

TNO report**TNO 2015 R11739 | Final report****Thermal fracturing due to low injection
temperatures in geothermal doublets****Energy/Geological Survey of
the Netherlands**Princetonlaan 6
3584 CB Utrecht
P.O. Box 80015
3508 TA Utrecht
The Netherlands

www.tno.nl

T +31 88 866 42 56

F +31 88 866 44 75

| | |
|----------------------|---|
| Date | 08 Apr 2016 |
| Author(s) | J.G. Veldkamp, D. Loeve, E. Peters, R. Nair, F. Pizzocolo, F. Wilschut |
| Copy no | |
| No. of copies | |
| Number of pages | 94 (incl. appendices) |
| Number of appendices | 8 |
| Sponsor | Energie combinatie Middenmeer ECW, GeoPower Oudcamp VOF, Green Well Westland BV, A.C. Hartman BV, IF Technology, Aardwarmte de Lier, Nature's Heat, Aardwarmte Vogelaer VOF, Kwekerij de Wieringermeer, Pieter Wijnen Egchel BV, Twan Wijnen Egchel BV, A+G van den Bosch BV, Gebr. Duijvestijn |
| Project name | IPC Geothermie 2.0 - part II: Thermal fracturing |
| Project number | 060.06962 |

All rights reserved.

No part of this publication may be reproduced and/or published by print, photoprint, microfilm or any other means without the previous written consent of TNO.

In case this report was drafted on instructions, the rights and obligations of contracting parties are subject to either the General Terms and Conditions for commissions to TNO, or the relevant agreement concluded between the contracting parties. Submitting the report for inspection to parties who have a direct interest is permitted.

© 2016 TNO

Summary

In the fall of 2013, a consortium consisting of a number of geothermal operators and IF Technology started a government funded project ('Innovatie Prestatie Contract' or IPC) to investigate ways to improve the operation of geothermal doublets. This report documents the results of a study done by TNO in the context of the IPC project on thermal fracturing as a consequence of lowering injection temperatures.

Enhanced cooling of the geothermal brine leads to a more viscous, denser fluid. The combined effect of viscosity and density on the flow in the well is positive but small (less injection pressure required). However, the effect of injection of a cold fluid into the reservoir is negative and large (more injection pressure required). The combined effect is that the injection pressure for the cooler fluid is larger than that of a warmer fluid.

An analytical model to calculate the dimensions of thermal fractures was implemented in Excel. This model was used to assess the likelihood (i.e. given the relatively large uncertainties in site-specific conditions) that thermal fracturing, and as a consequence enhanced flow, is taking place, given the essential reservoir and installation parameters, and current injection conditions. For four of the studied doublets it is considered likely that thermal fracturing occurs under current operating conditions. Four more doublets may encounter thermal fracturing. Four doublets are unlikely to experience thermal fracturing under current injection circumstances.

For three doublets, an analysis was made of production data. None of these doublets showed a permanently and consistently increased injectivity, and therefore no evidence of the *onset* of thermal fractures. Thermal fractures potentially start to grow at the beginning of the doublet operations. For none of the three doublets production data were available from the very beginning of operations. An effect on injectivity should be observed in current operations if thermal fracturing occurs.

The importance of accurate data in determining the uncertainty of predictions of thermal fracturing cannot be overemphasized. This holds for both data required as input for the modelling, and for the actual production data used to validate the models. The analytical tool is particularly sensitive to changes in reservoir depth, reservoir thickness, geothermal gradient, temperature of the injected water, thermo-elastic constant, and especially the magnitude of the minimum horizontal stress. Especially the minimum horizontal stress, which is often poorly constrained due to lack of data (i.e. well tests), plays a very important role. The available production data were sub-optimal, which plays an important role in the current analysis. Two data series did not cover the important first phase of operation, during which the fracture preferentially initiates. The third data series was too short to allow conclusive analysis. For new doublets, a continuous monitoring data record from the very start of production would be valuable for better assessing the likelihood of thermal fracturing.

Reduction of the injection temperature leads to increased risk of precipitation of some minerals. For silica (and barite in some cases), a significantly increased risk of scaling is predicted with additional cooling. Further cooling than done at present

is not advisable without a scaling prevention strategy. In fact, simulations indicate that the scaling potential of current operations is already significant.

Summarizing, it can be concluded that the positive flow effect of thermal fractures can be considerable, but prediction based on current datasets is difficult due to the large uncertainties in rock properties and local conditions. Moreover, increased risk of scaling associated with additional cooling may reduce or inhibit benefits of cooling on flow.

Samenvatting

Een consortium bestaand uit een aantal geothermie-operators en IF Technology startte in het najaar van 2013 een door de overheid gefinancierd project ('Innovatie Prestatie Contract' of IPC). Het doel van het project was om te onderzoeken hoe de operatie van geothermische doubletten verbeterd kon worden. Het onderliggende rapport beschrijft de resultaten van een studie naar thermisch scheuren ten gevolge van verlaagde injectietemperatuur die is uitgevoerd door TNO in de context van het IPC-project

Afkoeling van de geothermische brijn naar lagere temperatuur leidt tot een viskeuzere, zwaardere vloeistof. Het gecombineerde effect van viscositeit en dichtheid op de stroming in de put is positief maar klein (minder injectiedruk nodig). Daarentegen is het effect van het injecteren van een koudere vloeistof in het reservoir negatief en groot (meer injectiedruk nodig). Het gecombineerde effect van beiden tezamen is dat de benodigde injectiedruk voor koudere vloeistof groter is dan voor warmere vloeistof.

Een analytisch model dat de afmetingen van een thermische scheuren is in MS Excel geïmplementeerd. Dit model is gebruikt om te bepalen hoe waarschijnlijk het is dat het proces van thermisch scheuren optreedt (en als gevolg een vergroot debiet), gegeven de belangrijkste reservoir- en installatieparameters, en de injectiecondities. De onzekerheden in sommige van deze locatie-specifieke condities is groot. Het model voorspelt dat bij vier van de bestudeerde doubletten de kans groot is dat thermisch scheuren optreedt onder de huidige omstandigheden. Bij vier andere doubletten is het mogelijk dat dit effect optreedt. Bij de vier laatste doubletten is dit onwaarschijnlijk.

De productiegegevens van drie doubletten zijn geanalyseerd om te zien of deze aanwijzingen geven dat thermisch scheuren optreedt. Geen van de doubletten vertoont echter een permanent vergrote injectiviteit, en dus ook geen bewijs voor beginnende scheurvorming. Thermische scheuren beginnen in principe vrij snel te groeien na het begin van de exploitatie van het doublet. Van geen van de doubletten waren echter productiegegevens beschikbaar vanaf het begin van de exploitatie. Wanneer thermische scheuren worden gevormd, moet dit een effect hebben op de injectiviteit van het doublet.

De beschikbaarheid van nauwkeurige gegevens is zeer belangrijk om het optreden van thermisch scheuren te voorspellen. Dit geldt voor zowel de meetgegevens die nodig zijn als invoer voor de modellering, als de productiedata die gebruikt worden om de modellen te valideren. Het analytische model is zeer gevoelig voor (veranderingen in) de opgegeven reservoirdiepte, dikte, geothermische gradiënt, temperatuur van het geïnjecteerde water, thermo-elastische constante, en in het bijzonder de grootte van de minimale horizontale spanning. Deze laatste is vaak slecht bekend vanwege het gebrek aan gemeten gegevens (bijvoorbeeld uit well tests). De kwaliteit van de beschikbare productiegegevens was niet optimaal, hetgeen een zeer belangrijke rol in de analyse speelde. Twee van de drie sets productiedata besloegen de belangrijke eerste fase van productie, gedurende welke thermische scheuren in de regel beginnen, niet. De derde dataset was te kort om een afdoende analyse mogelijk te maken. Voor nieuwe doubletten is een

continue set productiegegevens, geregistreerd vanaf het eerste begin van de exploitatiefase, zeer waardevol om beter te kunnen bepalen of thermisch scheuren optreedt.

Verlaging van de injectietemperatuur leidt tot een verhoogd risico op het neerslaan van sommige mineralen. Een significant hoger neerslagrisico bij verlaging van de injectietemperatuur wordt voorspeld voor silica en, in sommige gevallen, bariet. Het verlagen van de injectietemperatuur wordt daarom afgeraden tenzij maatregelen tegen het neerslaan van mineralen worden genomen. Simulaties tonen aan dat het neerslagpotentieel bij de huidige omstandigheden als significant kan zijn.

Samenvattend kan geconcludeerd worden dat het positieve effect van thermische scheuren op het debiet aanzienlijk kan zijn, maar dat het voorspellen ervan moeilijk is vanwege de grote onzekerheid in de reservoir eigenschappen en het lokale spanningsveld. Het verhoogde neerslagrisico als gevolg van verlaagde injectietemperatuur kan het positieve effect ervan verminderen of teniet doen.

Contents

| | | |
|----------|---|-----------|
| 1 | Introduction | 7 |
| 1.1 | Context and background | 7 |
| 1.2 | Scope of work..... | 8 |
| 2 | First order thermal effects of cold fluid injection without thermal fracturing ... | 9 |
| 3 | Thermal fracturing | 12 |
| 3.1 | Fracture initiation and growth | 13 |
| 3.2 | Modelling the effect of thermal fracturing on flow..... | 15 |
| 3.3 | Literature observations of thermal fracturing..... | 19 |
| 4 | Thermal fracturing in Dutch geothermal systems | 20 |
| 4.1 | Doublet installation and reservoir parameters..... | 20 |
| 4.2 | Analysis of production data | 20 |
| 4.3 | Expected fracturing and injectivity based on analytical model | 31 |
| 4.4 | Differences between observed and theoretical BHP | 33 |
| 4.5 | Conclusions based on production data | 34 |
| 5 | Scaling potential at reduced injection temperatures | 36 |
| 6 | Conclusions and recommendations | 39 |
| 6.1 | Conclusions | 39 |
| 6.2 | Recommendations..... | 39 |
| | References | 41 |
| | Appendices | |
| | A Models for thermal fracturing and injectivity | |
| | B Changes in stress field and fracturing during injection and cooling | |
| | C Analytical model tool user guide | |
| | D Calculation of the axes of the elliptical fluid front | |
| | E List of symbols | |
| | F Determination of the minimum principal stress from well tests | |
| | G Additional plots Chapter 4 | |
| | H Doublet names (restricted) | |

1 Introduction

1.1 Context and background

In the fall of 2013, a consortium consisting of a number of geothermal operators, IF Technology and TNO started a government funded project ('Innovatie Prestatie Contract' or IPC) to investigate ways to improve the operation of geothermal doublets. The project was focused around two major topics: corrosion prevention and optimizing injection temperatures. Driven by priorities of the stakeholders in the project, TNO started with corrosion related activities. In a separate report the results of those activities were documented (Veldkamp et al., 2015). This report documents the results of the work done on thermal fracturing as a consequence of low injection temperatures.

In geothermal doublets, hot water is produced from a subsurface reservoir. After using the heat, the cooled water is injected back a. In a Dutch geothermal system, the temperature of the produced water is typically between 60-90°C, while water is re-injected at a temperature of around 30-35°C. The flow rates vary between 100 and 250 m³/hr. Some operators strive to further increase these rates.

Operating a geothermal doublet requires significant amounts of energy for the production and injection pumps, which are required to overcome flow resistance in the reservoir, the wells and the surface installations. In addition, energy is required by the heat exchanger and/or heat pump to cool the water. Flow resistance depends on water properties that vary with pressure and temperature (such as density and viscosity) as well as on reservoir properties. The flow capacity of the (near-well) reservoir can change when fractures form in the rock as a results of the combination of injection pressure and a high temperature difference between the reservoir and the injected water. The effect of temperature on the formation of fractures (i.e. thermal fracturing) is the central topic of the work described in this report. Injection-related fracturing in a rock formation is mainly determined by the complex interplay between pressure and temperature (apart from rock and fluid properties). Therefore the formation of fractures that occurs when the injection pressure exceeds the minimum principal stress (i.e. hydraulic fracturing) is included in the work where relevant. Hydraulic fracturing is the conventional method to stimulate flow in oil and gas reservoirs or enhanced geothermal systems.

The study addresses the question how reduction of the temperature of the injected water will affect the operation of geothermal systems:

- What is the effect of changes in the density and viscosity of the water to the flow in a geothermal system (without thermal fracturing)?
- Is thermal fracturing likely to occur in the current Dutch geothermal doublets, and does it occur when injection temperatures are reduced?
- If thermal fracturing occurs, how can the effect on the flow be estimated? What is the validity of the models used for such calculations?
- Is there any evidence of thermal fracturing in data of geothermal doublets that are currently operational (as provided by the operators)?
- Does reducing the injection temperature lead to increased risk of scaling in the injection well?

1.2 Scope of work

The scope of activities in the current study can be summarized as follows:

- It is explained how calculations with DoubletCalc can be made to estimate the performance of geothermal systems and, as an example of such calculations, it is demonstrated what the effect is of reduced temperatures on a 'typical' geothermal system without thermal fracturing.
- A relatively simple, analytical fracture propagation model has been implemented in an MS Excel environment. It can be used to estimate the onset and propagation of fractures and the corresponding improvement of the flow, which is expressed as a (negative) skin. The skin factor can be used in further calculations with DoubletCalc to estimate the flow enhancement.
- The MS Excel model has been validated by comparing its output to that of other analytical and numerical models.
- The MS Excel model has been used to predict whether or not thermal fracturing is likely to occur in present geothermal doublets.
- Data as obtained from three operators (time series of flow rates, temperatures and pressures) have been analysed to see if there is any evidence of thermal fracturing in these doublets.
- Results of a previous study on scaling have been reassessed to quantify (additional) scaling risk.

For the operators, predicting and optimizing flow is important. However, final (operational) decisions will also depend on other factors, such as consumer heat demand, subsidies, etc.. Design choices often have to be made before all information about the performance of the wells and the reservoir is available. The current study supports decision making on the basis of flow prediction. Economic evaluations are beyond the scope of this work. Pump efficiencies and/or other components in the geothermal system that are possibly influenced by changing flow conditions were not investigated either.

In the next chapter, the process of the thermal fracturing is explained. In chapter 2, the analytical fracture propagation model used in this study is described. Chapter 4 focusses on application of the models to Dutch geothermal systems, the production data and issues that exist with the data. In chapter 5, the effect of reduced injection temperatures on scaling risks is described. The analytical model is described in detail in the appendices.

2 First order thermal effects of cold fluid injection without thermal fracturing

The performance of a geothermal doublet is influenced by lowering the injection temperature. Both the density and the viscosity of the brine increase when the fluid is cooled (Figure 2.1). This triggers various effects:

- the water column in the injection well becomes heavier as a result of the density increase. Therefore the required injection pump pressure decreases;
- the friction in the injection well marginally increases¹ due to the higher fluid viscosity (). This increases the required injection pump pressure.
- warm water can more easily be injected in a reservoir than cold water. Therefore the required injection pressure increases due to the increased inflow resistance;
- the geothermal heat production increases due to the enhanced cooling.

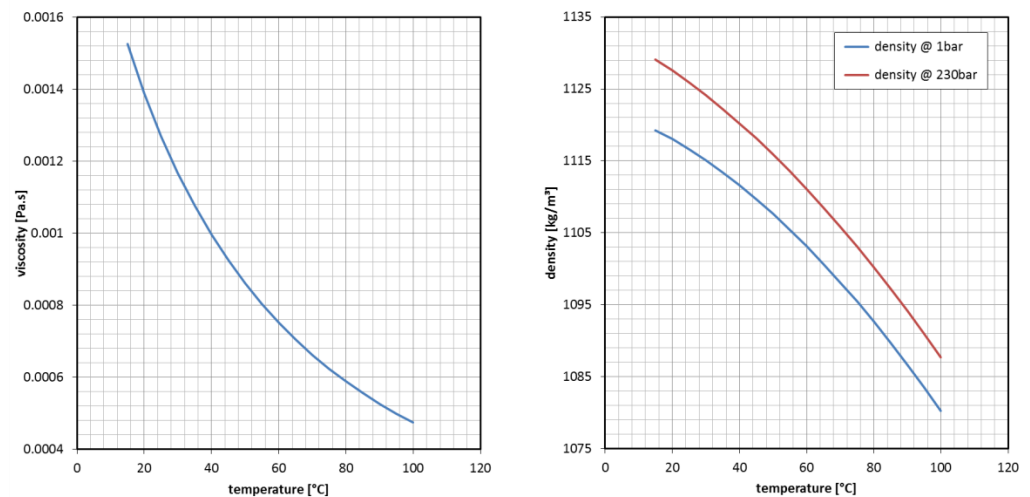


Figure 2.1 Batzle and Wang (1992) relationships between water temperature and viscosity (left), and water temperature and density (right) at different pressures.

The above mentioned effects are taken into account by the DoubletCalc software². In order to illustrate the effects, a DoubletCalc base case scenario was used, in which the original cooling to 35°C was changed to 20°C (Figure 2.2). The following paragraph shows the effects on density, viscosity and doublet performance.

¹ Friction is almost independent of viscosity. The main influencing factors on friction are the diameter of the well and the fluid velocity. In contrast, the fluid viscosity during hydraulic fracturing is very high due to the use of proppants, which requires the use of friction reducing chemicals.

² DoubletCalc is a software tool which can be used to calculate an indicative performance of geothermal doublets (Mijnlieff et al. 2014). The software can be downloaded from www.nlog.nl. It is widely used in the Dutch geothermal community, most importantly because DoubletCalc calculations are the basis for applications for the 'SEI' and 'SDE+' subsidy schemes.

Doublet Calculator 1.4.3

number of simulation runs () 1 Calculate Open Scenario Save Scenario Exit Program

Geotechnical input

A) Aquifer properties

| Property | min | median | max | Property | value |
|---------------------------------|--------|--------|--------|--------------------------------------|---------|
| aquifer permeability (mD) | 109 | 110 | 111 | aquifer kh/kv ratio (-) | 1.0 |
| aquifer net to gross (-) | 0.96 | 0.97 | 0.98 | surface temperature (°C) | 10.0 |
| aquifer gross thickness (m) | 164 | 165 | 166 | geothermal gradient (°C/m) | 0.03573 |
| aquifer top at producer (m TVD) | 1998.0 | 2220 | 2442.0 | (mid aquifer temperature product | 0.0 |
| aquifer top at injector (m TVD) | 2024.0 | 2249 | 2474.0 | (initial aquifer pressure at produc | 0.0 |
| aquifer water salinity (ppm) | 150000 | 165000 | 180000 | (initial aquifer pressure at injecto | 0.0 |

B) Doublet and pump properties

| Property | value |
|-------------------------------------|-------|
| exit temperature heat exchanger | 35 |
| distance wells at aquifer level (m) | 1243 |
| pump system efficiency (-) | 0.5 |
| production pump depth (m) | 687 |
| pump pressure difference (bar) | 87.5 |

C) Well properties

calculation length subdivision (m) 50

| Producer | | | | | Injector | | | | | | |
|----------|--------------------------------|------------------------------|------------------------|-------------------------|-------------------------------|---------|--------------------------------|------------------------------|------------------------|-------------------------|-------------------------------|
| Segment | pipe segment sections p (m AH) | pipe segment depth p (m TVD) | pipe diameter p (inch) | inner diameter p (inch) | pipe roughness p (milli-inch) | Segment | pipe segment sections i (m AH) | pipe segment depth i (m TVD) | pipe diameter i (inch) | inner diameter i (inch) | pipe roughness i (milli-inch) |
| 1 | 687 | 687 | 5.921 | 1.19 | 1.19 | 1 | 1286 | 1286 | 12.347 | 8.755 | 1.19 |
| 2 | 1200 | 1200 | 12.347 | 1.19 | 1.19 | 2 | 2298 | 2040 | 8.755 | 1.19 | 1.19 |
| 3 | 2130 | 2069 | 8.755 | 1.19 | 1.19 | 3 | 2531 | 2249 | 5.921 | 1.19 | 1.19 |
| 4 | 2213 | 2220 | 5.921 | 1.19 | 1.19 | 4 | | | | | |
| 5 | | | | | | 5 | | | | | |
| 6 | | | | | | 6 | | | | | |
| 7 | | | | | | 7 | | | | | |
| 8 | | | | | | 8 | | | | | |

optional

Figure 2.2 DoubletCalc example scenario used to assess density and viscosity effects due to enhanced cooling.

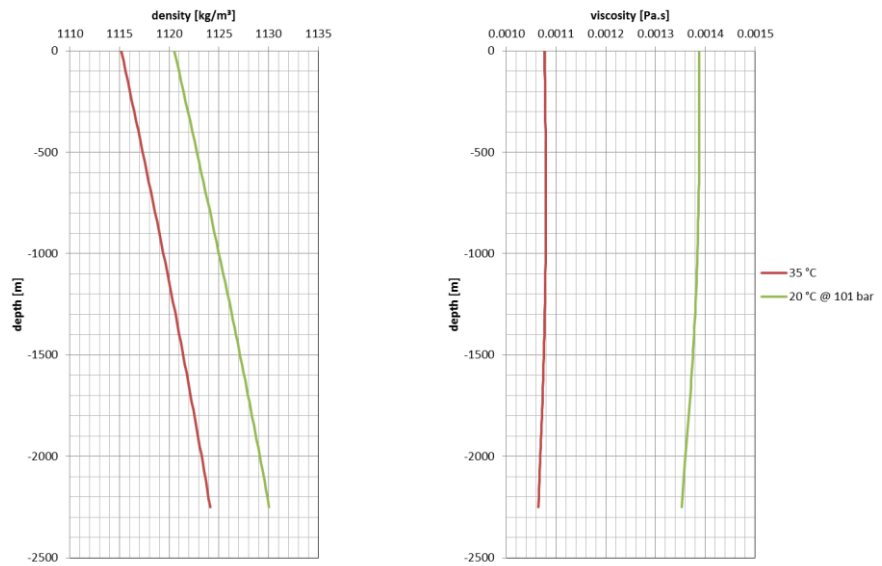


Figure 2.3 Density and viscosity changes with depth and injection temperature in the injector well, for 35 and 20°C injection temperature scenarios.

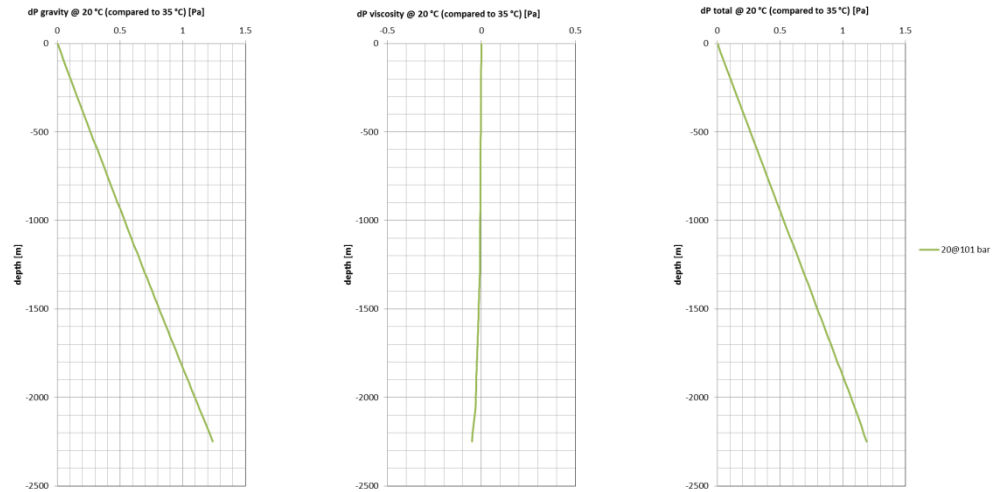


Figure 2.4 Increased pressure due to density effect (left), viscosity effect (middle) and combined effects (right) for increased cooling to 20°C @101 bar pump pressure difference.

Figure 2.4 shows that in the wellbore, the (positive) pressure effect of the increased density is much higher than the (negative) effect of viscosity (+1.25 vs -0.05 bar). The pressure drop due to increased viscosity becomes prominent during reservoir flow. The net pressure gain is about 1.2 bar at the bottom hole (Figure 2.4). The additional pump pressure required to maintain the same flow rate is about 13.7 bar (Table 2.1), so the negative effect of increased inflow resistance is 13.7 + 1.2 = 14.9 bar. The extra power generated is 1.7 MW (compared to the original 13.8 MW), which is about a 12% increase.

Additional power was generated by the enhanced cooling. At the same time a higher pump pressure (and therefore higher power consumption) was required to maintain the same flow rate. Both effects influence the coefficient of performance (COP) in opposite directions. The COP is defined as the ratio of the generated geothermal power to the summed power required to produce the hot water and to inject the cold water.

The extra cooling leads to a COP increase from 12.1 to 15.3. As a comparison, 13.7 bar extra pump pressure without extra cooling adds 1.9 MW (15%), at the expense of a lower COP (10.5). Cooling to 20°C with an identical target power (13.8 MW) requires only 77 bar pump pressure. The volume flow rate is lower, and the friction losses are less. The COP is raised to 17.3.

| temperature [°C] | pump pressure [bar] | flow rate [m³/hr] | power [MW _{th}] | COP [-] |
|------------------|---------------------|-------------------|---------------------------|---------|
| 35 | 87.5 | 234.7 | 13.8 | 12.1 |
| 20 | 87.5 | 207.6 | 15.5 | 15.3 |
| 20 | 101.2 | 234.7 | 17.5 | 13.3 |
| 35 | 101.2 | 265.5 | 15.7 | 10.5 |
| 20 | 77.0 | 186.4 | 13.8 | 17.3 |

Table 2.1 Resulting flow rate, power and COP as a result of multiple combinations of exit temperature and pump pressure difference. The highest COP is achieved with a combination of low temperature and low pump pressure / flow rate.

3 Thermal fracturing

The injection of fluid at temperatures different from the reservoir rock will cause cooling or heating of that rock. This will in turn cause a volume change as the rock shrinks as it cools, and expands when it heats. The rock volume is not free to expand or contract in the lateral direction, because it is connected to neighbouring rock volumes. Therefore, the temperature-induced volume change of the rock will lead to a change of the forces acting on the reservoir rock volume that were already present before drilling the well. In other words, the in-situ stress state changes. This effect is called thermal stressing or thermo-elastic stressing.

This effect which can, either by itself or in combination with pore pressure changes, open and propagate fractures that already exist in the rock or initiate new tensile fractures (Figure 3.1). The type of failure (Figure 3.2) will depend on:

- the magnitude and direction of the in-situ stress already present in the subsurface;
- the orientation of pre-existing fractures and faults;
- the magnitude and direction of thermo-elastic stresses and pore pressure changes.

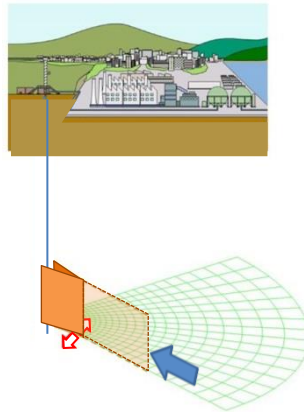


Figure 3.1 Side view of a propagating tensile crack (orange; in the vertical plane). The red arrows indicate the tangential stresses. The blue arrow indicates the maximum horizontal stress.

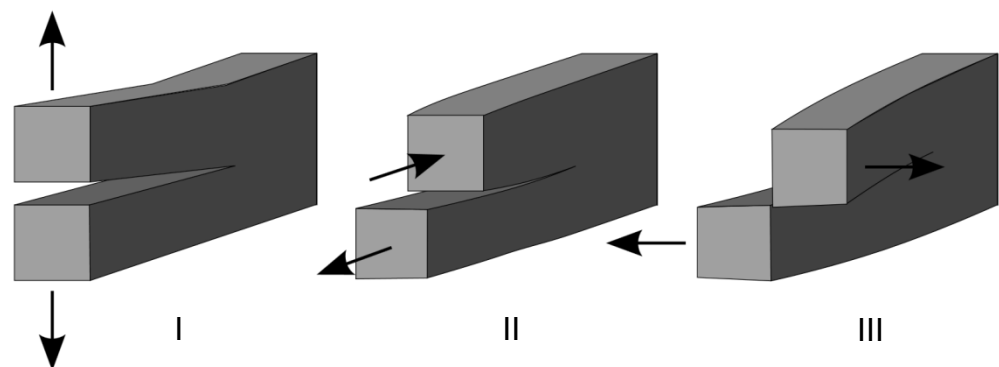


Figure 3.2 Three modes of fracture mechanics (I: opening, II: in-plane shear and III: out-of-plane shear). Source: wikimedia.

In this chapter the development of newly formed tensile fractures (Mode I in Figure 3.2 and Figure 0.22) is described. These fractures initiate around the wellbore, where temperature and pressure effects are largest. As it is unclear whether natural fractures are present in the geothermal reservoirs, only tensile fracturing (mode I) is considered when analysing thermal effects on injectivity. Shear fracturing (mode II) may occur if natural fractures are hydraulically connected to the injection well (Figure 0.22).

3.1 Fracture initiation and growth

Several criteria can be adopted to model the initiation and propagation of a tensile fracture. Appendix A.1 describes the criteria that are used in this study to predict whether tensile failure of the rock, and thereby initiation and/or propagation of hydraulic fractures, occurs. The local stress state around a geothermal injection well (within a distance of approximately 2-3 times the well radius) changes due to the injection of large volumes of fluid colder than the reservoir rock. It is generally assumed that hydraulic fractures initiate when the injection pressure exceeds the sum of the minimum principal stress and the tensile strength of the rock. As temperature differences between reservoir and injected fluid will decrease with time due to cooling of the reservoir, thermal stresses will be largest at the start of injection. Therefore, thermal fractures will likely initiate and grow at the beginning of doublet operations.

The initial magnitude and direction of minimum principal stress before injection are controlled by the local geological setting. The tensile strength is a mechanical property of the undamaged rock matrix. Usually, the drilling process has caused some damage to the rock near the wellbore. Therefore, the tensile strength within the damage zone is reduced compared to the undamaged rock matrix. It is difficult to quantify how the damaged zone affects the rock's strength. In general it is easier to initiate or propagate a fracture within the damaged zone. In most cases the tensile strength of the rock near the wellbore is assumed to be negligible. Accordingly, the condition of hydraulic fracture initiation is met when the pressure equals the minimum principal stress.

A tensile fracture can be initiated when the criteria for tensile opening are met due to changes in thermal stress and/or pore pressure. Most parts of the Netherlands are dominated by a normal faulting regime which means that the minimum principal stress (σ_3) is equal to the minimum horizontal stress ($\sigma_{h,min}$), the intermediate principal stress (σ_2) is equal to the maximum horizontal stress ($\sigma_{H,max}$) and the maximum principal stress (σ_1) is equal to the vertical stress (σ_v). In this case, the fracture will open in the direction of the minimum horizontal stress because this requires the smallest amount of energy. The fracture will propagate in the direction of the maximum horizontal stress, which is oriented at right angles to the minimum horizontal stress. The propagation of the fracture depends on the in-situ stress state, the thermal stress changes and the injection pressure, but also on the rock strength and the fracture length itself. An analytical model for fracture propagation described by Koning (1988) was implemented in an Excel environment. The model includes the effects of pore pressure changes and thermal stress changes due to the fluid injection and heat extraction typical for a geothermal doublet. Appendix A.2 provides more details about the implementation and the theoretical background.

The main assumptions of the model are:

- The fracture is assumed to be vertical. It extends laterally from a single well in an infinite reservoir. The surface of the fracture is rectangular and has height h and half-length L . The reservoir and fracture heights are constant. In top view, the fracture tips are elliptical (Figure 3.3).
- The rock volume that experiences the effect of pressure change is larger than the rock volume that experiences the temperature change. The outer boundaries of both volumes are described by the fluid-front and the cold-front respectively. The shapes of both fronts are approximated by ellipses. The ellipse axes are parallel to the fracture at all times (Figure 3.4).
- The fluid and temperature changes remain uniform over the height of the reservoir during the growth of the elliptical fronts (piston-like behaviour, Figure 3.5).

One of the simplifications seen in literature is the assumption of one-dimensional leak-off in the direction perpendicular to the fracture wall (along the y -axis in Figure 3.3). This assumption is not valid in a geothermal doublet because the production well is close to the injection well and therefore the pressure field and the flow pattern is 2-dimensional. The influence of pressure field on a 2-dimensional flow pattern on the leak-off should be taken into account. Therefore a two-dimensional leak-off model is used in the analytical model presented here.

Among the results of the analytical model are the dimensions of the fracture after the specified analysis period, and the equivalent negative skin factor.

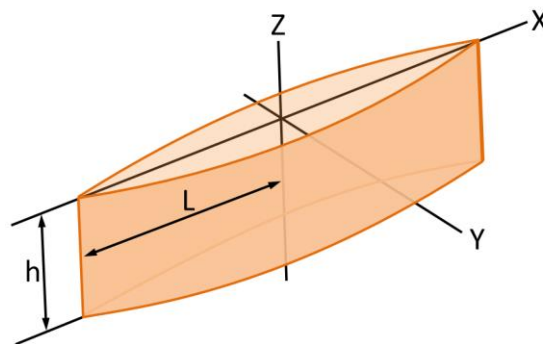


Figure 3.3 Fracture shape and naming conventions (after Koning, 1988).

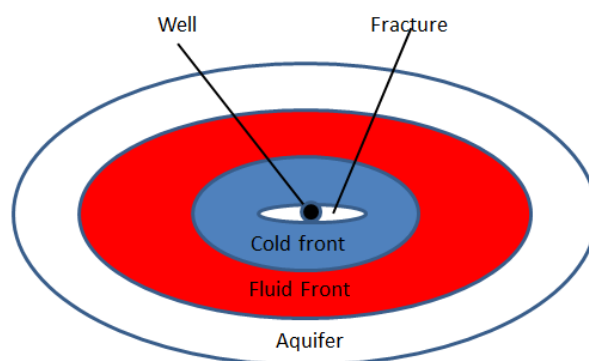


Figure 3.4 Elliptical shape of the cold and fluid fronts around the injection well (top view).

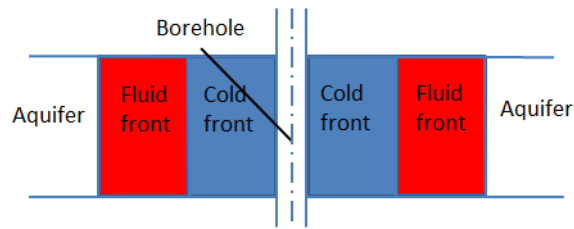


Figure 3.5 Piston like displacement of the fluid fronts (side view).

The injection pressure is relatively well known in a doublet. The minimal principal stress however is difficult to assess. Analyses of well tests (e.g., extended leak-off tests- XLOT) can be used, but their availability is limited due to relatively high costs involved. Appendix F describes how (local values for) $\sigma_{h,min}$ can be calculated from an extended leak-off test. In absence of well tests, $\sigma_{h,min}$ can be estimated using regional trends in leak-off pressure. Analysis of Verweij et al. (2012) suggests that the ratio between the horizontal and vertical stress ($\sigma_{h,min}/\sigma_v$) for various on- and offshore structural elements in most of the Netherlands is between 0.55 and 0.60 although variation of leak-off pressures is high and the ratio varies with depth (Figure 3.6). Note that locally $\sigma_{h,min}$ should be between the hydrostatic pressure and leak-off pressure. The data suggest a value for $\sigma_{h,min}/\sigma_v$ of 0.5 as a conservative estimate.

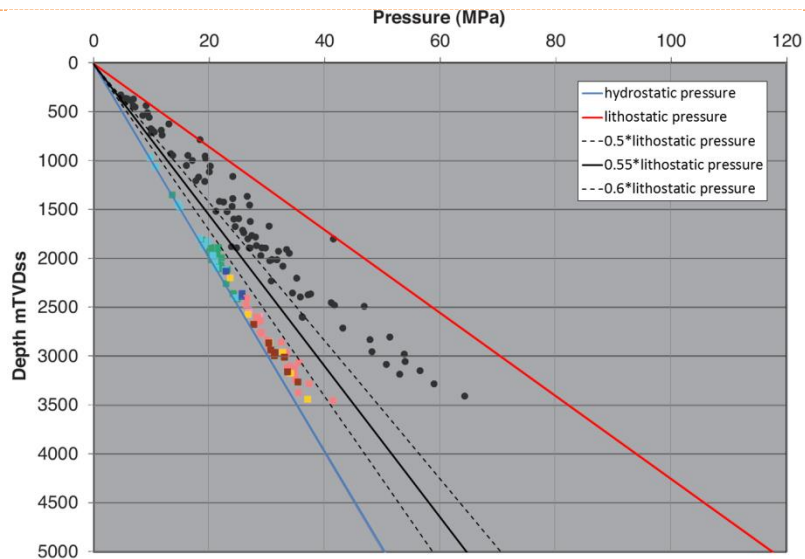


Figure 3.6 Fluid pressure (coloured dots) and leak-off pressure (black dots) for the main lithostratigraphic units in the West Netherlands Basin (after Verweij et al. 2012). The lower bound of the leak-off pressure is indicative of the horizontal minimal stress.

3.2 Modelling the effect of thermal fracturing on flow

For modelling purposes, the simplest possible well (a 'standard well') is vertical and unstimulated. Stimulation of a well can include thermal or hydraulic fracturing, acidizing, radial jetting and/or the drilling of laterals. The opposite effect of stimulation can be caused by well damage, where the relevant flow properties of the reservoir around the wellbore (in particular permeability) are affected by processes like mud invasion, scaling and perforation damage. These processes will cause the flow rate to decline under constant drawdown pressure.

3.2.1 *Injectivity index*

The productivity (or injectivity) index is defined as the amount of fluid that can be produced (or injected) per unit of time per bar pressure. It is expressed in cubic meters per hour per bar ($\text{m}^3/\text{hr}/\text{bar}$). Stimulation will increase the productivity / injectivity index. Well damage will have the opposite effect. As thermal fractures will likely initiate at the beginning of doublet operations (c.f. section 3.1) an effect on injectivity should be observed during the early stages of injection (i.e. during the first year or even first days of injection).

3.2.2 *Skin*

It is common practice to compare the productivity / injectivity of non-standard wells to that of a standard well by means of a so called skin factor. Any non-standard well has a productivity / injectivity equal to that of the standard well plus a skin factor. A skin factor is a dimensionless number that can either be positive or negative. A positive skin factor indicates that the well underperforms with respect to the standard well. A well that has negative skin performs better than a standard well. Deviated wells are generally modelled as a vertical well with a negative skin factor to account for their increased reservoir connectivity in comparison to a standard well.

Different types of skin are mechanical skin (caused by wellbore damage), completion skin, geometric skin (slant well) and rate dependent skin. The effect of a thermal or hydraulic fracture or radials can also be expressed as a (negative) skin factor. The skin factor and injectivity of a geothermal well that has been thermally fractured can be calculated if the dimensions of the fracture are known.

Figure 3.7 shows the resulting fracture length and corresponding skins as calculated by the analytical model, for different values of the ratio between horizontal and vertical stress. For the calculations, parameter values for a 'typical' doublet were used, as given in Table 3.1. The positive effect thermal fractures have on flow can be considerable. Their prediction is however difficult due to the large uncertainties in the relevant rock properties and local conditions. Figure 3.8 shows that the changes of the injectivity index for various values of (fracture) skin can be several tens of percent. For the modelled doublet, it increases from less than six to more than ten.

| parameter | value | unit |
|---|-------|----------------------|
| K_{IC} (critical stress intensity factor) | 10 | bar.m ^{1/2} |
| α (Verweij constant) | 0.6 | - |
| depth | 2330 | m |
| density rock | 2300 | kg/m ³ |
| $L_{initial}$ | 0.09 | M |
| E (Young's modulus) | 13.8 | GPa |
| ν (Poisson ratio) | 0.25 | - |
| T_{fluid} | 25 | °C |
| T_{rock} | 96.8 | °C |
| vertical stress | 526.4 | bar |
| horizontal stress | 315.8 | bar |
| density fluid | 1000 | kg/m ³ |
| initial pressure | 229 | bar |

Table 3.1 'Typical' rock and fluid properties.

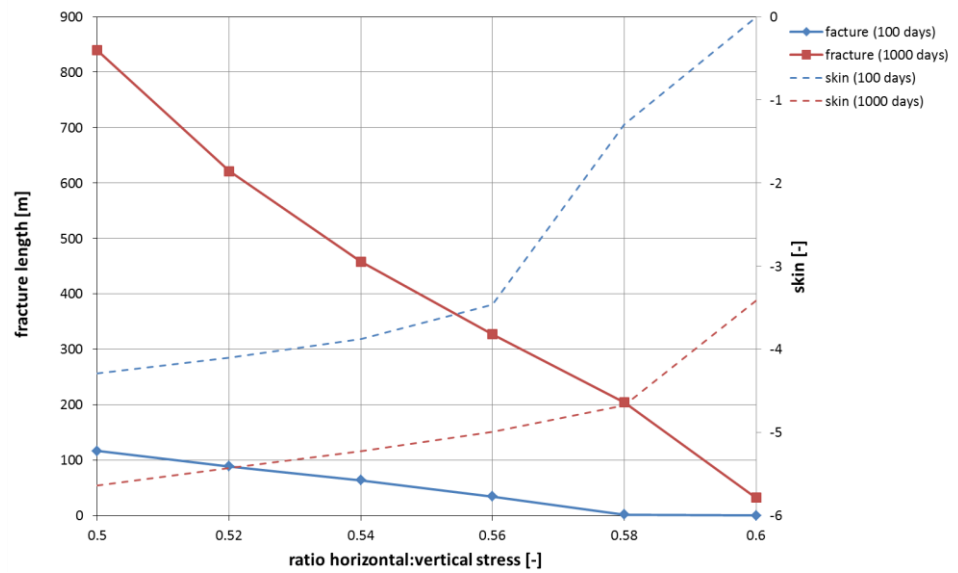


Figure 3.7 Fracture and skin development for a 'typical' doublet using varying horizontal : vertical stress ratios.

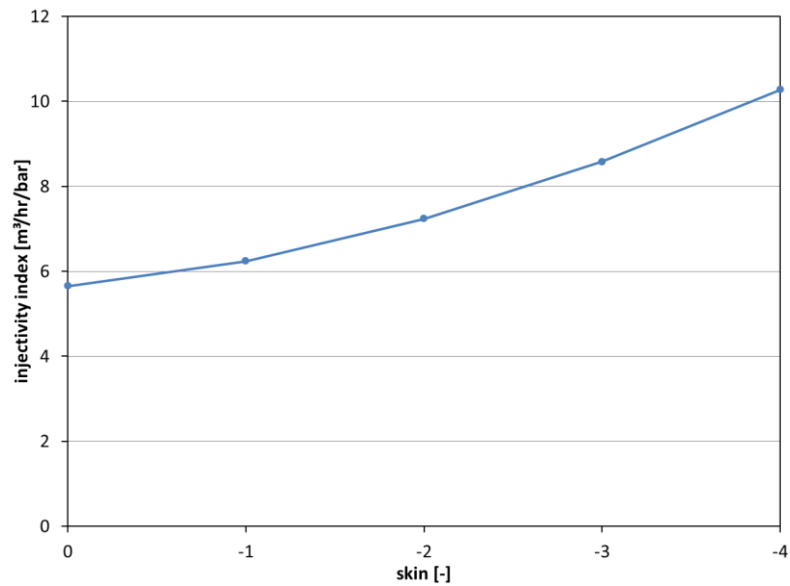


Figure 3.8 Theoretical relation between negative skin (for instance, fracture induced) and injectivity index for a 'typical' doublet. The increase in injectivity index is in the order of tens of percent for a (very high) skin of -4.

3.2.3 *Doublet performance calculation using a skin*

DoubletCalc can account for the effects of flow stimulation by specifying a skin factor. In contrast to the skin resulting from the deviation angle (which is automatically calculated by DoubletCalc using an analytical formula), other types of skin have to be calculated outside DoubletCalc and entered manually (Figure 3.9). The thermal fracture skin that is calculated by the analytical model can be accounted for in DoubletCalc using the relevant skin factor.

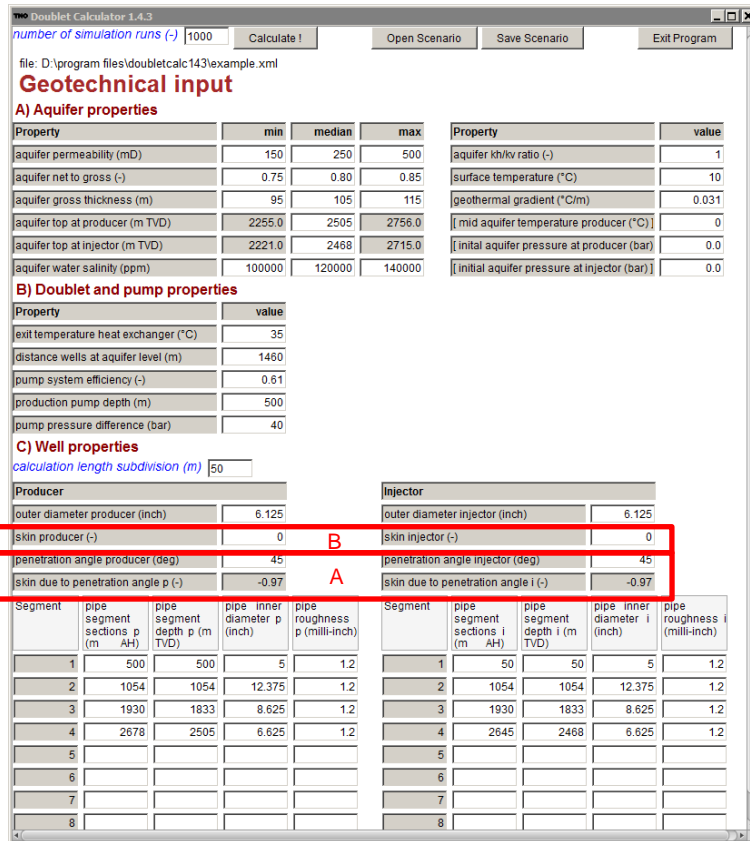


Figure 3.9 DoubletCalc input screen showing well inclination and automatically calculated penetration angle skin (A). Additionally, a 'skin producer' and / or 'skin injector' can be specified manually (B).

3.3 Literature observations of thermal fracturing

Thermally induced fracturing is common in water injection wells in the petroleum industry (Bellarby, 2009) and many examples have been presented. The effect has frequently been reported in geothermal wells too (Benson et al, 1987; Tulinius et al, 2000). Bellarby (2009) states that thermally induced fracturing is indeed observed to such an extent that filtration of fines is reduced on many North Sea platforms. Cold fracturing is even observed in relatively soft, unconsolidated formations where according to theory fracturing should be limited (Santarelli et al., 2008). Most examples found in the literature report sharp increases in injectivity shortly (< 5 days) after start-up (Svendsen et al., 1991; Santarelli et al., 2008). Long term phenomena (>year) were studied by Detienne et al. (1998), Slevinsky (2002) and Suri et al. (2011). Slevinsky (2002) analysed three water injection wells. Neither of these wells showed an overall increase in injectivity over a period of 29, 700 and 1500 days respectively. The authors concluded however that in all three wells plugging effects were offset by increasing fracture length. The data typically showed alternating gradual decrease (plugging) and sharp increases (fracturing) in injectivity. Suri et al. (2011) analysed the history of an injection well in an oil field. Despite extensive analysis and modelling, the simulated fracture length remained highly uncertain.

4 Thermal fracturing in Dutch geothermal systems

4.1 Doublet installation and reservoir parameters

The development of a thermal fracture will enhance the injectivity index (c.f. section 3.2.1). In order to obtain insight into the possibility that thermal fracturing plays a role for the Dutch geothermal sector, the injectivity index was studied.

Doublet and installation parameters of most Dutch doublets were collected or estimated. Production data of four doublets were obtained and analysed by calculating the injectivity index and studying its development over time. For all doublets, the Excel model tool was used in order to estimate whether thermal fracturing is likely to occur under the present production circumstances.

4.2 Analysis of production data

Production data were made available from doublets labelled D1, D2, D3 and D4. The data from the D2 doublet was lacking pressure data and could not be used. All other data included production and injection flow rate, injection temperature and (injection) pump pressure for varying periods in time. In section 3.2.1, it was pointed out that the effect of increased injectivity due to thermal fracturing is expected during the first year or even first days of injection. Only for the D1 doublet the data covering the first months of production were available.

4.2.1 Description of the production data

| location | drilling finished | date from | date to | days | rate [m ³ /hr] | temp. [°C] | pressure [bar] |
|----------|-------------------|------------|------------|------|---------------------------|------------|----------------|
| D1 | 24/10/2013 | 24/08/2014 | 24/02/2015 | 184 | 214 | 36 | 37 |
| D3 | 22/01/2011 | 01/01/2014 | 30/12/2014 | 363 | 128 | 36 | 36 |
| D4 | 16/07/2007 | 03/06/2013 | 02/07/2015 | 759 | 183 | 30/15 | 14 |

Table 4.1 Characteristics of the analysed production data.

The raw data were filtered and corrected for incomplete time intervals (e.g. during shut-in, pressure data were sometimes lacking). The injectivity index was estimated by calculating the bottom hole pressure (BHP) from the injection pressure (tubing head pressure THP). This was done by assuming a vertical well. In a deviated well, due to the increased length, the pressure losses due to friction are higher. However, the extra friction losses are significant only for high velocity gas flow (Mijnlieff et al. 2014, eq. 29). In the case of water flow, the effect is small and can be neglected.

Two components contribute to the conversion from THP to BHP:

- gravitational forces (the weight of the water column)
- pressure losses due to friction forces.

To this end, the density and viscosity were calculated as a function of the salinity, injection temperature and pressure. The pressure conversion is described by the Fanning equation, which is explained in more detail in the DoubletCalc manual (Mijnlieff et al. 2014). The heating of the fluid during injection in the well (see Appendix A.6) is ignored, because of its limited magnitude (around 1°C). The

pressure measurements data are generally noisy, probably as a result of non-uniform turbulent flow in the well and its influence on the pressure sensor. The magnitude of the noise is assumed to be relatively small compared to the pressure effects due to varying flow rate and temperature.

Different analyses were performed on the production data:

- Hall plots of the production data were created. A Hall plot analyses steady-state flow in an injection well (Figure 4.1). In general, the slope of a Hall plot is interpreted as an indicator of the average well injectivity. When injection conditions do not change over time, the plot is a straight line. Deviations from the straight line indicate changes in injection conditions. Hall plots have been used earlier by other authors to detect the effectivity of thermal stimulation (Bradford et al., 2014, Figure 4.2).
- A more detailed analysis was performed in order to investigate whether the observed BHP or injectivity index could be explained by theoretical outflow equations. Calculated injectivity indices were added to the Hall plots to facilitate the interpretation.
- Time against flow rate – injection temperature, injection pressure – injection temperature and flow rate – injection pressure plots were generated for one week periods (both in summer and winter) to interpret relevant phenomena that may act on a short (daily) time scale.

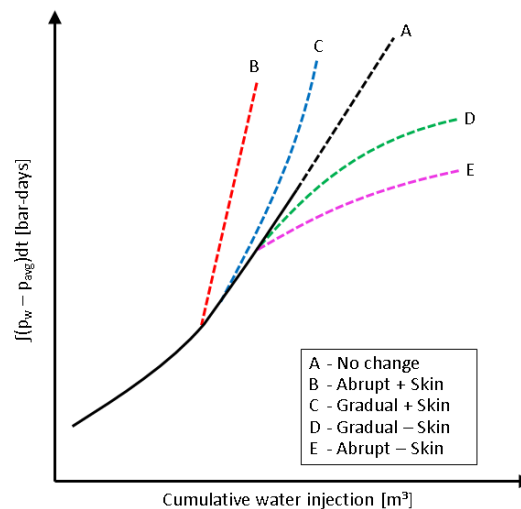


Figure 4.1 Possible characteristics of a Hall plot (after www.fekete.com).

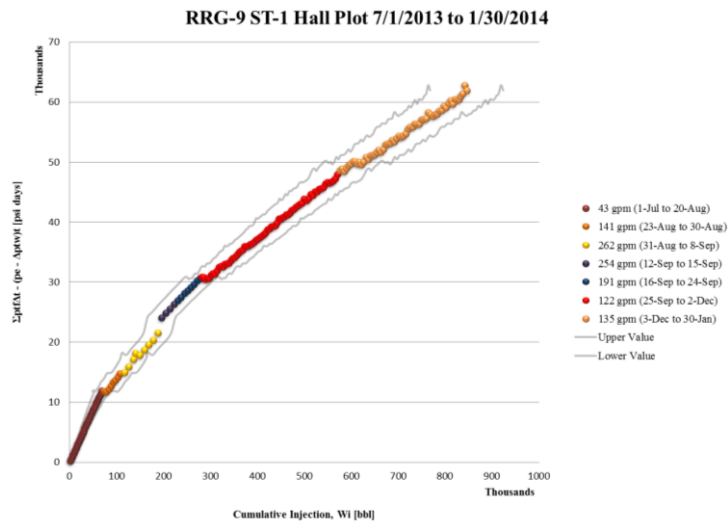


Figure 4.2 Field example of a hall plot analysis on an injector well in the Raft River geothermal field (Bradford et al., 2014). 'Cooler' colours represent cold water injection.

4.2.2 D1 doublet

The D1 doublet was drilled in between June and October 2013. Seven months of production data between August 2014 and February 2015 were made available. Figure 4.3 shows the production data, averaged per day. The injection temperature remained relatively constant around 36°C. The flow rate varied around 240 m³/hr, with some intervals of lowered injection rate near the end of November.

The combined Hall and injectivity index plot (Figure 4.4) shows negligible deviation from the expected trend for a non-fractured reservoir. The injectivity index shows a number of spikes (numbered in Figure 4.3 and Figure 4.4), all related to short shut-in periods. Especially the first 50 days shows a higher injectivity index for higher flow rate. This is a possible indication of a fractured reservoir (Mohamed et al. 2014, Settari 2000). However, after 100 days this effect is not dominant anymore³.

A clear feature in this well was the increased injectivity observed after various shut-ins (e.g. point 3). This is possibly caused by the pressure build-up around the well during injection. This reservoir has the lowest permeability of the three sites investigated (110 mD, see Table 4.2). Due to the injection, the pressure around the well builds up. After a period of shut-in the increased pressure around the well has dissipated and injection is easier when operations are restarted (needs less injection pressure). This effect is more dominant when the permeability is lower.

The injection temperature varied little in this well. Some brief periods of increased temperature occur, which coincide with increased injectivity. This is consistent with the decreased viscosity at higher temperature as discussed in Section 3.1.

³ The result depends very much on the estimate of the reservoir pressure. The reservoir pressure initially used was taken from DoubletCalc. DoubletCalc assumes a linear gradient in the salinity to calculate the reservoir pressure which results in a value of 232.7 bar, which results in a strong correlation between well II and flow rate. In reality the reservoir pressure is higher, according to a welltest the pressure is 240 bar (Report Panterra G1008), with the outcome the relation largely disappears. This is shown in Figure 4.5, where the injectivity is shown for a reservoir pressure of 240 bar.

Figure 4.6 shows that the variability of the injectivity index on a daily scale is in the order of 0.02 m³/hr/bar. On a scale of several months, the injectivity index does not change significantly. It is therefore concluded that the production data do not show evidence of thermal fracturing.

| input | symbol | unit | value |
|----------------------------|----------------|--------------------|-------|
| reservoir depth | - | m | 2249 |
| net reservoir height | - | m | 165 |
| porosity | phie | - | 0.18 |
| permeability | K | mD | 110 |
| salinity | - | kg/kg | 0.165 |
| geothermal gradient | - | °C/m | 0.035 |
| temperature injected water | - | °C | 35 |
| well radius | r _w | inch | 4.25 |
| well distance | D | m | 1243 |
| injection rate | - | m ³ /hr | 240 |

Table 4.2 D1 doublet parameters.

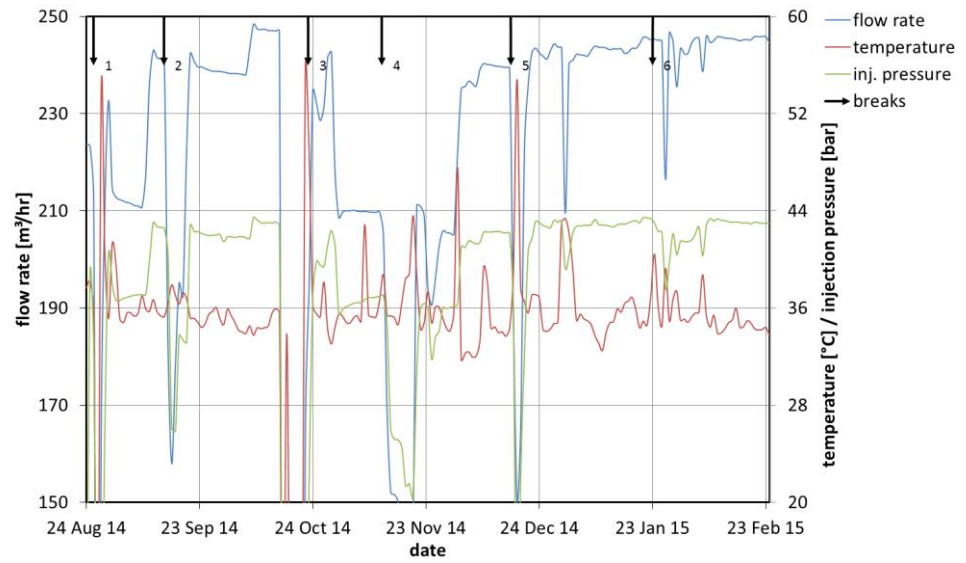


Figure 4.3 Complete production data D1 doublet (daily average) showing flow rate, injection temperature and injection pressure.

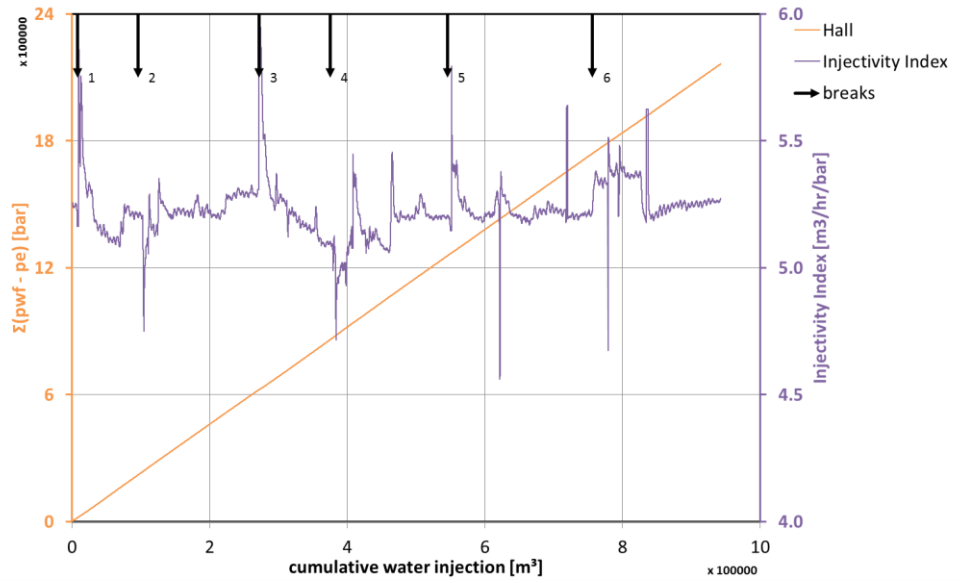


Figure 4.4 Hall plot and injectivity index of the D1 doublet. Arrows indicate marked changes in injectivity index. From start to end, the injectivity index does not show a significant permanent increase that is expected if thermal fracturing would have occurred.

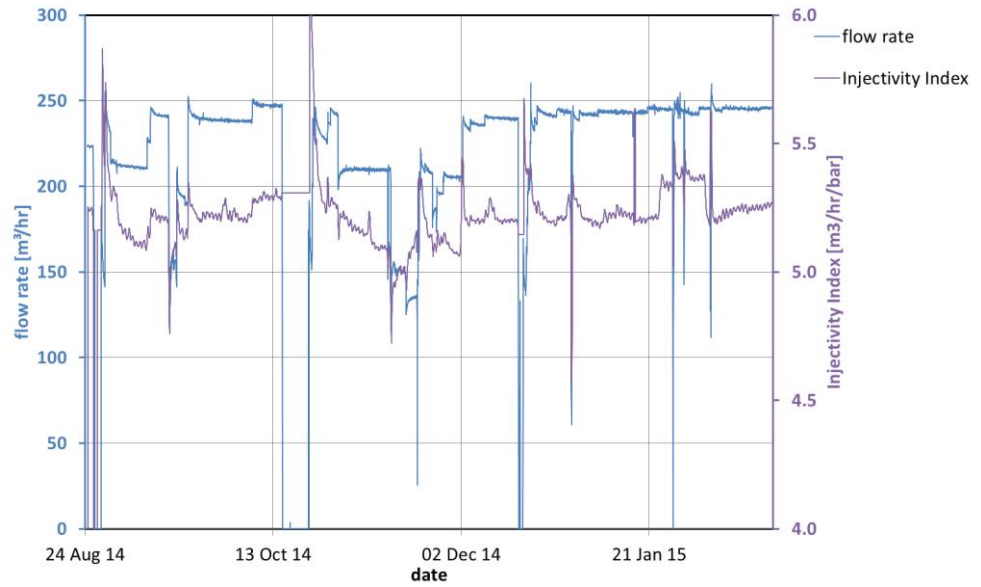


Figure 4.5 Injectivity index and flow rate of the D1 doublet.

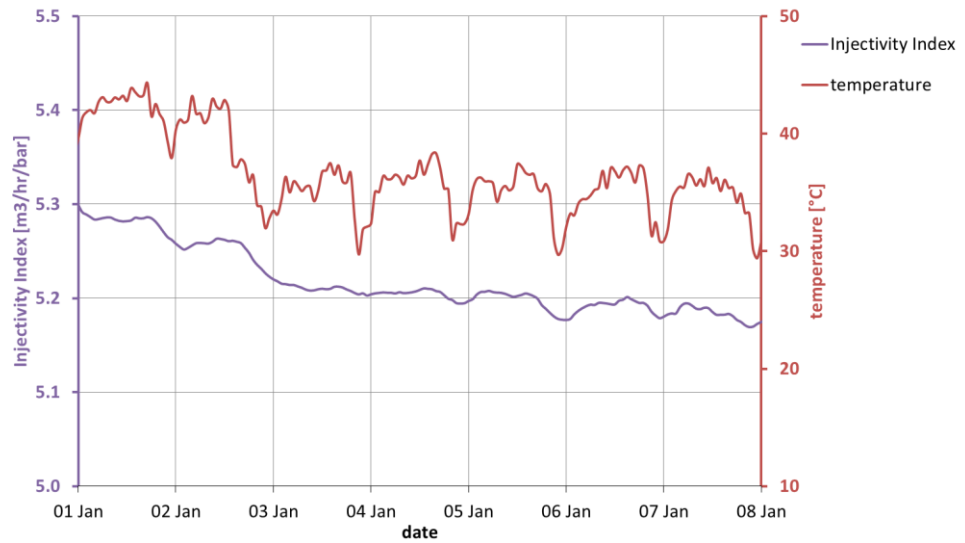


Figure 4.6 D1 doublet production data for one week in January showing the injectivity index and the temperature. The daily temperature cycle is very clear.

| BHP [bar] | salinity [ppm] | BHT [°C] | viscosity [cP] | density [kg/m³] |
|-----------|----------------|----------|----------------|-----------------|
| 280 | 165000 | 34 | 1.09 | 1124 |
| 280 | 165000 | 40 | 0.99 | 1122 |
| % change: | | | -9.2% | -0.2% |

Table 4.3 Effect of bottom hole temperature BHT on the viscosity and density of D1 doublet.

4.2.3 D3 doublet

The D3 doublet was drilled between August 2010 and January 2011. One year of production data was made available covering the year 2014. The properties of the D3 doublet are given in Table 4.4. Figure 4.7 shows the raw production data, averaged per day. The injection temperature remained relatively constant around 35°C. The flow rate varied between 100 and 170 m³/hr and shows several shut-ins.

The production data (Figure 4.7) and the combined Hall and injectivity index plot (Figure 4.8) show few notable features. Most striking is the increase in injectivity at point 6. This coincides with a drop in temperature of around 10°C (from 40°C to 30°C), a high flow rate (180 m³/hr). Based on the analysis in Chapter 2, a decrease in injectivity is expected for a drop in temperature. The expected drop in injectivity due to the temperature change for this particular case is 16% (see Table 4.5). The observed increase of injectivity index from around 3 to 3.8 m³/hr/bar (change of more than 25%) may be an indication of a thermal fracture.

A closer look to at the data around the 25th of November shows that there is a shut-in of the well just before the strong increase of the injectivity index (Figure 4.9). As for D1, there is a tendency for the injectivity index to briefly increase after a shut-in period. The injection temperature drops here to 24°C. This could indicate the initiation of a fracture. A few hours later the injection rate becomes higher and the pressure as well. This could keep the fracture open for a certain period of time and maintain the enhanced injectivity. A subsequent decrease in flow rate to 110 m³/hr

coincides with a gradual decrease in injectivity index from 5.5 to 3.5 m³/hr/bar – this may indicate closing of the fracture again.

However, where the daily cycle in the injectivity for D1 was very small (Figure 4.6) and showed a small increase with increasing temperature, the daily variability in injectivity for the D3 doublet is in the order of 5% (Figure 4.10) and is high for low temperature. When investigated in detail, the daily cycle showed an increasing injectivity for low temperature (Figure 4.10). The time shift that can be seen to exist in this figure between the temperature and the injectivity index can be explained by the first order thermal effects described in Chapter 2: the injectivity index of cold water is less than that of warm water due to effects on density and viscosity. The time shift exists because the effect of the cold water only becomes noticeable when a significant amount of cold water has been injected. The decrease in injectivity index therefore follows the decrease in temperature of the injected water.

In general, the injectivity index remained relatively stable during the analysis period. Therefore it is concluded that during the period for which the production data were analysed it is considered unlikely that thermal fractures were initiated.

| input | symbol | unit | value |
|---|--------|--------------------|-------|
| reservoir depth | - | m | 1951 |
| net reservoir height | - | m | 100 |
| porosity | Φ | - | 0.23 |
| permeability | K | mD | 450 |
| salinity | - | kg/kg | 0.095 |
| geothermal gradient | - | °C/m | 0.031 |
| temperature injected water (bottomhole) | - | °C | 30 |
| well radius | r_w | inch | 4.25 |
| well distance | D | m | 1784 |
| injection rate | - | m ³ /hr | 160 |

Table 4.4 D3 doublet parameters

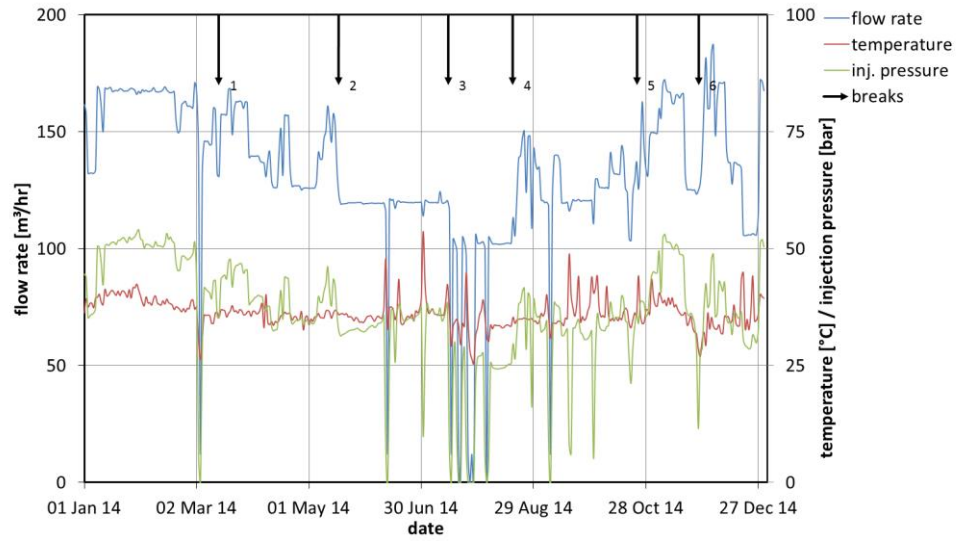


Figure 4.7 Complete production data D3 doublet (daily average) showing flow rate, injection temperature and injection pressure.

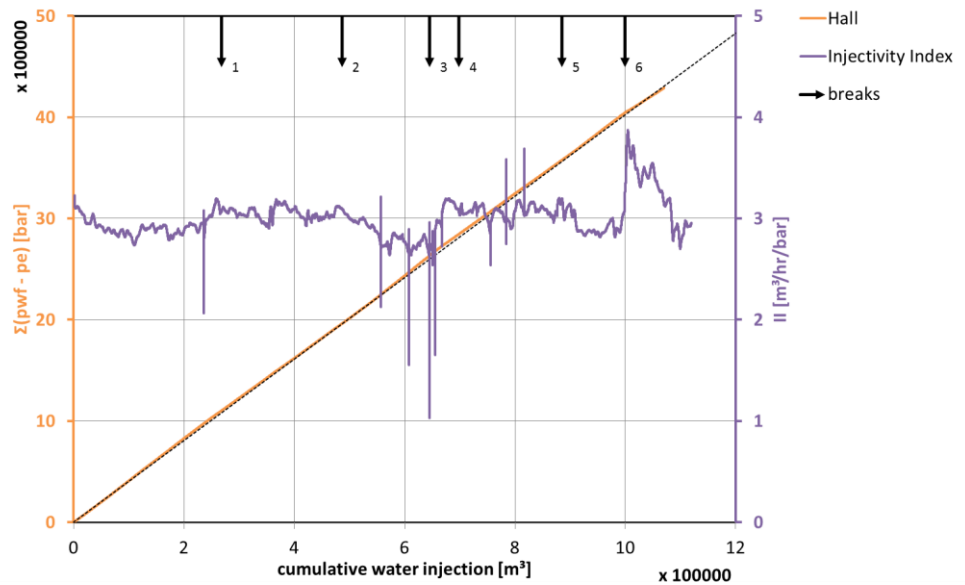


Figure 4.8 Hall plot and injectivity index of the D3 doublet. From start to end, the injectivity index does not show a significant permanent increase that is expected if thermal fracturing would have occurred.

| BHP [bar] | salinity [ppm] | BHT [°C] | viscosity [cP] | density [kg/m³] |
|-----------|----------------|----------|----------------|-----------------|
| 204 | 90000 | 40 | 0.89 | 1076 |
| 204 | 90000 | 30 | 1.03 | 1080 |
| % change: | | | 15.7% | 0.4% |

Table 4.5 Effect of temperature on the viscosity and density of the D3 doublet. Constant injection is assumed.

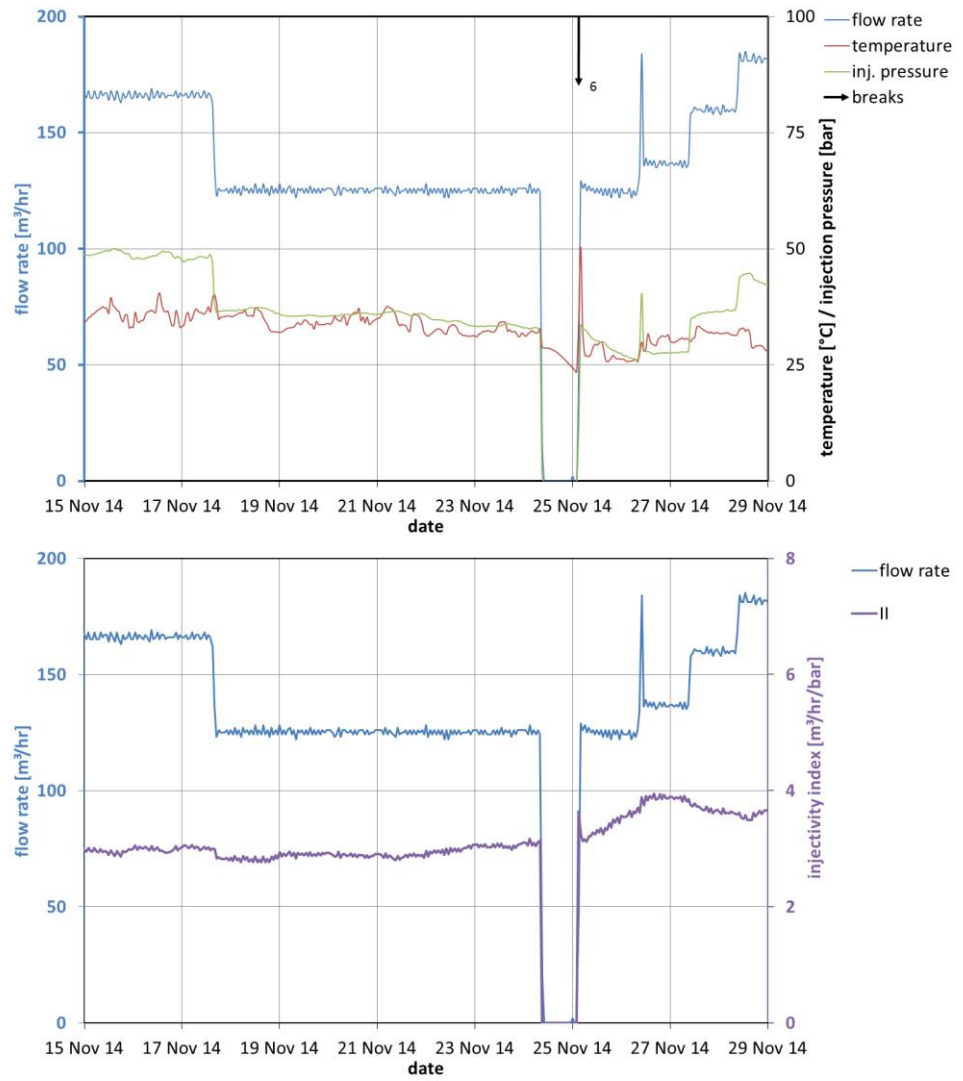


Figure 4.9 D3 doublet production data for two weeks in November showing flow rate, temperature, injection pressure and injectivity index.

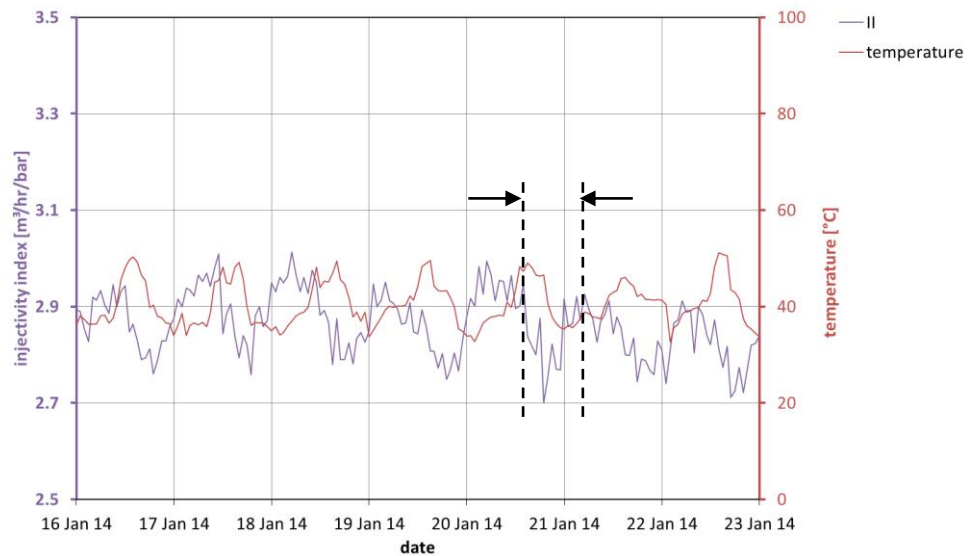


Figure 4.10 D3 doublet production data for a week in January showing Injectivity index and temperature. There is a time shift between the two signals (black arrows).

4.2.4 D4 doublet

The D4 doublet was drilled between October 2006 and July 2007. The properties of the this doublet is given in Table 4.7. Two years of production data were made available covering the period from June 2013 through June 2015. After June 2014 the injection temperature was changed from about 30°C to about 15°C. This is an interesting period for detailed analysis because enhanced cooling could lead to enhanced development of thermal fractures.

Figure 4.11 shows the production data, averaged per day. The injection temperature fluctuates. The flow rate shows several shut-in moments, but is relatively constant between 185 and 190 m³/hr. The injection pressure is remarkably constant with a minimum of 11.8 bar. The daily maximum pressures coincide with the temperature high, as is also visible for the other doublets. The current hypothesis is that the pattern of the pressures should also follow the temperature lows. The flat line appearance of the pressure graphs (also see Figure 0.47) suggests that perhaps a lower cut off was applied to the reported pressures.

From the production data (Figure 4.11) and the combined Hall and injectivity index plot (Figure 4.12) several observations can be made. Points 1 through 3 are probably operational related (shut-ins). A constant injectivity index of around 11.8 m³/hr/bar is observed for the first period from June 2013 to the end November 2013. Within this period a short sharp decrease of injectivity index is observed after a well shut-in (point 1).

From the end of November 2013 until the begin of April 2014 after a shut-in period the Hall slope slightly decreases. The well behaves completely different compared to the previous period. The injectivity index is significantly higher since the shut-in (point 2); at the same flow rate as the previous period a much injection lower pressure was needed. It is assumed that during this shut-in period the well was cleaned or stimulated in another way.

During August 2014, there is a decrease in the injection temperature from around 36°C to 20°C. This decrease in temperature is accompanied by an increase in flow rate at a relatively constant injection pressure. Moreover, Figure 4.12 shows an increase in the injectivity and a decrease in the skin during this period. This trend shows that there is indeed a response in the injectivity to the temperature changes in the D4 doublet. From December 2014 (point 4) the injection temperature is lowered even more to 15°C. Simultaneously the injectivity index is also decreasing due to the viscosity effect (Table 4.6).

Generally, it can be concluded that the injectivity index did not change significantly after the additional cooling started, apart from a number of operations-related changes in the injectivity index. Despite some uncertainty regarding the causes for increased injectivity after shut-in around end of November 2013 (point 2), the production data do not allow to conclude that thermal fracturing occurred.

| BHP [bar] | salinity [ppm] | BHT [°C] | viscosity [cP] | density [kg/m ³] |
|-----------|----------------|----------|----------------|------------------------------|
| 175 | 90000 | 17 | 1.24 | 1069 |
| 175 | 90000 | 30 | 0.99 | 1065 |
| % change: | | | -20% | -0.4% |

Table 4.6 Effect of temperature on the viscosity and density of D4 doublet.

| input | symbol | unit | value |
|----------------------------|--------|--------------------|---------|
| reservoir depth | - | m | 1520 |
| net reservoir height | - | m | 80 |
| porosity | Φ | - | 0.2 |
| permeability | K | mD | 330 |
| salinity | - | kg/kg | 0.09 |
| geothermal gradient | - | °C/m | 0.031 |
| temperature injected water | - | °C | 30 / 15 |
| well radius | r_w | inch | 4.25 |
| well distance | D | m | 1865 |
| injection rate | - | m ³ /hr | 190 |

Table 4.7 D4 doublet parameters.

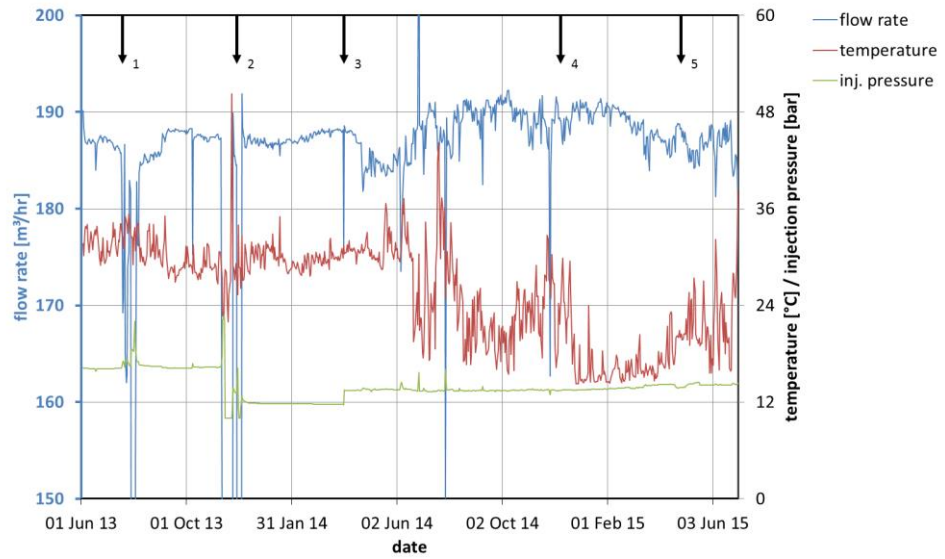


Figure 4.11 Complete production data D4 doublet (daily average), showing flow rate, injection temperature and injection pressure.

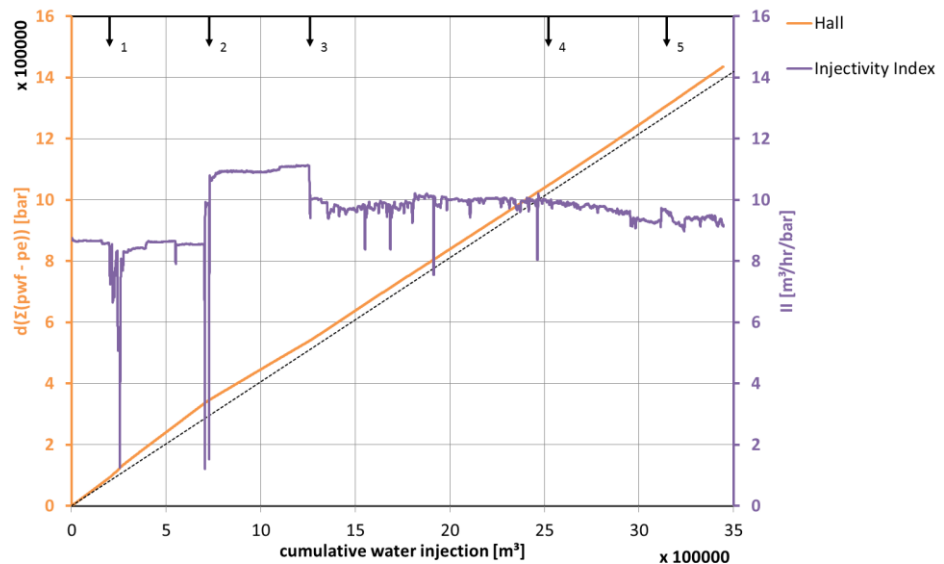


Figure 4.12 Hall plot and injectivity index of the D4 doublet. Arrows indicate marked changes in injectivity index. From start to end, the injectivity index does not show a significant permanent increase that is expected if thermal fracturing would have occurred.

4.3 Expected fracturing and injectivity based on analytical model

The likelihood that thermal fractures develop under current operating conditions was calculated for all doublets using the analytical model described in Chapter 2. A ratio of horizontal to vertical stress of 0.6 was used. Table 4.8 shows the analytical model results for the four doublets D1-D4. For eight more Dutch doublets no production data were available, but the relevant doublet and reservoir parameters required for the analysis could be collected. The first part of the table shows the expected fracture length and resulting skin for an injection temperature of 35°C. The second part shows the same results for an injection temperature of 20°C. The last part shows the results for the currently known injection temperature. The calculated fracture length and skin are reported after 100 and 1000 days.

The model sometimes calculates very high skin values. It should be realised that these skin values are calculated assuming a single fracture of infinite permeability⁴ in the fracture. In reality both the fracture geometry and permeability will be more complex, which results in lower skin values. Accordingly, the calculated skin values should be regarded as upper bounds for actual values.

| doublet number | D1 | D2 | D3 | D4 | D5 | D6 | D7 | D8 | D9 | D10 | D11 | D12 |
|------------------------|------|------|-----|------|-----|------|------|------|------|------|------|------|
| temperature [°C] | 35 | | | | | | | | | | | |
| frac length 100 d [m] | 3 | 0 | 0 | 0 | 0 | 0 | 1 | 0 | 0 | 2 | 0 | 0 |
| frac length 1000 d [m] | 77 | 76 | 0 | 0 | 0 | 0 | 62 | 0 | 2 | 170 | 0 | 0 |
| skin 100 d [-] | -2.3 | -0.1 | 0.0 | 0.0 | 0.0 | 0.0 | -1.3 | 0.0 | 0.0 | -1.7 | 0.0 | 0.0 |
| skin 1000 d [-] | -4.5 | -4.6 | 0.0 | 0.0 | 0.0 | 0.0 | -4.6 | 0.0 | -1.9 | -4.9 | -1.1 | 0.0 |
| temperature [°C] | 20 | | | | | | | | | | | |
| frac length 100 d [m] | 25 | 15 | 0 | 12 | 0 | 0 | 19 | 0 | 21 | 168 | 28 | 80 |
| frac length 1000 d [m] | 187 | 165 | 0 | 243 | 0 | 178 | 188 | 134 | 247 | 1310 | 299 | 592 |
| skin 100 d [-] | -4.0 | -3.7 | 0.0 | -3.0 | 0.0 | 0.0 | -4.0 | 0.0 | -3.9 | -5.3 | -4.1 | -4.4 |
| skin 1000 d [-] | -5.5 | -5.5 | 0.0 | -4.9 | 0.0 | -5.4 | -5.8 | -5.4 | -5.6 | -6.7 | -5.7 | -5.7 |
| temperature [°C] | 35 | 35 | 30 | 15 | 35 | 40 | 40 | 35 | 35 | 35 | 30 | 30 |
| frac length 100 d [m] | 3 | 0 | 0 | 47 | 0 | 0 | 0 | 0 | 0 | 2 | 0 | 0 |
| frac length 1000 d [m] | 77 | 76 | 0 | 384 | 0 | 0 | 16 | 0 | 2 | 170 | 20 | 2 |
| skin 100 d [-] | -2.3 | -0.1 | 0.0 | -4.0 | 0.0 | 0.0 | -0.1 | 0.0 | 0.0 | -1.7 | -0.4 | -0.2 |
| skin 1000 d [-] | -4.5 | -4.6 | 0.0 | -5.4 | 0.0 | 0.0 | -3.5 | 0.0 | -1.9 | -4.9 | -3.6 | -1.9 |

Table 4.8 Expected fracture lengths after 100 and 1000 days, and equivalent skin factors for the 4+8 doublets, and various return temperatures (35, 20 and currently known temperature). Theoretical skins between -1 and -4 in red, below -4 in bold red.

The theoretical calculations for the 35°C, 20°C and actual temperature scenarios in Table 4.8 show that for the D1 doublet, fracturing is expected to occur at the actual injection temperature (35°C, doublet scenario 7). After 100 days, a skin of -2.3 is calculated. This skin is not supported by the observations discussed in section 4.2.2, although the possibility cannot be excluded that the small increase in injectivity observed at the end of the data is associated with the development of a small fracture. The calculations show initially no fracture initiation for the D2 doublet, but similar fracture as for D1 does develop in a later stage (1000 days). The settings for these two doublets are very similar with the exception of the permeability which is slightly higher for D2. It may be that the uncertainty of the permeability is determining the difference in fracture initiation.

For the D3 doublet, no thermal fracturing is expected, which is supported by the steady injectivity index (c.f. Figure 4.8).

⁴ If the permeability of a fracture is very high compared to the permeability of the reservoir, it can be considered to be infinite. This is a reasonable assumption for a thermal fracture, which does not contain proppants. For a fracture containing proppants, the fracture width can be used to estimate the fracture permeability

For the D4 doublet, no fractures are predicted by the model for 35°C, but significant fracturing for 20°C. This effect is not supported by the data (c.f. section 4.2.4).

4.4 Differences between observed and theoretical BHP

Because for neither of the three doublets the production data cover the very start of the production phase (although D1 is rather close), it is possible that thermal fractures developed before the start of the analysed production data. For that reason an additional analysis was performed. If thermal fractures are present, the measured BHP required to inject the water should be significantly lower than the theoretical BHP calculated using the given reservoir parameters.

D1

The same analysis was performed on the D1 data for August 24, 2014. The result was a negative skin factor of -1.1. The recorded data show that a BHP of 279 bar is needed to maintain the recorded flow rate. From a theoretical point of view a pressure of 295 bar would be required. An injection pressure of 279 bar would be achieved by introducing a skin factor of -1.1. Part of the total skin factor is due to the deviation of the well, which can contribute to the skin factor by a value of approximately -1.

D3

On 1-1-2014, the skin factor was estimated based on the D3 data. The recorded data show a BHP of 247 bar, however only 216 bar is expected according to the parameters in Table 4.4. This result means that a skin factor of +12.5 was needed to achieve this BHP of 247 bar. A skin factor > +10 is unrealistic and probably the reservoir thickness or the permeability of the reservoir is lower than anticipated. This view is strengthened since a pumping volume of 293 m³/h was expected (based on Panterra report), but the data shows around 170 m³/h was realised.

D4

The flow rate, THP, injection temperature and injectivity index on June 3rd 2013 were used to calculate the observed BHP. The theoretically required BHP to inject the water was estimated using the analytical model tool, using the input parameters shown in Table 4.7.

The resulting estimated value of the injection BHP is 174 bar, which is in the same order than the 170 bar that was calculated from the recorded THP. Less pressure appears to be required in theory than in practice. A skin factor of +0.7 would be required to match this pressure to the recorded flow rate – given the reservoir and operational parameters. The positive skin factor can be due to scaling or damage around the well. It should be noted that inaccurate assumptions for the other parameters, in particular the reservoir permeability, may offer alternative explanations for the deviation between observed and computed injection BHP.

4.5 Conclusions based on production data

Neither of the three doublets shows the abrupt increase in injectivity which can be related to thermal fracturing. The production data, therefore, provide no evidence of the onset of thermal fractures.

Although variations in the injectivity index are observed, the average value of the injectivity index does not increase over the analysed period, as would be expected when fractures grow.

The largest temperature and stress changes are expected to occur at the start of doublet operations, or just after a significant decrease of the injection temperature. Therefore the effects of thermal fracturing are assumed to be best observed during this period. Although the largest stress changes are in this period, this does not necessarily mean a thermal fracture will develop. It requires thermal stresses large enough to bring the minimum horizontal stress close to or below the BHP during injection.

The BHP and BHT are the most critical observations for detecting fracture effects. These values are not measured directly but they are derived from surface measurements. This derivation introduces additional uncertainty because of effects such as pressure losses due to wellbore friction.

The D1 data show variations in the injectivity index that are most likely related to operations (shut-ins, cleaning). D1 shows a negative skin, both predicted by the fracture model and deduced from the production data. However the fracture model shows a gradual decrease to -4.5, while hardly any change of injectivity (and therefore skin) is observed in the production data. Therefore it is expected that currently no fracturing occurs in this doublet. The analysis could be improved if production data for a longer period would become available.

The D4 data also show variations in the injectivity index that are most likely related to operations (shut-ins, cleaning). The D3 doublet may show signs of fracturing in parts of the analysed data, but predictions by the analytical Koning model do not indicate fracture initiation. Furthermore the expected operational conditions were lower than anticipated resulting in a positive skin, probably the reservoir performance (e.g. permeability, thickness) was lower than earlier expected

It is expected that, for the three analysed doublets, a lowering of the injection temperature will not lead to thermal fracturing and associated increased injectivity.

Table 4.9 summarizes the predicted skin factors as a result of thermal fracturing (section 4.3) and the calculated skin (difference between calculated and observed injectivity index; section 4.4).

| | D1 | D3 | D4 |
|-------------------------------|--------------|-------|------|
| analytical tool fracture skin | -2.3 to -4.5 | 0 | 0 |
| fitted from production data | -1.1 | +12.5 | +0.7 |

Table 4.9 Calculated skin factors for the analysed doublets.

The adapted analytical Koning model predicts the development of thermal fractures and their related skin factor for simplified fracture geometries. The analysed production data do not provide convincing evidence for thermal fracturing. Therefore it was impossible to test the model performance with field data.

5 Scaling potential at reduced injection temperatures

Geochemical simulations were performed with the software PHREEQC to predict the geochemical effects of additional cooling (Wasch 2014). Cooling of the formation water will disturb the chemical equilibrium of the water and as a result dissolved elements can come out of solution and form solid minerals. The performed simulations were part of a theoretical model study to assess the scaling potential for different geothermal doublets in the Netherlands. Here, the geochemical simulations of cooling are presented without the effect of degassing. The simulations predict the formation of mainly ferrihydrite ($\text{Fe}(\text{OH})_3$), barite (BaSO_4) and silica due to the temperature decrease (Figure 5.1). For all minerals precipitation increases with cooling. Not all minerals show a substantial increase between 30°C and additional cooling to 15°C, as shown for ferrihydrite. For silica (and barite in some cases), a significantly increased risk of scaling is predicted with additional cooling.

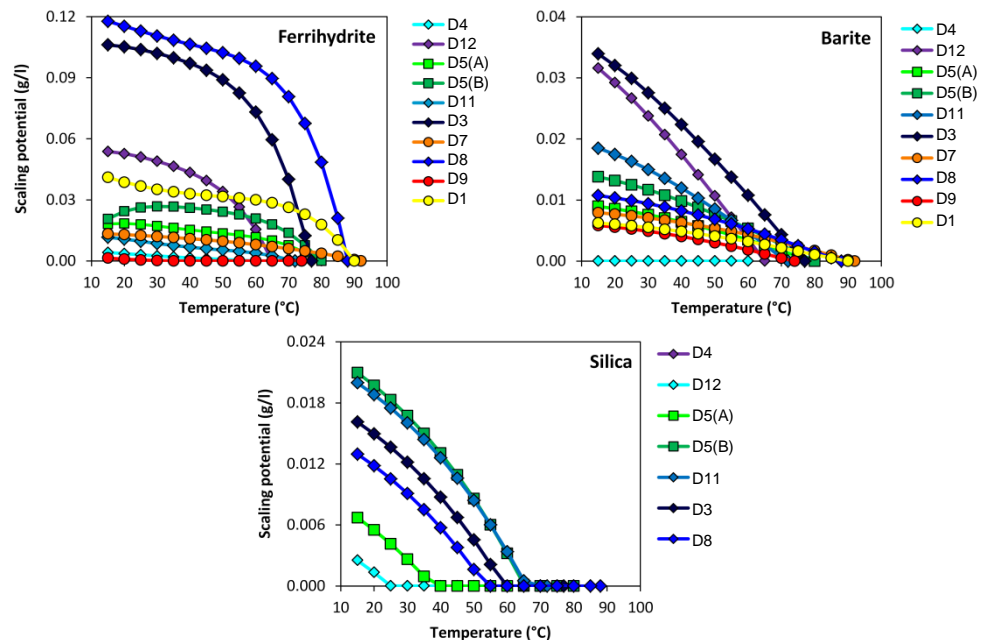


Figure 5.15.4 Scaling potential of ferrihydrite, barite and silica (in g/l) with cooling as predicted for various geothermal doublets of the Netherlands.

Previous simulations were done without taking into account the rate of reactions. If precipitation is delayed due to the reaction rates (kinetics), precipitation may not occur at the location of cooling (heat exchanger) but may occur further along the installation, possibly within the reservoir. This is of interest for potential porosity/permeability clogging and flow reduction in the reservoir. Considering production time scales, the amount of barite precipitation was calculated per hour. Assuming a total volume of 50 m³ in the injection well a total amount of barite scale will be roughly two kg after five years.

The time effect of chemical reactions is illustrated for barite (Figure 5.2). The simulation predicts that precipitation increases steadily in the first four years, after which precipitation slows down until the final amount is reached. Comparing cooling

to 30°C and further cooling to 15°C, the final amount of barite formed is higher (as was shown above). However, it is now shown that in the first period (~ three years) the amount of precipitation is roughly similar for both temperatures. As a first indication, barite precipitation appears to be equal for 30°C and 15°C *at the onset of cooling* (the first three years). This can be explained by the small difference in reaction rates at these temperatures. Hence the amount of mineral formed is roughly similar per unit of time. A third scenario was calculated for which the temperature was raised again after three year. This roughly simulates possible re-heating of the injected fluid within the reservoir. Figure 5.2 shows that re-heating would decrease the final amount of barite formed. 2D transport simulations are required to better assess the actual effect of delayed precipitation within the reservoir (and re-heating) on the characteristics of mineral formation in time and space. It should also be noted that the location of precipitation does not depend solely on kinetics, also nucleation sites and flow dynamics are of influence.

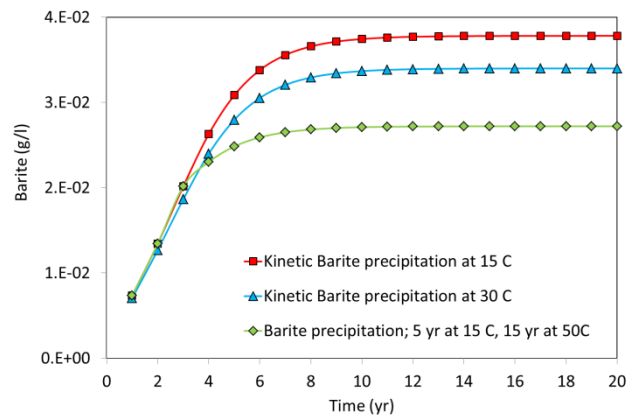


Figure 5.2 Predicted precipitation of barite in time for 20 years. Three scenarios were run for precipitation at 15°C, precipitation at 30°C and precipitation at 15°C for three years and subsequent precipitation at 50°C.

The following conclusions and recommendations were already presented in the report by Wasch (2014):

- Further cooling than done at present is not advisable without a scaling prevention strategy; in fact, simulations indicate that the scaling potential of current operations is already significant.
- It is advisable to take measures to keep CO₂ in solution or re-introduce CO₂ or another pH decreasing agent during degassing, to minimize the precipitation of carbonates. Note, however that such precipitation is not expected to increase when the injection temperature is lowered from 30°C to 15°C.

GPC-IP and KWR conclude accordingly (presentation at TNO-IPC meeting, Delft, February 2015 and concept report, 2015) – although the study by GPC and KWR focused in improved injectivity rather than on the effects of reducing injection temperatures: ‘the main cause for accumulation of minerals on filters and as scaling is due to degassing of CO₂’. Especially carbonates were observed in the investigated wells. Several remediation measures were mentioned, including higher than bubble point production wellhead pressures (keep CO₂ in solution), injection of inhibitors and pressure sustained CO₂ injection. Again, these recommendations are independent of the injection temperature.

Both their and this study agree in their recommendations and further stress the importance of (standardized) analyses of brine, gases and scale samples to better understand and predict the chemical processes in the geothermal (injection) wells.

6 Conclusions and recommendations

6.1 Conclusions

Enhanced cooling of the geothermal brine leads to a more viscous, denser fluid. The combined effect of viscosity and density on the flow in the well is positive but small. The effect of injection of a cold fluid into the reservoir is negative and large. Accordingly, the injection pressure of a cooler fluid is larger than that of a warmer fluid.

Thermal fractures may initiate if a cold fluid is injected in a warm reservoir. This effect will increase the injectivity.

An analytical model for thermal fracture growth was implemented in an Excel environment. The model calculates the dimensions of the thermal fracture given the reservoir and operating conditions of the doublet. According to the model, several Dutch doublets are likely to develop thermal fractures under current operating conditions.

It has not been possible to validate the analytical model for thermal fracture growth against actual production data.

If a doublet, under given reservoir and operation conditions, is likely to develop thermal fractures, the onset will likely be in an early stage of operations.

Convincing evidence for the growth of thermal fractures could not be found in the production data of either of the three analysed doublets.

The recorded production data is noisy and therefore of limited use. Pressure P , temperature T and flow rate Q are recorded at surface level instead of at reservoir level. Therefore P , T and Q at reservoir level must be calculated from the surface data. This introduces additional uncertainty.

Reduction of the injection temperature leads to an increased risk of precipitation of some minerals. Measures should be taken to assess the size of the risk, and prevent the scaling.

6.2 Recommendations

The analytical model for predicting the growth of thermal fractures is sensitive to a number of poorly constrained parameters like rock properties and the magnitude of the minimum horizontal stress. Some of those parameters can be estimated from extended leakoff tests, or from well logs. Collecting these data in a consistent way will be of great value for predicting the formation of thermal fractures.

Validation of the analytical fracture model using actual production data would increase the value of the model.

The analytical fracture model was benchmarked using a reformulated definition of the critical intensity factor. A benchmark using a geomechanical 2D or 3D approach could increase the confidence in the analytical model.

The growth of thermal fractures is best studied using injection data that are a) collected bottom hole and b) available from the onset of production. The former is desirable but unlikely to be feasible for geothermal doublets. The latter, however, could be realised for new doublets.

The ultimate proof of thermal fractures is achieved if they are actually generated by ramping up injection rates to give a bottom hole pressure BHP above the fracturing pressure ($\sigma_{h, \min}$) to constrain local stress conditions. Theoretical models can subsequently be used to determine if thermal fracturing can take place, i.e. is the effect of thermal stresses large enough to overcome the difference between BHP pressure and $\sigma_{h, \min}$? Perhaps such operations need additional license from the State Supervision of the Mines SodM because it involves hydraulic fracturing (though without the use of added chemicals).

The availability of production data for other doublets than the three studied – especially those that are likely to develop thermal fractures according to the analysis using the analytical fracture tool - would increase the insight into the possibility that the process of thermal fracturing is indeed taking place.

According to some operators, the theoretically occurring first order effects of lowered injection temperatures (higher injection pressure required) do not take place in their production data. If this is true, an additional unidentified process is taking place in the well or the reservoir. This has not been observed in the currently analysed production data. It would be valuable to identify this potential process in actual production data.

References

- Batzle M. and Wang Z. (1992). Seismic properties of pore fluids. *Geophysics* v57, p1396-1408.
- Bellarby, J. (2009). Well completion design. *Developments in Petroleum Science* 56. Elsevier, Amsterdam, The Netherlands.
- Benson, S.M., J.S. Daggett, E. Iglesias, V. Arellano and J. Ortiz-Ramirez (1987). Analysis of Thermally Induced Permeability Enhancement in Geothermal Injection Wells. PROCEEDINGS, Twelfth Workshop on Geothermal Reservoir Engineering, Stanford University, Stanford, California, January 20-22, 1987, SGP-TR-IW.
- Bradford, J., Ohren, M., Osborn, W.L., McLennan, J., Moore, J. and R. Podgorney (2014). Thermal Stimulation and Injectivity Testing at Raft River, ID EGS Site. Proceedings, Thirty-Ninth Workshop on Geothermal Reservoir Engineering, Stanford University, Stanford, California, February 24-26, 2014.
- Chang, C., Zoback M.D., and A. Khaksar (2006). Empirical relations between rock strength and physical properties in sedimentary rocks. *Journal of Petroleum Science and Engineering* 51, p223–237.
- Dake, L.P.(1978): Fundamentals of reservoir engineering, Elsevier, *Developments in Petroleum Science* 8
- Detienne, J-L. Creusot, M. Kessler, N. Sahuquet, B. and J-L. Bergerot (1998). Thermally Induced Fractures: A Field-Proven Analytical Model. *SPEREE*, Feb. 1998.
- Economides, M. J., and K. G. Nolte (2000). *Reservoir Stimulation*, 3rd ed. John Wiley and Sons, West Sussex, England
- Fjaer, E., Holt, R.M., Horsrud, P., Raaen, A.M., Risnes, R. (2008) *Petroleum related rock mechanics*. Elsevier 491 p.
- GPC, KWR (2015). Report assessment of injectivity problems In geothermal greenhouse heating wells. Concept, 39p.
- Hoek, E., Kaiser, P.K. and W.F. Bawden (1998). Support of underground excavations in hard rock. Balkema, Rotterdam, 215 pp.
- Koning E. J. L. (1988). Waterflooding under fracturing conditions. Dissertation, Delft Technical University.
- Lin, W., Yamamoto, K., Ito, H., Masago, H., Kawamura, Y. (2008). Estimation of Minimum Principal Stress from an Extended Leak-off Test Onboard the Chikyu Drilling Vessel and Suggestions for Future Test Procedures. *Scientific drilling* 6. doi: 10.2204/iodp.sd.6.06.2008.
- Mijnlieff H.F., Obdam A.N.M., van Wees J.D.A.M., Pluymaekers M.P.D. and Veldkamp J.G. (2014). DoubletCalc 1.4 manual. English version for DoubletCalc 1.4.3. TNO report R11396, 54p.
- Mohamed I.M., Block, G.I., Abou-Saued, O.A., Elkhatatny S.M., Abou-Sayed A.S. (2014), Flow rate dependent skin in water disposal injection well: Case Study, *ARMA* 14-7758
- Perkins T.K. and Gonzalez J.A. (1985). The effect of thermo-elastic stresses on injection well fracturing. *SPE journal* 11332, 11p.
- Santarelli F.J., Havmoller O and Naumann M. (2008). Geomechanical aspects of 15 years water injection on a field complex: an analysis of the past to plan the future. *SPE* 112944, 15p.

- Settari, A., (2000) Note on the calculation on PWRI well injectivity index, www.Advntk.com
- Sheorey, P.R. (1994). A theory of in-situ stress in isotropic and transversely isotropic rock. *Int. J. Rock Mech. Min. Sci. Geomech.* 31 (1), 23-34.
- Slevinsky, B.A. (2002). A model for analysis of injection-well thermal fractures. SPE77568.
- Svendsen, A.P. Wright, M.S. Clifford P.J. and P.J. Berry (1991) Thermally Induced Fracturing of Ula Water Injectors. *SPEREE Nov 1991*, p 384-390.
- Suri, A., M.M. Sharma and E.J. Peters (2011) Estimates of fracture lengths in an injection well by history matching bottomhole pressures and injection profile. *SPEREE Aug. 2011*, p 405-417.
- Panterra G1008m (2014). Analysis of welltest of MDM-GT-03-S2.
- Smith F., Verlinden V., McIntosh K., Tovar J. and Ibukun O. (2013). Thermal fracturing in high and low permeability sandstone reservoirs in the North Sea. First EAGE/SBGf Workshop, Rio de Janeiro - Fractures in Conventional and Unconventional Reservoirs. 14p.
- Tulinius, H., H. Correia, O. Sigurdsson (2000). Stimulating a high enthalpy well by thermal cracking. *Proceedings World Geothermal Congress 2000, Kyushu - Tohoku, Japan, May 28 - June 10, 2000.*
- Veldkamp J.G., Goldberg T.V., Bressers P.M.M.C. and Wilschut F. (2015). Corrosion in Dutch geothermal systems. TNO report R10160, 96p.
- Verruijt, A. (1970): *Theory of Groundwater Flow*. Macmillan, 1970.
- Verweij J.M., Kunakbayeva G., Klomp A.L., Ghazaryan L., Koolmees H.H., Pluymaekers M.P.D. and Hegen, D. (2014). Pressure information system of the onshore and offshore Netherlands. 76th EAGE Conference and Exhibition 2014, 16-19 June 2014, Amsterdam, p1356-1360.
- Verweij J.M., Simmelink H.J., Underschultz J. and Witmans N. (2012). Pressure and fluid dynamic characterisation of the Dutch subsurface. *Netherlands Journal of Geosciences* 91-4, p465-490.
- Wasch L.J. (2014). Geothermal energy – Scaling potential with cooling and CO₂ degassing. TNO report R11661, 19p.
- Zoback, M.D. (2007) *Reservoir Geomechanics*. Cambridge University Press.
- Zoback, M.D., C.A. Barton, M. Brudy, D.A. Castillo, T. Finkbeiner, B.R. Grollmund, D.B. Moos, P. Peska, C.D. Ward, D.J. Wiprut (2003). Determination of stress orientation and magnitude in deep wells. *International Journal of Rock Mechanics and Mining Sciences*. Vol. 40, pp 1049-1076.

A Models for thermal fracturing and injectivity

In this study, an analytical model was developed to estimate onset and growth of thermal fractures in geothermal doublets. The theoretical background and equations behind this model are provided in paragraphs A.1 and A.2. The correctness of the implementation in the Excel tool is described in paragraph A.3. A short benchmark is presented in paragraph A.4.

A.1 Criteria for initiation and propagation of fractures

For a horizontal reservoir that is laterally constrained ($\Delta\varepsilon_{hor} = 0$; $\Delta\sigma_v = 0$ with ε indicating strain) and free to move in vertical direction, the thermal stress difference $\Delta\sigma_{thermal}$ that results from the injection of water colder than its environment is given by (Fjaer et al. 2008):

$$\Delta\sigma_{thermal} = \alpha \cdot \frac{E}{(1-\nu)} \cdot (T_{init_res} - T_{cooling}) \quad \text{eq. 1}$$

where:

α thermal expansion coefficient

E Young's modulus

ν Poisson's ratio

T_{init_res} initial temperature of the reservoir

$T_{cooling}$ new temperature caused by injection of the cold fluid.

When considering a circular horizontal cross section around the injection well, the thermal stress can be resolved into two principal components: a radial and tangential stress.

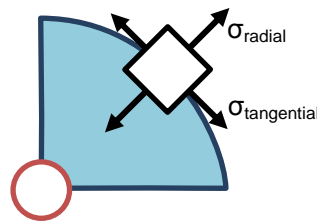


Figure 0.1 Plane view representation of the radial and tangential components of the thermal stress in a horizontal plane. Injection well in red, cold front in blue.

The radial ($\sigma_{th,rad}$) and tangential ($\sigma_{th,tang}$) thermal stress can be evaluated by the following equations:

$$\sigma_{th,rad} = \alpha \cdot \frac{E}{(1-\nu)} \cdot (T_{init_res} - T_{cooling}) \cdot \frac{1}{r^2} \cdot \int_{r_0}^{r_a} r dr \quad \text{eq. 2}$$

$$\sigma_{th,tan} = \alpha \cdot \frac{E}{(1-\nu)} \cdot (T_{init_res} - T_{cooling}) \cdot \frac{1}{r^2} \cdot \left[\int_{r_0}^{r_a} r dr - r^2 \right] \quad \text{eq. 3}$$

where:

- r radial distance of the cooling front from the well
- r_0 wellbore radius
- r_a distance from the injection well.

Thermal fractures are typically initiated by the tensile (tangential) stress. They propagate in the direction of the maximum in situ stress, and they open in the direction of the minimum in situ stress (Figure 3.2- Mode I).

Different failure criteria exist that describe the initiation and propagation of fractures. In this study the criterion of the critical stress intensity factor K_{IC} (also called fracture toughness) is considered to model the initiation of fracture growth. Using this criterion, fractures will grow when the critical stress intensity factor is reached:

$$P_f - \sigma_h \geq \frac{K_{IC}}{\sqrt{\pi L}} \quad \text{eq. 4}$$

where:

- P_f pressure in the fracture, equal to the bottom hole pressure (BHP) (Pa)
- σ_h horizontal stress (Pa)
- L half-length of the fracture (m)
- K_{IC} critical stress intensity factor (typically $10 \text{ bar}\cdot\text{m}^{-1/2}$)

$$\sigma_h = \sigma_{h,min} + \sigma_{poro} - \sigma_{th,tan} \quad \text{eq. 5}$$

$$\sigma_{poro} = 0.5 \cdot \frac{1 - 2\nu}{1 - \nu} \cdot (P_f - P_{in}) = C \cdot (P_f - P_{initial}) \quad \text{eq. 6}$$

where:

- $\sigma_{h,min}$ minimum horizontal stress
- σ_{poro} poro-elastic stress
- $\sigma_{th,tan}$ tangential component of the thermal stress
- C constant (based on Poisson ratio ν)

The criterion for fracture propagation based on the critical stress intensity factor can be compared to a criterion for initiation of tensile (mode I) fracturing based on the minimum in situ stress (eq. 7.). For this criterion, initiation and propagation of a fracture occurs when the pressure inside the fracture exceeds the minimum horizontal stress:

$$P_f \geq \sigma_{h,min} \quad \text{eq. 7}$$

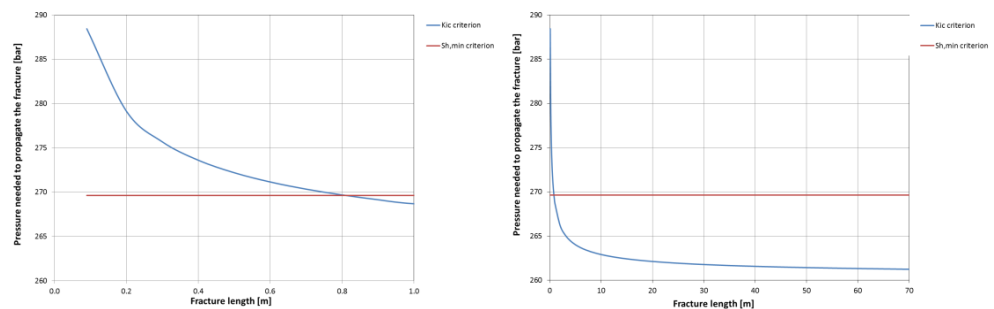


Figure 0.2 Comparison between the 'critical stress intensity factor' and 'minimum in situ stress' failure criteria (left: short distance (0-1m); right: long distance (0-70m)).

The required pressure inside the fracture to propagate the fracture for the stress intensity factor criterion K_{IC} is higher than the pressure required by the minimum in-situ stress criterion at small fracture lengths (Figure 0.2, fracture length < 0.8 m in this example). However, once the fracture starts propagating, the pressure required to continue the propagation rapidly decreases below $\sigma_{h,min}$. The criterion of the stress intensity factor is generally considered the more realistic criterion to model fracture propagation. However, in most practical applications it is assumed that fractures initiate if the minimum horizontal stress is exceeded.

A.2 Analytical model for propagation of thermal fractures

An analytical model based on the dissertation by Koning (1988) 'Waterflooding under fracturing conditions' was developed in Excel. The model calculates the possible development of thermal (mode I) fractures based on the relevant doublet and reservoir parameters. Among the results of the model are the length of the developed fracture, and the equivalent skin factor.

Some small adjustments to the Koning model were made to make it suitable for application to a geothermal doublet. The adjustments are described below.

Assumptions

For the construction of a simple analytical fracture propagation model the following assumptions are made:

- A vertical fracture with a rectangular surface area having height h and half-length L extends laterally from a single well in an infinite reservoir. The reservoir and fracture heights are constant. The shape of the fracture is elliptical (Figure 0.3).
- The fracture has infinite conductivity. Therefore the fluid pressure drop along the fracture can be neglected.
- The total leak-off rate from the fracture into the reservoir equals the constant injection rate from the well into the fracture.
- The fracture propagates sufficiently slow with respect to the velocity of the pressure transients that the fluid leak-off from the fracture into the reservoir can be described as a 2-D pseudo-radial model.

- The shapes of the fronts that separate the cold-flooded and the warm-flooded parts of the reservoir are approximated by ellipses that are confocal with the fracture tips at all times (Figure 0.4).
- The reservoir is homogeneous.
- The displacement is piston-like, i.e. the reservoir is horizontal, laterally constrained ($\Delta\varepsilon_{\text{hor}} = 0$; $\Delta\sigma_v = 0$), and free to move in vertical direction (Figure 0.5).

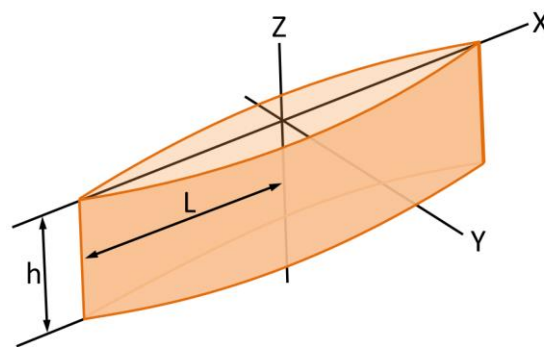


Figure 0.3 Shape of the fracture and naming conventions (from Koning, 1988).

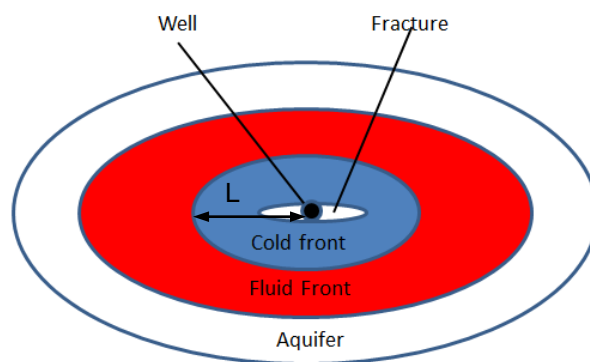


Figure 0.4 Elliptical shape of the cold and fluid front around the injection well (top view).

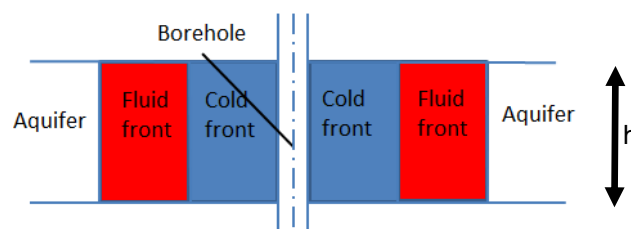


Figure 0.5 Piston like displacement of the fluid fronts (side view).

One of the simplifications seen in literature is the assumption of one-dimensional leak-off in the direction perpendicular to the fracture wall (along the y-axis in Figure 0.3). Since in a geothermal doublet a production well is close to the injection well this assumption is not valid; the influence of the producer on the pressure field and

the flow pattern is such that the 2-dimensional the leak-off should be taken into account. Therefore a two-dimensional leak-off model is used.

Fracture propagation

Continuing from eq. 4, the pressure in the fracture is given by:

$$P_f = P_i + \Delta P_0 \quad \text{eq. 8}$$

where:

P_i injection pressure
 ΔP_0 pressure change in fracture

$$\frac{2\pi h}{q} \Delta P_0 = \frac{1}{\lambda_1} \text{Ln} \left(\frac{a_c + b_c}{L} \right) + \frac{1}{\lambda_2} \text{Ln} \left(\frac{D}{a_c + b_c} \right) \quad \text{eq. 9}$$

where:

λ_1 mobility of the cold front ($\text{m}^2/\text{Pa s}$)
 λ_2 mobility of the warm front ($\text{m}^2/\text{Pa s}$)
 a_c, b_c major and minor axis of the cold front (m)
 a_F, b_F major and minor axis of the warm front (m)
 D distance between the wells (m)

Koning (1988) uses a one well approach. A time dependent exterior radius is used ($R_e(t)$) instead of the distance D used above in eq. 9. The time-dependent exterior radius is the distance from the well affected by the change in pressure due to injection, which is dynamic for a one well system. In a doublet, a steady state pressure profile between the injector and producer wells is established after a period of time. Therefore the exterior radius is replaced by the distance between the two wells (D) of the geothermal doublet. For completeness the definition of the time dependent exterior radius $R_e(t)$ is given below

$$R_e(t) = 1.5\sqrt{\eta t} \quad \text{eq. 10}$$

where:

η hydraulic diffusivity $\eta = k/\phi\mu c_t$
 t time

In order to evaluate eq. 9, the major and minor axis of the cold front have to be calculated according to Perkins and Gonzalez (1985) (see Appendix D).

The minimum horizontal stress is given by the sum of the initial (far field) horizontal stress and the poro- and thermo-elastic stress changes due to the cold water injection:

$$S_h = S_{hi} + \Delta\sigma_{yP} + \Delta\sigma_{yT} \quad \text{eq. 11}$$

where:

S_{hi} initial minimum horizontal stress
 $\Delta\sigma_{yP}$ poro-elastic stress change

$\Delta\sigma_{yT}$ thermo-elastic stress change

Poro-elastic stress changes

The poro-elastic stress changes at the fracture face can be calculated from the following expressions (Koning 1988):

$$\Delta\sigma_{yPD} = \frac{1}{2} \Delta P_D(0) - R + \Delta S_{HpD} \quad \text{eq. 12}$$

where:

$\Delta P_D(0)$ stress change due to injection at the fracture tip (given by eq. 9)

R correction term due to elliptical coordinates

ΔS_{HpD} apparent change in far field stress

The subscript D denotes dimensionless stress which is defined as:

$$\Delta\sigma_{yPD} = \frac{\Delta\sigma_{yP} 2\pi kh}{A_p q\mu} \quad \text{eq. 13}$$

where:

A_p poro-elastic constant, which can be expressed as $\left(\frac{1-2\vartheta}{1-\vartheta}\right) \left(1 - \frac{c_g}{c_m}\right)$

ϑ Poisson ratio

c_g compressibility of the grains

c_m compressibility of the bulk matrix

The correction term R is given by:

$$R = \frac{1}{2} \frac{e_c}{(1+e_c)} + \frac{1}{2} \frac{\lambda_1}{\lambda_2} \left(\frac{1}{2} - \frac{e_c}{(1+e_c)} \right) \quad \text{eq. 14}$$

where:

$$e_c = \frac{b_c}{a_c}$$

λ_1 mobility of the cold front

λ_2 mobility of the warm front

The apparent far field stress ΔS_{HpD} is given by:

$$\Delta S_{HpD} = \frac{1}{2} \Delta P_D(0) - \frac{1}{4} Q \left(\frac{L}{2} \right) + \frac{1}{4} \left(1 - \frac{\lambda_1}{\lambda_2} \right) Q \left(\frac{a_c + b_c}{2} \right) + \frac{1}{4} \frac{\lambda_1}{\lambda_2} Q(D) \quad \text{eq. 15}$$

After some time the pressure penetration radius will be in the order of the reservoir height and plane strain conditions no longer apply. This means that the fracture toughness ceases to be constant. This deviation can be accounted for by changing the boundary condition that at infinity the horizontal stresses become equal to an apparent change in the far field stress.

Thermal elastic stress changes

The thermal elastic stress change is given by an expression found by Perkins and Gonzalez (1985):

$$\Delta\sigma_{yTD} = \frac{e_c}{(1 + e_c)} + \frac{(1 + e_c)^{-1}}{1 + 0.5[1.45(h_D)^{0.9} + 0.35(h_D)^2][1 + (1 + e_c)]^{0.774}} \quad \text{eq. 16}$$

where:

$$h_D = h/2b_c$$

The subscript D denotes the dimensionless number. The conversion to real numbers is done by:

$$\Delta\sigma_{yT} = \Delta\sigma_{yTD} A_t \Delta T \quad \text{eq. 17}$$

where:

A_t thermo-elastic constant (Pa/°C)

ΔT temperature difference between reservoir and injected fluid (°C)

Numerical calculation of fracture propagation

At every time step t the pressure in the fracture (P_f) and the in situ horizontal stress can be evaluated (S_h) by eq. 8 and eq. 11. Substitution of P_f and S_h into eq. 6 will lead to a nonlinear algebraic equation for the fracture half-length for every time step t .

This equation is solved by a Newton-Raphson iteration method implemented in Excel using Visual Basic. The starting value of the fracture length was set to be the borehole radius (0.09 m). Convergence is reached when the following criterion is satisfied:

$$Abs\{2 * (L_i - L_{i-1}) / (L_i + L_{i-1})\} < 0.001 \quad \text{eq. 18}$$

where:

L_i fracture length at iteration i

L_{i-1} fracture length at iteration $i-1$

Well skin factor

The analytical expression which returns the required pressure difference to sustain a given flow rate in a doublet system in a homogeneous aquifer is given by Verruijt (1970) and Dake (1978):

$$\Delta p = P_{BHP} - P_{res} = q \frac{\mu}{2\pi k h} \left(\ln\left(\frac{D}{r_w}\right) + s \right) \quad \text{eq. 19}$$

where:

Q flow rate

ΔP pressure difference between BHP and reservoir pressure

P_{BHP} bottom hole pressure (BHP)

P_{res} reservoir pressure

μ viscosity

r_w well bore radius

| | |
|---|----------------------------|
| s | skin factor |
| k | permeability |
| h | thickness |
| D | distance between the wells |

The efficiency with which a wells is operating is defined in terms of productivity (PI) or injectivity index (II) (Dake 1978):

$$II = \frac{q}{P_{BHP} - P_{res}} = 1 / \left(\frac{\mu}{2\pi k h} \left(\ln \left(\frac{D}{r_w} \right) \right) \right) \quad \text{eq. 20}$$

The larger the injectivity index, the larger the injection rate q for a given pressure difference. This means that a lower pressure difference, hence less energy is needed to inject (or produce) the same injection rate. In reality additional pressure loss (due to formation damage), or enhancement due to potentially generated thermal fractures has to be taken into account for the estimation of the injectivity index:

$$II = \frac{q}{P_{BHP} - P_{res} - \Delta P_{skin}} = 1 / \left(\frac{\mu}{2\pi k h} \left(\ln \left(\frac{D}{r_w} \right) + s \right) \right) \quad \text{eq. 21}$$

Based on the fracture propagation theory, the BHP of a geothermal doublet with thermal fractures and related injectivity (injectivity index_{fracture}) can be estimated. Furthermore the expected BHP can be estimated using eq. 20 and finally the ideal injectivity (injectivity index_{ideal}). In case there is an thermal fracture then injectivity index_{fracture} > injectivity index_{ideal}. In reality both definitions of injectivity have the same value. The reduced pressure drop due to thermal fracturing can be accounted for by using the skin factor as shown in eq. 21. The equivalent skin factor for each time step t is then calculated using a 'goal seek' type of optimization in Excel.

A.3 Model implementation validation

Koning (1988) described the analytical model for oil reservoirs. The assumptions used by Koning were translated for application to a geothermal injection well. The Excel implementation of the model was compared to the results published by Koning, using the same values as described in the dissertation.

The input parameters used are given in Table A.1. As can be observed in Figure 0.6 (Excel implementation) and Figure 0.7 (Koning 1988), the pressure profile and the propagation of the fracture show similar behaviour. There is a slight difference in pressure behaviour, because in the Koning dissertation an infinite reservoir is modelled with an oil phase attached to it. Since the viscosity of oil is higher, a higher injection pressure is expected. The largely similar behaviour however shows that the model was correctly implemented.

| Input | value | unit |
|----------------------------------|----------|----------------------|
| reservoir depth | 4500 | m |
| reservoir height | 120 | m |
| porosity | 0.24 | - |
| permeability | 250 | mD |
| temperature difference | 70 | °C |
| radius of well | 0.09 | m |
| water injection rate | 8000 | m ³ /d |
| simulation duration | 730 | days |
| thermal elastic constant | 1 | bar/C |
| poro elastic constant | 5.00E-01 | 1/bar |
| heat capacity of formation | 2100 | Kj/m ³ .K |
| critical stress intensity factor | 10 | bar m ^{1/2} |
| initial pressure | 450 | bar |
| Initial horizontal stress | 500 | bar |
| viscosity water (cold) | 7.80E-04 | Pa.S |
| viscosity water (hot) | 2.67E-04 | Pa.S |

Table A.1 Input parameters used in the dissertation of Koning (1988).

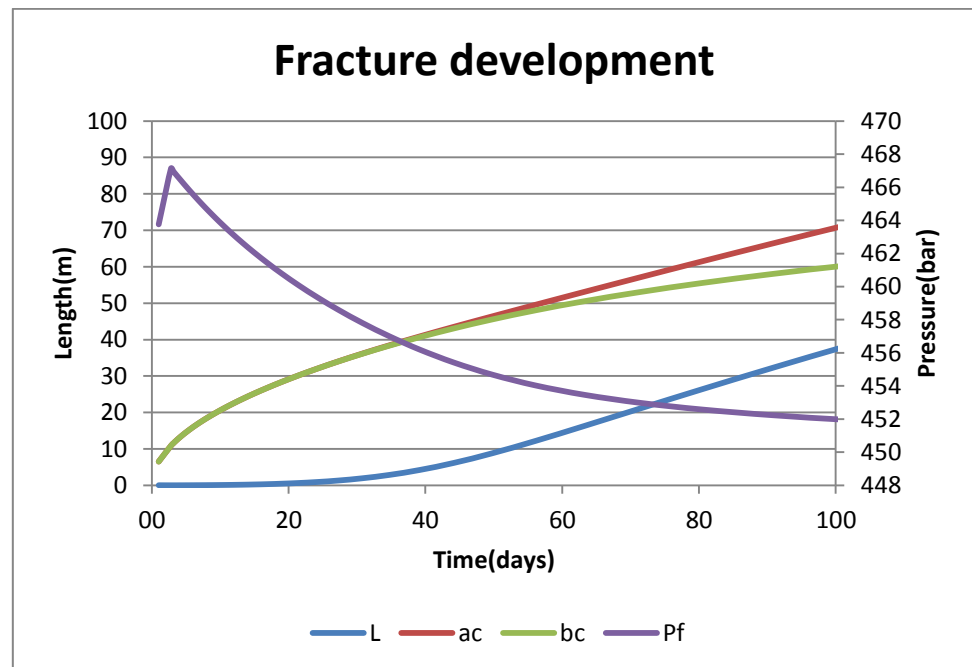


Figure 0.6 Propagation of the fracture (L), long axis of the heat front ellipsoid (ac), short axis of the heat front ellipsoid (bc) and pressure in the fracture (Pf).

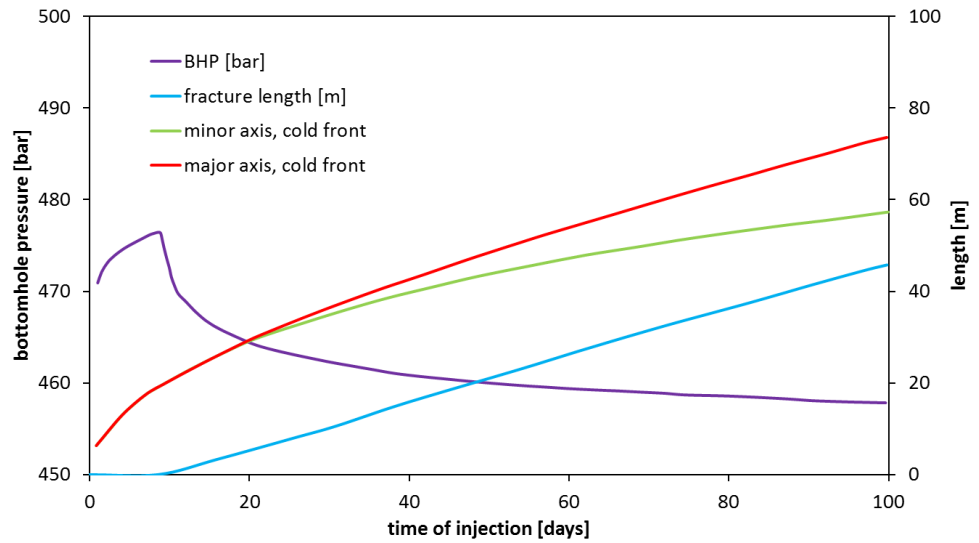


Figure 0.7 Simulation output after Koning

A.4 Model benchmark

In order to validate the analytical model tool, the criterion based on the critical intensity factor has been reformulated. In the new formulation the only parameters required are the temperature of the fluid and the length of the fracture to be generated. The output is the pressure inside the fracture that it is needed to generate such a fracture. This is considered to be a valuable way to represent the criterion: the injection pressure and the temperature of the fluid are the two parameters that the operator can actually control. The critical pressure required to propagate the initial fracture is derived from eq. 22 (K_{IC} is given as input parameter):

$$P_{fC} = \frac{K_{IC}}{\sqrt{\pi L}} + \sigma_h \quad \text{eq. 22}$$

Or, after substitution,

$$P_{fC} - \sigma_{h,min} - CP_f + CP_{in} + \sigma_{th,tan} = \frac{K_{IC}}{\sqrt{\pi L}} \quad \text{eq. 23}$$

But $P_{fC} = P_{in} + \Delta P_C$, therefore

$$P_{in} + \Delta P_C - \sigma_{h,min} - CP_f + CP_{in} + \sigma_{thermal} = \frac{K_{IC}}{\sqrt{\pi L}} \quad \text{eq. 24}$$

After some mathematical steps it is possible to derive ΔP_C (and then P_{fC}) as function of the temperature of the fluid and the length of the fracture (L) that the user wants to generate:

$$\Delta P_c = \frac{1}{1 - \nu} \left(\frac{K_{IC}}{\sqrt{\pi L}} + \sigma_{h,min} - P_{in} - \sigma_{th,tan} \right) = \text{eq. 25}$$

$$= 2 (1 - \nu) \left(\frac{K_{IC}}{\sqrt{\pi L}} + \sigma_{h,min} - P_{in} - \sigma_{th,tan} \right)$$

$\sigma_{h,min}$ is calculated as a fraction of the vertical stress, which is defined by density and depth (Figure 0.9). Assuming Young's modulus to be about 10-20 GPa (which can be considered as a representative value for sandstone, see Figure 0.8), it is possible to predict Figure 0.9 predicts $\sigma_{h,min} / \sigma_v$ to be around 0.5 for depths between two and three kilometers. This prediction is based on a model on elastic static thermal stresses of the earth (Sheorey 1994). The equation used to estimate the ratio between the horizontal and vertical stresses (k) is:

$$k = 0.25 + 7E_h \left(0.001 + \frac{1}{z} \right) \text{eq. 24}$$

Where z is the depth below the surface and E_h (GPa) the average deformation modulus of the upper part of the earth's crust measured in horizontal direction, or simplified the Young's modulus.

An approximation of the ratio between horizontal and vertical stress for various on- and offshore structural elements in the Netherlands is given by Verweij et al. (2012). Figure 0.10, for the West Netherlands Basin, suggests a value between 0.55 and 0.60 for $\sigma_{h,min} / \sigma_v$. Appendix F provides some more details on more reliable determination of (local values for) $\sigma_{h,min}$ using well tests.

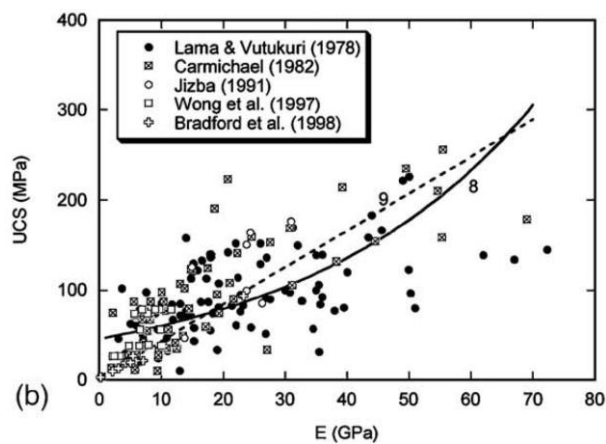


Figure 0.8 Dependence of the uniaxial compressive strength (UCS) of 260 sandstones on Young's modulus E (Chang, Zoback and Khaksar 2006).

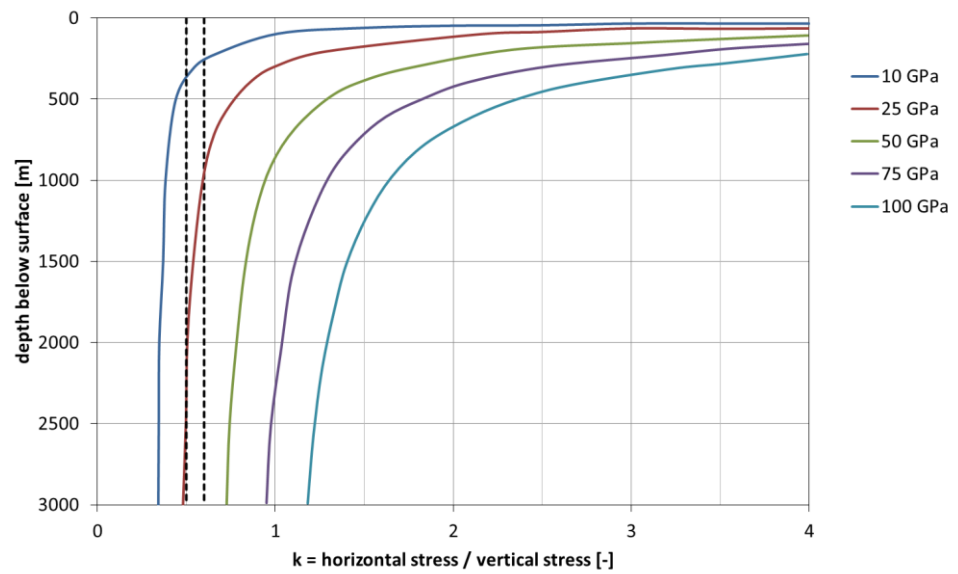


Figure 0.9 Ratio between horizontal and vertical stress as function of depth for various values of Young's modulus (after Hoek, 1998). The dashed lines $k=0.5$ and $k=0.6$ correspond to those in Figure 0.10.

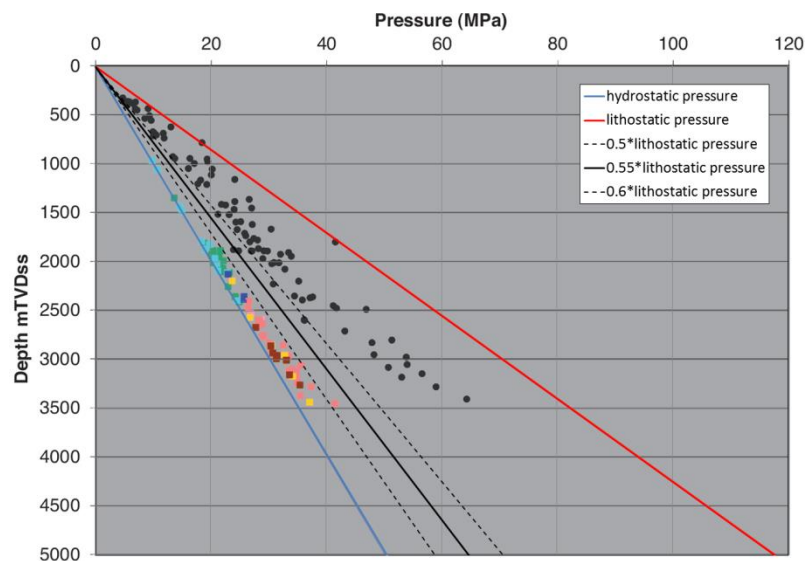
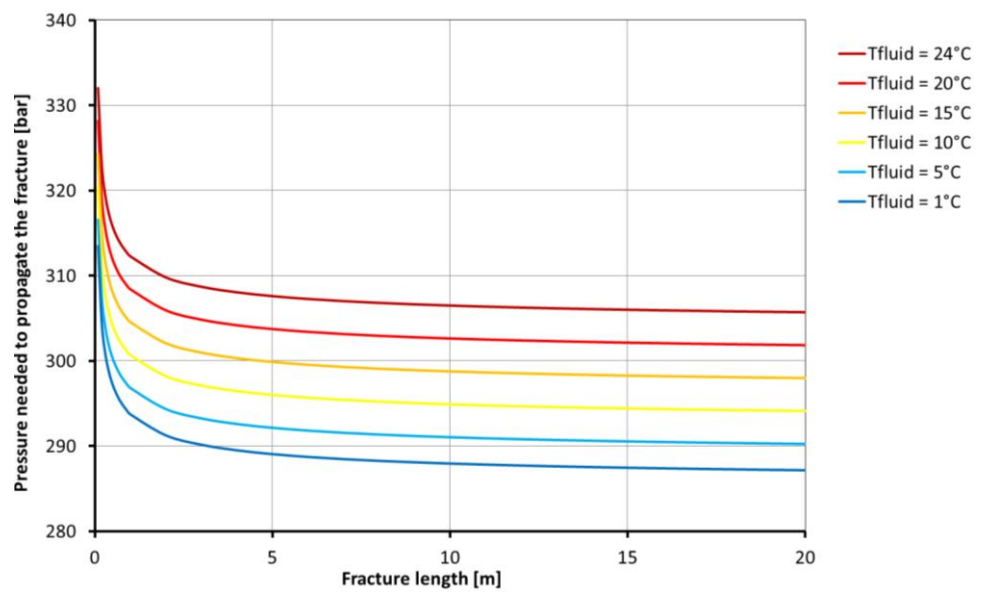


Figure 0.10 Fluid pressure (coloured dots) and leakoff pressure (black dots) for the main lithostratigraphic units in the West Netherlands Basin (Verweij et al. 2012). The lower bound of the leak-off pressures is indicative of the horizontal minimal stress.

| parameter | value | unit |
|---|-------|----------------------|
| K_{IC} (critical stress intensity factor) | 10 | bar.m ^{1/2} |
| α (Verweij factor) | 0.6 | - |
| depth | 2330 | m |
| density rock | 2300 | kg/m ³ |
| $L_{initial}$ | 0.09 | M |
| E (Young's modulus) | 13.8 | GPa |
| ν (Poisson ratio) | 0.25 | - |
| T_{fluid} | 25 | °C |
| T_{rock} | 96.8 | °C |
| vertical stress | 526.4 | bar |
| horizontal stress | 315.8 | bar |
| density fluid | 1000 | kg/m ³ |
| initial pressure | 229 | bar |

Table A.2 Rock and fluid properties used for the benchmark.

Figure 0.11 Injection pressure required to propagate the initial 9 cm long fracture for different fluid temperatures (coefficient of thermal expansion = $5.6 \cdot 10^{-6}$ [1/C]).

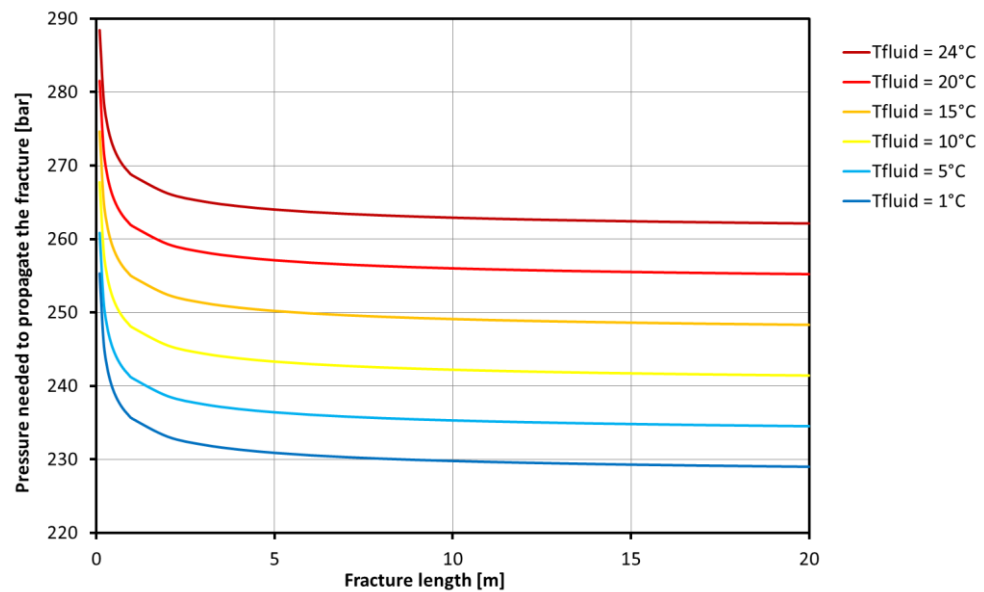


Figure 0.12 Injection pressure required to propagate the initial 9 cm long fracture for different fluid temperatures (coefficient of thermal expansion = $10 \cdot 10^{-6}$ [1/C]).

Figure 0.11 and Figure 0.12 show the results obtained by solving the equation for different fluid temperatures and for two different coefficients of thermal expansion. They also show that the *initiation* of the fracture requires considerably more pressure than the *continuation*. When the fracture reaches a length of approximately 20 meter, the pressure required to continue propagating the fracture remains almost constant because the term $\frac{K_{IC}}{\sqrt{\pi L}}$ (eq. 25) becomes very small (1.2 bar for $L = 20$ m), and the term $\sigma_{h,min} - P_{in} - \sigma_{th,tan}$ remains approximately constant.

Figure 0.13 especially illustrates the importance of choosing the coefficient of thermal expansion properly. Depending on the choice of this coefficient, the pressure that is required to propagate the initial fracture can differ up to 55 bar.

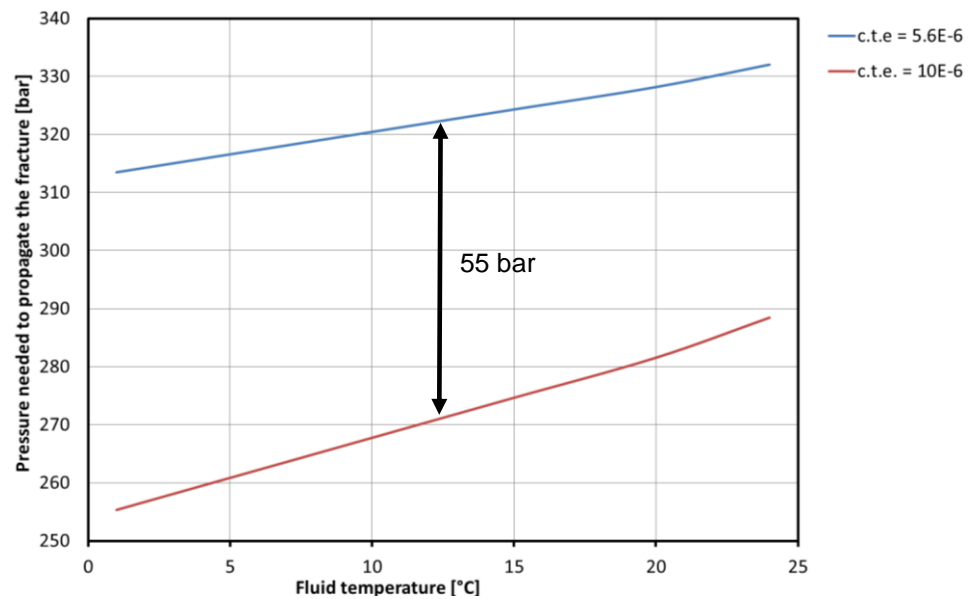


Figure 0.13 Pressure required to propagate the initial fracture as function of the fluid temperature, for two values of the coefficient of thermal expansion (c.f. Figure 0.11, Figure 0.12).

Comparing the thermal and poro-elastic stresses (Figure 0.14, Figure 0.15) it is possible to notice substantial differences between the formulation of the analytical model and the formulation described in this section (equation 25).

These differences are due to the different ways that the geometry of the fracture is taken into account. In the formulation described in this section a 1D geometry of the fracture is modelled or in other words only the length. In contrast in the analytical model is described according to the equations of Koning, a full 3D (and then more accurate) geometry of the fracture is considered (length, width and height).

The differences in pressure between of the two different approaches are given in Figure 0.14 and Figure 0.15 is due to the different geometry of the fracture used in both models. The difference of 10 bars is an acceptable difference, because measurements of the poro-elastic stress within one specific unit is varying with 10 bar and more (see Figure 0.10).

The same geometrical differences in the approach of the fracture play a role in Figure 0.16. Again, a difference of up to 10 bars is acceptable. The fracture pressures calculated by the analytical tool are probably more realistic due to the 3D approach.

Taking into account the differences in the formulations, the mechanical behaviour of fracture during propagation modelled with the analytical tool has been verified.

To conclude, it is important to remark the importance of considering all the factors that have a role in the fracture initiation and propagation: the increase of the pore pressure in the reservoir and in the fracture and the raise of the thermal stress induced by the temperature gradient. Figure 0.17 demonstrates that if thermal

stress is not taken into account (HM model) the pressure that is needed to propagate the fracture is overestimated. If the poro-elastic stress changes (TM model) are not considered, the pressure needed inside the fracture to propagate would be underestimated. To properly described the mechanical behaviour, a reliable measure of the mechanical properties (Young's modulus, Poisson's ratio and coefficient of thermal expansion) and of the minimum in situ stress (via a leak-off test) is crucial.

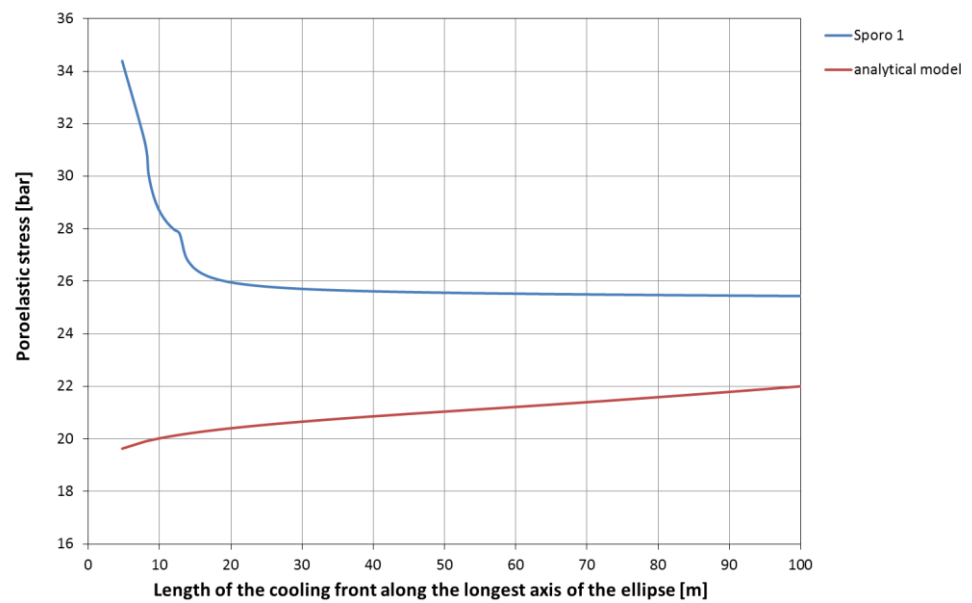


Figure 0.14 Poro-elastic stress calculated using the analytical model and minimum in situ stress model.

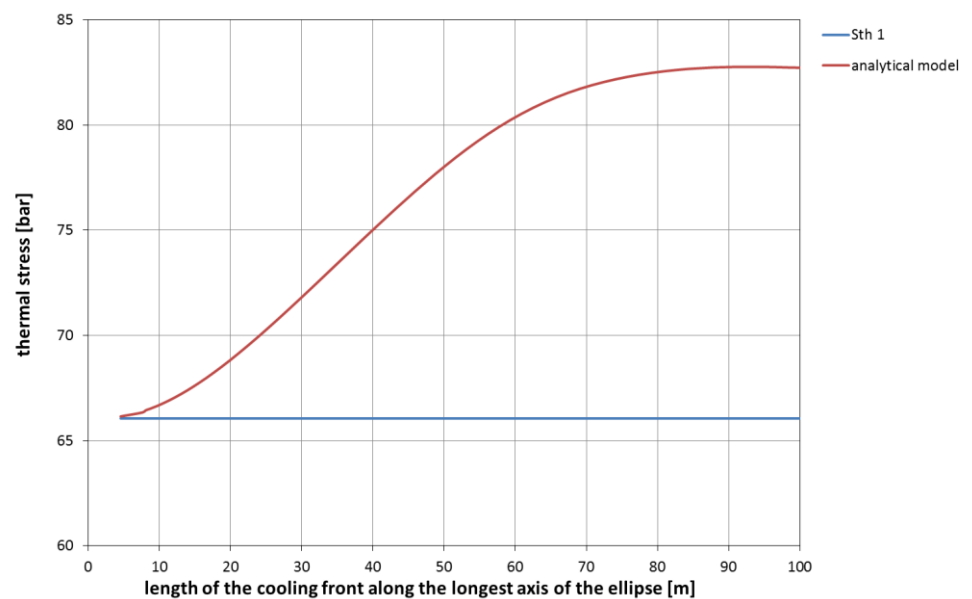


Figure 0.15 Thermal stress calculated using the analytical model eq. 3.

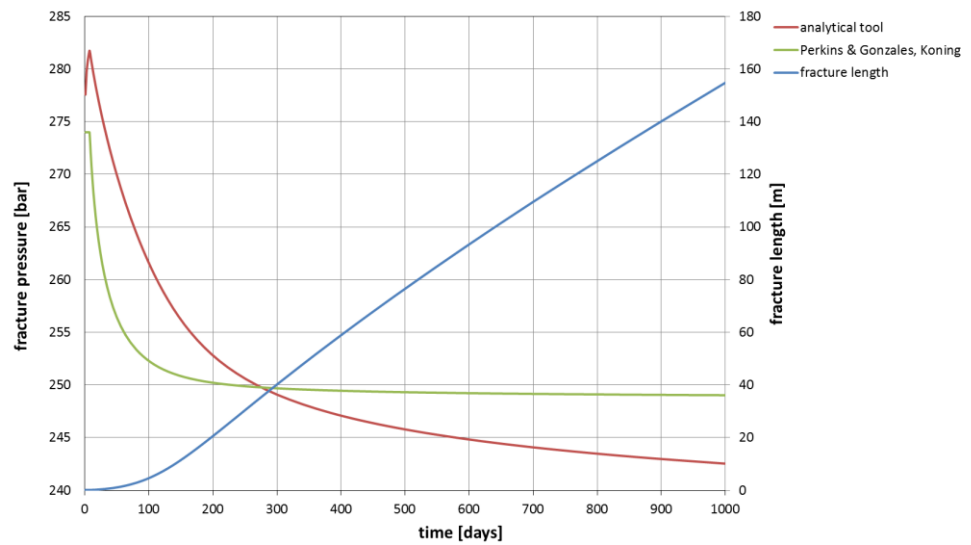


Figure 0.16 Pressure required to propagate the initial fracture for the two models. The right hand vertical axis represents the length of the fracture.

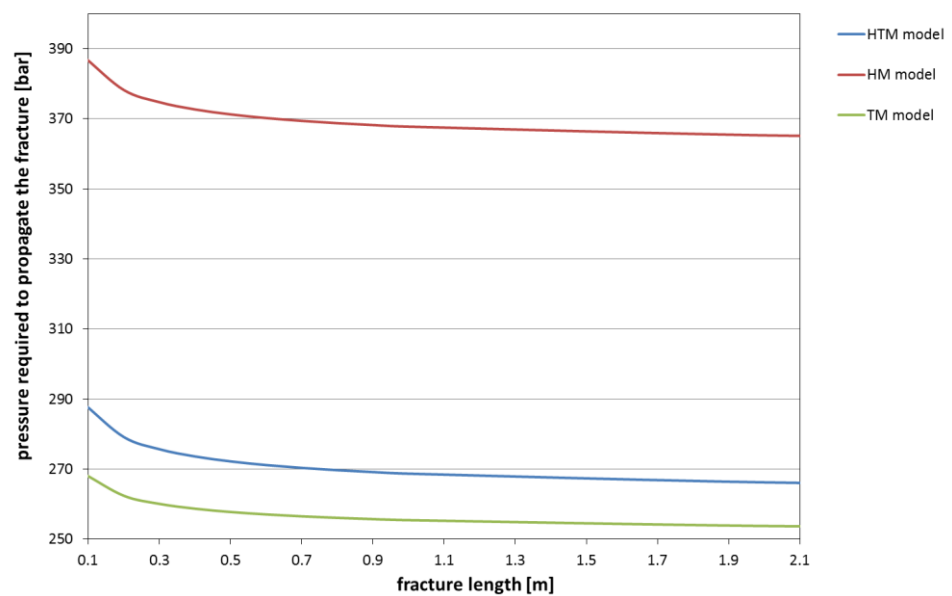


Figure 0.17 Comparison between different hydro-mechanical (HM), thermo-mechanical (TM) and hydro-thermo-mechanical (HTM) models

A.5 Sensitivity of the analytical model to input parameters

The analytical tool requires various reservoir and doublet parameters to be entered prior to execution (green cells in the tools Input sheet). Most are calculated and/or estimated during or after drilling as they are required to run DoubletCalc. Hence, they are considered to be relatively well known. Other parameters however are rock properties that are less well documented or extremely variable, such as Young's modulus (Figure 0.8), Poisson ratio, the thermal and poro-elastic constants, heat capacity, and others (grey cells). The analytical tool suggests values for those

parameters, obtained from Koning (1988), Economides (2000) and Santarelli (2008), as well as ECLIPSE300 standard values. This does not mean that those values are necessarily optimal for all installations.

In order to obtain an idea of the sensitivity of the various input parameters, various runs of the tool were made for a specific hypothetical doublet, each time varying one of the input parameters specified in Table A.3 by 10%. The fracture length for this doublet as predicted by the analytical tool is 29.3 meters after 1000 days for the base case parameters in Table A.3. Figure 0.18 shows the results of the analysis. It becomes apparent that, *for this installation and reservoir setting*, a difference of plus or minus 10% does not influence the length of the fracture *for most of the parameters* – it remains at 29.3 meters. Not surprisingly, fracture dimensions are most sensitive to the geothermal gradient and the temperature of the injected water (which together determine the thermal stress), and the pressure gradient (which determines the minimum horizontal stress). Also the reservoir depth and thickness and the thermal elastic constant play a role. The fact that a 10% difference of various parameters does not change the resulting fracture dimension for this case, does not imply that the formation of a fracture is always insensitive to those parameters – it may just be the case that, for this scenario, the parameter is not critical.

| parameter | unit | value |
|-----------------------|-------------------|-------|
| reservoir depth | m | 2000 |
| reservoir height | m | 100 |
| porosity | % | 0.2 |
| permeability | mD | 250 |
| salinity | kg/kg | 0.1 |
| temperature gradient | °C/km | 0.031 |
| Injection temperature | °C | 30 |
| well radius | m | 0.100 |
| well distance | m | 1500 |
| injection rate | m ³ /d | 4800 |

Table A.3 Reservoir and doublet parameters used for the sensitivity analysis (Figure 0.18).

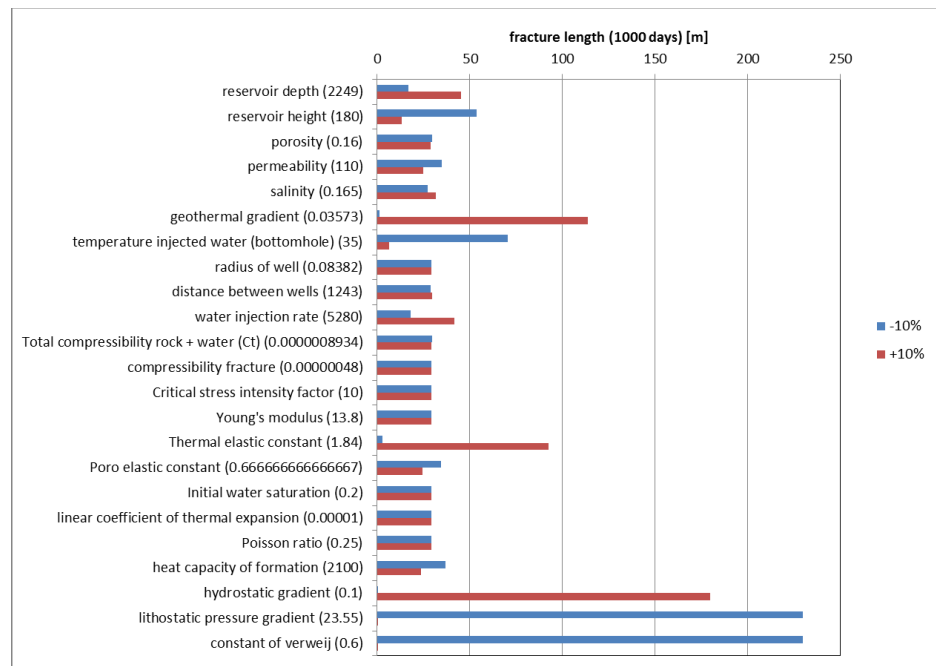


Figure 0.18 Sensitivity plot showing the effect of increasing or decreasing the various input parameters by 10% for a specific doublet.

For illustration purposes, various calculations were performed on an 'average doublet' using varying ratios of the horizontal and vertical stress. Figure 0.9 and Figure 0.10 suggest that the value for this ratio approximately lies between 0.5 and 0.6. A higher value indicates a larger horizontal stress, hence a fracture will develop less easily. This is illustrated by Figure 0.19. An optimistic scenario – from an economical point of view where fractures lead to better injectivity – has a small horizontal stress and hence a low ratio (0.5). For the chosen doublet and reservoir parameters, a fracture starts to develop which reaches >800m after 1000 days. A pessimistic scenario having a high ratio (0.6) shows that, in this case, the fracture will hardly develop. It illustrates the large control of the local stress state on fracture initiation and growth. Accordingly, efforts to better constrain the local stress state (e.g., constraining $\sigma_{h,min}$ from extended leakoff tests) will considerably improve predictions of fracture dimensions.

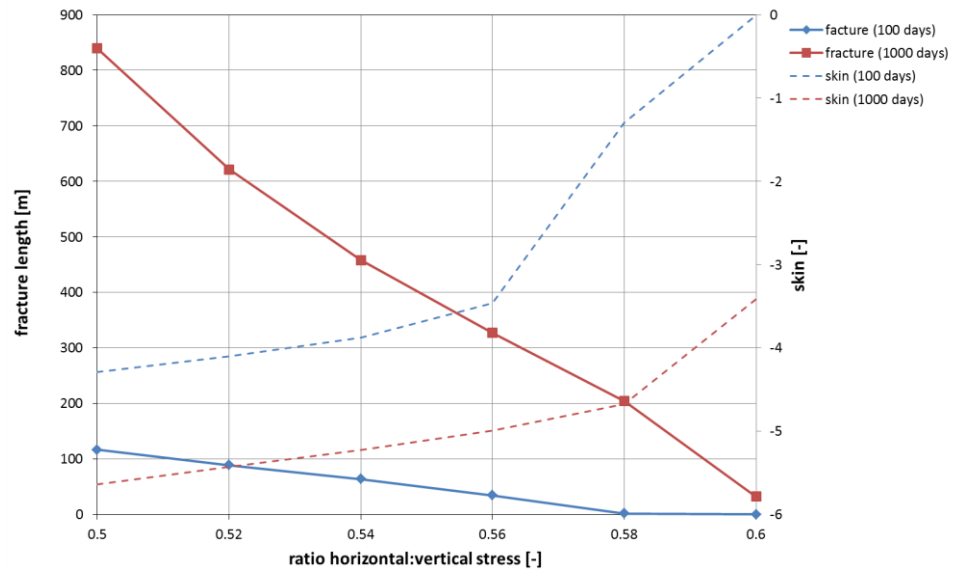


Figure 0.19 Fracture and skin development for a 'typical' doublet using varying horizontal : vertical stress ratios.

A.6 The effect of heat exchange with the reservoir on injectivity

The accuracy of the injectivity calculations is influenced by the temperature of the injected water and the reservoir. During injection, the well and the injected water exchange heat with the surrounding reservoir rock. At a plotow depth, the injected water cools because the reservoir rock is colder than the injected water. At larger depth, the water reheats because the reservoir rock is warmer than the injected water. As a result, the temperature (and therefore density and viscosity) of the water injected into the reservoir differs from the temperature at the exit of the heat exchanger. The magnitude of this effect was calculated as follows. The heat loss per length unit in the well is estimated by:

$$Q_{w,well} = \frac{4\pi k_r (T_c - T_r)}{\left(\ln \left(\frac{4\alpha t}{\sigma r_c^2} \right) \right)} \quad \text{eq. 27}$$

where:

- $Q_{w,well}$ heat loss per length unit (W/m)
- k_r thermal conductivity of the rock (typical value 3 W/mK)
- T_c temperature of the casing
- T_r temperature of the rock
- α thermal diffusion coefficient of the rock (typical value 1.2e-6 m²/s)
- t time
- σ constant with the value 1.781072
- r_c radius of the casing

The heat loss of the injected water can be estimated by the energy balance equation:

$$Q_{w,well} = Q_m C_p \frac{dT_{well}}{dl} \quad \text{eq. 28}$$

where:

Q_m mass flow rate

C_p water heat capacity

$\frac{dT_{well}}{dl}$ temperature profile within the well

The magnitude of the effect was calculated using values for an 'average' Dutch doublet (see Table A.4). It can be shown that the effect is the highest after one day of injection. In this case, the water is heated by a maximum of 3.5°C. After a longer period of injection, for instance one year, the environment around the well has heated up at shallower depths, and cooled down in the deeper parts of the subsurface. Therefore, the magnitude of the effect on temperature is reduced to a maximum of about 1°C at high injection rates. At lower injection rates, the reservoir around the well heats slower and the temperature difference after one year is still larger.

| Input | value | unit |
|---|---------|-------------------|
| reservoir depth | 2250 | m |
| geothermal gradient | 0.03573 | °C/m |
| temperature injected water (bottomhole) | 35 | °C |
| radius of well | 0.12 | m |
| injection rate (high) | 4800 | m ³ /d |
| Injection rate (low) | 2400 | m ³ /d |

Table A.4 Input parameters for the assessment.

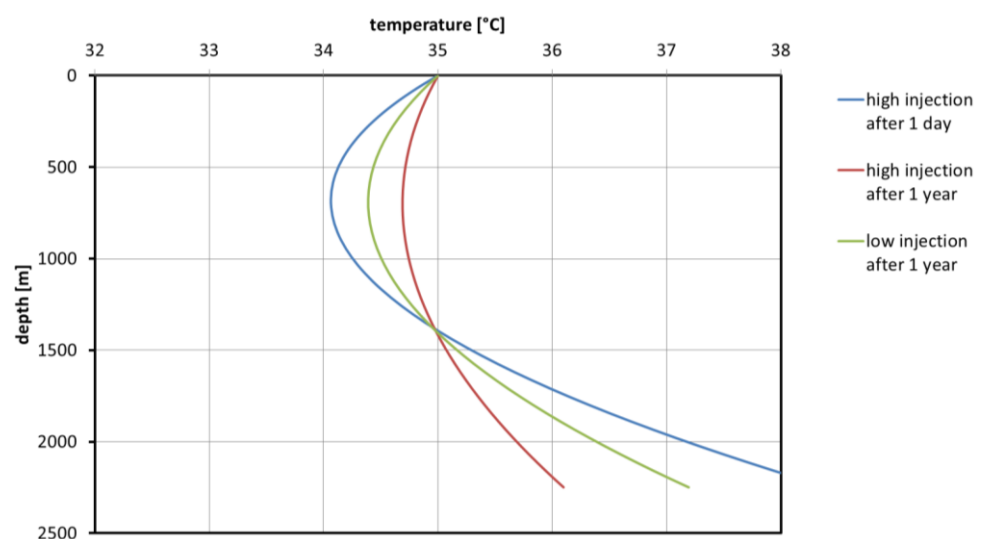


Figure 0.20 Temperature profile in the well.

With the exception of the D1 data, the data provided by the operators start at least one year after the onset of production. This means that a temperature difference between 1.0 and 2.0°C can be expected. This difference has a very small effect on density. The change in viscosity is between -1.6 and -3.1% (see Table A.5).

| parameter | value | unit | value | unit | % difference |
|----------------|-----------|-------------------|-----------|-------------------|--------------|
| injection rate | 4800 | m ³ /d | 4800 | m ³ /d | |
| temperature | 36 | °C | 35 | °C | |
| density | 1174.2 | kg/m ³ | 1175.39 | kg/m ³ | -0.10% |
| viscosity | 1.046E-03 | Pa.S | 1.063E-03 | Pa.S | -1.60% |

| | | | | | |
|----------------|-----------|-------------------|----------|-------------------|--------|
| injection rate | 2400 | m ³ /d | 2400 | m ³ /d | |
| temperature | 37.2 | °C | 35 | °C | |
| density | 1172.9 | kg/m ³ | 1175.39 | kg/m ³ | -0.21% |
| viscosity | 1.027E-03 | Pa.S | 1.06E-03 | Pa.S | -3.11% |

Table A.5 The effect of well heating on density and viscosity for two injection rates.

The difference in density and viscosity between the injected water at surface level and bottom hole implies that the injectivity index is different as well. The effect on the injectivity index over time is shown in Figure 0.21 for the high flow rate. An increased injection temperature also increases the injectivity index. The combined viscosity and density effects initially increased the injectivity index. This effect decreases with time.

The injectivity index depends on bottom hole temperature (BHT). Therefore it is important to measure the BHT directly if possible using a downhole installed sensor. The temperature effect in the well is estimated but gives rise to uncertainty of the exact value of the injectivity index.

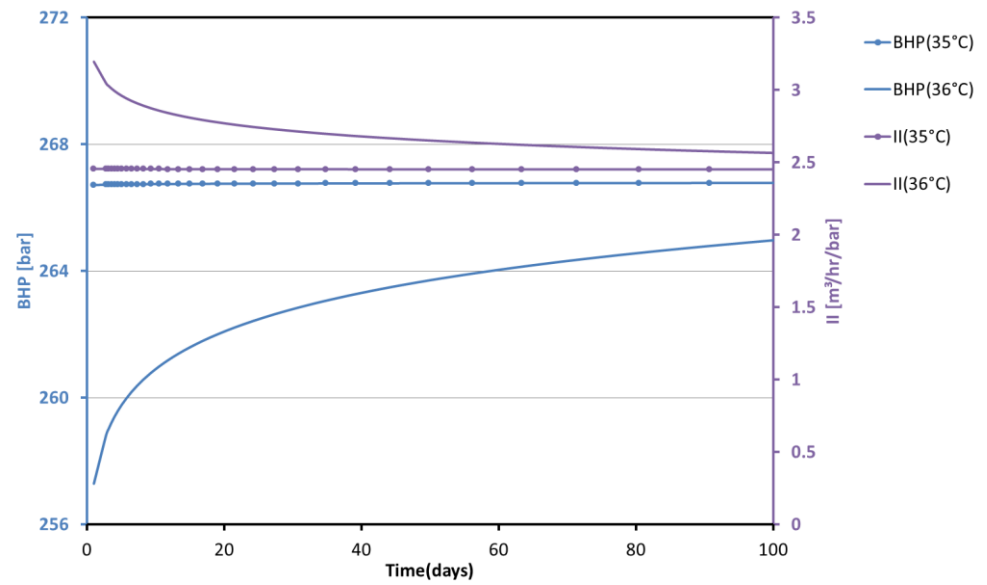


Figure 0.21 Development of BHP and injectivity index with constant injection rate of 4800 m³/day with constant injection temperature of 35°C, and including time dependent heating (indicated by calculated temperature of 36°C).

B Changes in stress field and fracturing during injection and cooling

This appendix describes the importance of tensile (thermal) fracturing (mode I) with respect to shear fracturing (mode II). Some knowledge of Mohr circles is assumed.

Figure 0.22 shows the local stress state is indicated by Mohr circles (half circles in black, green and purple) and can be fully constrained by three total stresses (S_v , S_{Hmax} , S_{Hmin} , thick black lines) or effective stresses (σ'_v , σ'_{Hmax} , σ'_{Hmin} , thin black lines). Fracturing is controlled by the effective stresses. The pressure in the reservoir (P_p) and Biot's constant α determine the difference between total and effective stresses (indicated by the black arrow). During injection without cooling (I- green arrow), the reservoir pressure increases, and effective stresses decrease (green Mohr circles). The size of the Mohr circle decreases due to poro-elastic effects in the reservoir. During injection with cooling (II- purple arrow), σ'_{Hmin} decreases and σ'_v remains approximately constant (purple Mohr circles). Therefore, the Mohr circles increase in size compared to injection without cooling. Shear fracturing may occur if the Mohr circles cross the Mohr failure criterion (red lines). Several Mohr failure criteria are indicated with similar cohesion (S_w) and different friction coefficients (μ_w), assuming existing natural fractures form planes of weakness (c.f. Fjaer et al. 2008). The Mohr failure criterion for intact rock with cohesion (S_i) and internal friction coefficient (μ_i) is also indicated. Some fractures at a critical angle (λ^*_{ini}) to σ'_v may be critically-stressed at initial stress conditions (red/black dot) due to a relatively low friction coefficient ($\mu_w = 0.44$ in this example), which means they can open even for small variations in pore pressure at the start of injection. Other fracture orientations (black dots) will be stable at initial stress conditions and do not move. As effective stresses decrease during injection more fractures may become critically stressed and start to move, i.e. the range of critical fracture angles becomes larger (red/green dot). Also, fractures with higher friction coefficient ($\mu_w = 0.6$ in this example) can become critically stressed and may move (at critical angle λ^*_{ini}). If existing fractures at critical orientations are absent or not hydraulically connected to the injection point at the well, cooling (II- purple arrow), may decrease stresses so that σ'_{Hmin} becomes negative and equal to the tensile rock strength (T). In this case, tensile (thermal) fractures will initiate and grow.

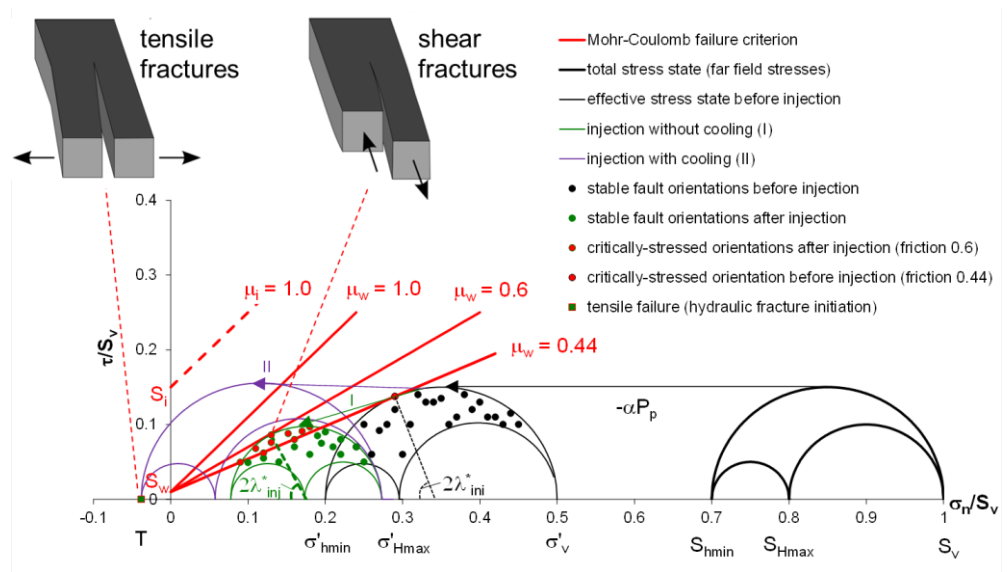


Figure 0.22 Schematic diagram showing the potential effects of water injection on the local stress state for a normal faulting regime.

C Analytical model tool user guide

The Excel sheet contains six tab sheets. The hidden sheets are provided only for advanced users.

- Input
- Output
- Newton Raphson (hidden)
- Time steps (hidden)
- Conversions and constants (hidden)
- Pressure (hidden)

Input sheet

In this sheet the following input parameters can be entered:

- The values for depth, reservoir thickness, water injection rate, water injection temperature, porosity and permeability should be determined locally and are considered to be relatively well-known.
- Various others properties, such as rock compressibility, critical stress intensity factor, Young's modulus a.o. (see Figure 0.23) are often less well known and can for instance be derived from text books.
- The cells shaded in yellow are calculated automatically and should not be changed manually.
- The temperature of the reservoir is calculated by default using a geothermal gradient of 0.031°C/m.
- The pressure of the reservoir is calculated by using a hydrostatic gradient of 0.1 bar/m.
- The initial horizontal stress strongly depends on the local stress situation, which can be found in the Pressure SNS database (Verweij et al. 2014). As a rule of thumb the initial horizontal stress is calculated as 60% of the lithostatic pressure (Verweij et al. 2012). The lithostatic pressure gradient is about 23 MPa/km.
- The density of water depends on pressure, salinity and temperature. It is estimated according to the correlations of Batzle en Wang (1992).
- The viscosity of water depends on salinity and temperature. It is estimated according to the correlations of Batzle en Wang (1992).

| Input | symbol | value | unit | comment |
|---|--------|---------|-------------------|---------|
| reservoir depth | | 2333 | m | |
| reservoir height | | 165 | m | |
| porosity | phia | 0.25 | - | |
| permeability | K | 110 | mD | |
| salinity | | 0.165 | kg/kg | |
| geothermal gradient | | 0.03573 | °C/m | |
| temperature injected water (bottomhole) | | 25 | °C | |
| radius of well | Rw | 0.11 | m | |
| distance between wells | D | 1243 | m | |
| water injection rate | | 5832 | m ³ /d | |
| simulation duration | | 1000 | days | |

| Reservoir rock properties | symbol | value | unit | comment |
|---|--------|----------|----------------------|---|
| Total compressibility rock + water (Ct) | Ct | 8.93E-07 | kPa ⁻¹ | standard ECLIPSE300 values |
| compressibility fracture | Cf | 4.80E-07 | kPa ⁻¹ | not used |
| Critical stress intensity factor | K_ic | 10 | bar m ^{3/2} | E.J.L. Koning (1988) --> 10 M.J. Economides (2000) 1000-3500 psi*inch ^{1/2} typical 2000 |
| Young's modulus | E | 1.38E+01 | GP | Santarelli et al (2008) --> range 0.2 - 50 (not used) |
| Thermal elastic constant | At | 1.84 | bar/C | E.J.L. Koning (1988) --> 1 Santarelli et al (2008) --> 0.18 - 0.38 bar/C |
| Porosity elastic constant | Ap | 6.67E-01 | 1/bar | E.J.L. Koning (1988) |
| Initial water saturation | Swi | 0.2 | | not used |
| linear coefficient of thermal expansion | beta | 1.00E-05 | mm/mm.K | Santarelli et al (2008) --> range 10e-5 - 10e-6 (not used) |
| Poisson ratio | v | 0.25 | | Santarelli et al (2008) --> range 0 - 0.5 (not used) |
| heat capacity of formation | Cp | 2100 | KJ/m ³ .K | E.J.L. Koning (1988) |

| Reservoir fluid properties | symbol | value | unit | comment |
|---|----------|-------------|----------------------|--|
| heat capacity formula | Cpw_mass | 5.160999415 | KJ/kg.K | Grunberg (1970) |
| density aquifer water (@injection conditions) | RhoW | 1188 | Kg/m ³ | calculated automatically (Batzle en Wang (1992)) |
| density sweet water (@injection conditions) | | 1.080 | g/cm ³ | calculated automatically (Batzle en Wang (1992)) |
| heat capacity of injected water | Cpw | 4200 | KJ/m ³ .K | E.J.L. Koning (1988) |
| viscosity water (cold) | Visw | 1.25E-03 | Pa.S | calculated automatically (Batzle en Wang (1992)) |
| viscosity water (hot) | Visw | 4.85E-04 | Pa.S | calculated automatically (Batzle en Wang (1992)) |
| Reservoir temperature | | 96.78795 | C | calculated automatically |
| density aquifer water (@reservoir conditions) | RhoW | 1111 | Kg/m ³ | calculated automatically (Batzle en Wang (1992)) |
| density sweet water (@reservoir conditions) | | 1.036 | g/cm ³ | calculated automatically (Batzle en Wang (1992)) |

| | | | | |
|-------------------------------|--|-------|--------|---|
| hydrostatic gradient | | 0.1 | bar/m | |
| lithostatic pressure gradient | | 23.55 | MPa/km | |
| constant of verweij | | 0.6 | - | ratio overburden pressure en min hor stress |
| initial pressure | | 234 | bar | calculated automatically |
| initial horizontal stress | | 330 | bar | calculated automatically |

Figure 0.23 Screenshot of the Input tab sheet, Required properties in green, optional input in grey. Values in yellow are automatically calculated.

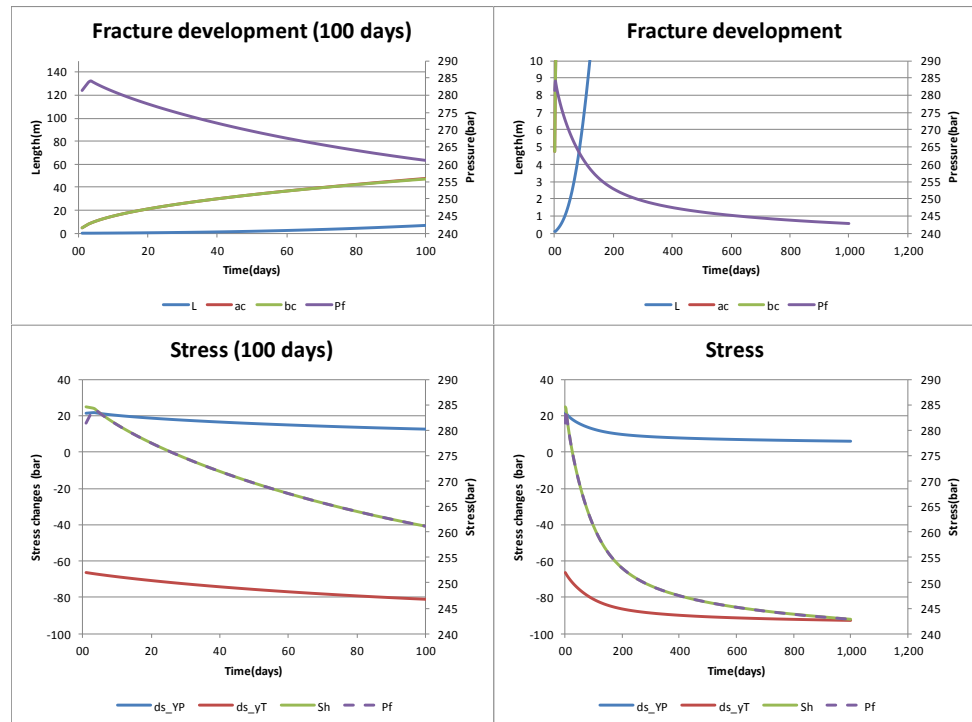


Figure 0.24 Input tab sheet graphics showing the fracture and stress development in the geothermal doublet over time.
Upper panels: L: fracture length; ac, bc: long and short axis of the ellipsoid of the cold front; Pf: pressure in the fracture.
Lower panels: ds_YP: change of the initial stress perpendicular to the fracture due to poro-elastic effects (positive); ds_yT: change of the initial stress perpendicular to the fracture due to thermal-elastic effects (negative); Sh: current stress at the tip of the fracture; Pf: pressure in the fracture, which is equal to the initial stress from the moment the fracture starts to propagate.

The top two panels of Figure 0.24 show the fracture growth over time. The lower two panels show the stress development over time.

Output sheet

In the output sheet the skin belonging to the enhanced injectivity can be calculated by pressing the button 'Find skin' as shown in Figure 0.25. Furthermore in the output sheet skin factor progressing over time is visualized (Figure 0.26). The user can apply these skin factors in the DoubletCalc software to estimate the injectivity and related economics.

A number of hidden sheets are available for advanced users of the analytical fracture tool. They can be visualised by right-clicking one of the visible sheets and selecting 'unhide'.

Newton-Raphson sheet (hidden)

At every time step a Newton-Raphson procedure is started to estimate the fracture length. This is a method for finding successively better approximations to the roots (or zeroes) of a real-valued function. This sheet is available for debug purposes only.

Time steps (hidden)

In this sheet the fracture growth (L), in situ stress (Sh), poro-elastic (ds_YP) and thermo-elastic stress changes (ds_yT) as well as the major (ac) and minor (bc) axes of the cold front are shown for every time step.

Based on the data in this sheet different graphical presentations of the development of the fracture through time can be made.

Conversions and constants (hidden)

A help sheet with conversion factors and constants.

Pressure (hidden)

The output of the pressure profile around the well for every time step.

| Input parameters from input sheet | | Output analytical model | | |
|-----------------------------------|---------------|-------------------------|--------|----------|
| | | t | Pf | Skin |
| | | days | bar | |
| Water Injection rate | 5832 m3/d | | | |
| Height | 165 m | | | |
| Viscosity water (visw) cold | 1.25E-03 Pa.S | 1.0 | 281.39 | -0.00665 |
| Permeability (K) | 110 mDarcy | 2.8 | 283.73 | -0.00665 |
| rw | 0.10795 m | 3.2 | 284.00 | -0.00665 |
| d | 1243 m | 3.6 | 284.16 | -0.01796 |
| Initial pressure | 234.3 Bar | 4.0 | 283.90 | -0.06943 |
| Viscosity water (visw) hot | 4.85E-04 | 4.5 | 283.63 | -0.12263 |
| | | 5.1 | 283.32 | -0.17904 |
| | | 5.7 | 282.99 | -0.23719 |
| Output | | 6.5 | 282.64 | -0.29795 |
| | | 7.3 | 282.26 | -0.36154 |
| | | 8.2 | 281.85 | -0.42822 |
| | | 9.3 | 281.40 | -0.49825 |
| | | 10.5 | 280.91 | -0.57187 |
| | | 11.8 | 280.38 | -0.65006 |
| | | 13.3 | 279.81 | -0.7322 |
| | | 15.0 | 279.19 | -0.81899 |
| | | 16.9 | 278.52 | -0.91075 |
| | | 19.1 | 277.79 | -1.00782 |
| | | 21.5 | 277.01 | -1.11051 |
| | | 24.2 | 276.16 | -1.21912 |
| | | 27.3 | 275.25 | -1.3339 |
| | | 30.8 | 274.28 | -1.45506 |
| | | 34.7 | 273.23 | -1.58386 |
| | | 39.2 | 272.11 | -1.71898 |

Figure 0.25 Output sheet: press the 'find skin' button to estimate the skin factor belonging to the enhanced injectivity estimated in the input sheet.

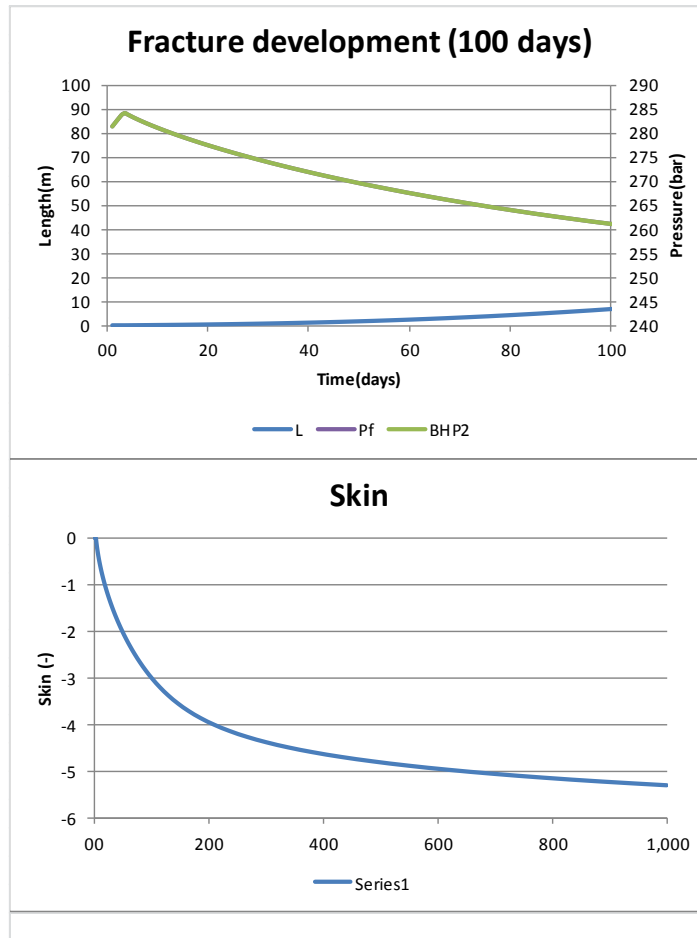


Figure 0.26 Visualization of the skin factor and fracture development over time

The procedure to estimate the fracture growth and the resulting skin factor is as follows:

- Select the Input sheet
- Set all the required input parameters.
- Run the program by pressing the “Run the program” button on the input sheet
- On the input sheet some predefined graphics indicate the fracture growth and BHP development over time.
- To estimate the skin factor switch to the Output sheet
- Press the button 'Find Skin' on the Output sheet. This will imitate the Excel 'goal seek' method and find the skin belonging to the fracture scenario modelled in step 2
- On the Output sheet some predefined graphics indicate the skin and BHP development over time.

D Calculation of the axes of the elliptical fluid front

Perkins and Gonzalez (1985) assume a simple piston-like displacement of the fluid and cold front around the well. The flood front advances through the reservoir faster than the cold front. The general volume balance of the flood front is:

$$V_F = \frac{qt}{\phi} \quad \text{eq. 29}$$

where:

V_F volume of the fluid flood front
 qt injection rate multiplied by time
 ϕ porosity

The cold front is equal to heat balance:

$$V_c = \frac{M_w}{M_r} qt \quad \text{eq. 30}$$

where:

V_c volume of the cooling front
 M_w heat capacity of the injected water
 M_r heat capacity of the fluid filled reservoir rock

$$V_c = \pi L^2 h \sinh \xi_c \cosh \xi_c \quad \text{eq. 31}$$

The major and minor elliptical axes are respectively $a_c = L \cosh \xi_c$ and $a_c = L \sinh \xi_c$. Hence, it follows that:

$$a_c = \frac{L}{2} \left(\sqrt{F_c} + \frac{1}{\sqrt{F_c}} \right) \quad \text{eq. 32}$$

$$b_c = \frac{L}{2} \left(\sqrt{F_c} - \frac{1}{\sqrt{F_c}} \right) \quad \text{eq. 33}$$

where:

$$F_c = \frac{2V_c}{\pi L^2 h} + \frac{1}{2} \left[\left(\frac{2V_c}{\pi L^2 h} \right)^2 + 4 \right]^{1/2} \quad \text{eq. 34}$$

E List of symbols

| | |
|-----------------------------|--|
| a_c, b_c | major and minor axis of the cold front |
| a_F, b_F | major and minor axis of the warm front |
| A_p | poro-elastic constant, which can be expressed as $\left(\frac{1-2\vartheta}{E}\right)\left(1 - \frac{c_g}{c_m}\right)$ |
| A_t | thermo-elastic constant |
| BHP | Bottom Hole Pressure |
| BHT | Bottom Hole Temperature |
| c_g | compressibility of the grains |
| c_m | compressibility of the bulk matrix |
| c_t | total compressibility |
| D | distance between the wells |
| E | Young's modulus |
| $e_c = \frac{b_c}{a_c}$ | |
| h | reservoir height |
| k | permeability |
| K_{ic} | critical stress intensity factor (typically $10 \text{ bar}\cdot\text{m}^{-1/2}$) |
| L | fracture half length |
| M_w | heat capacity of the injected water |
| M_r | heat capacity of the fluid filled reservoir rock |
| P_f | pressure in the fracture (equal to the BHP) |
| $\frac{1}{2} \Delta P_D(0)$ | stress change due to injection at the fracture tip |
| q | injection rate |
| R | correction term due to elliptical coordinates |
| r_w | wellbore radius |
| s | skin factor |
| S_h | horizontal total rock stress |
| S_{hi} | in situ horizontal total rock stress |
| ΔS_{Hp} | apparent change in far field stress |
| T | time |
| ΔT | temperature difference between reservoir and injected fluid |
| V_c | volume of the cold front |
| V_F | volume of the flood front |

Greek

| | |
|---------------------|--|
| α | Verweij constant |
| λ_1 | mobility of the cold front |
| λ_2 | mobility of the warm front |
| η | hydraulic diffusivity $\eta = k/\phi\mu c_t$ |
| $\Delta\sigma_{yP}$ | poro-elastic stress change |
| $\Delta\sigma_{yT}$ | thermo-elastic stress change |
| ϑ | Poisson ratio |
| ϕ | porosity |
| ξ | elliptical coordinate |
| μ | viscosity |

Subscripts:

| | |
|---|----------------|
| c | cold front |
| f | fluid front |
| D | dimensionless |
| P | poro-elastic |
| T | thermo-elastic |

F Determination of the minimum principal stress from well tests

A mini-frac or extended leak-off test (XLOT) can be performed to determine the magnitude of the minimum principal stress (i.e. the minimum horizontal stress $\sigma_{h,min}$ in case of a normal or strike slip faulting regime). The most accurate determination of $\sigma_{h,min}$ using well tests can be derived from an XLOT (Figure 0.27). The best estimate of $\sigma_{h,min}$ is from the fracture closure pressure (FCP) because formation stresses and fracture pressure are in a state of mechanical equilibrium (Lin et al. 2008). However, in practice full ('ideal') XLOTs are rare because

- they are expensive to conduct with two pumping cycles;
- a full XLOT causes formation damage which may lead to failure of the formation near the wellbore, and fines migration or fluid losses.

A mini-frac test is a small fracturing treatment before the main fracturing treatment to obtain some information on the stress field and fluid leak-off rate. The fracture propagation pressure (FPP) often has a constant value in the time interval that the fracture is propagating away from the well. In the case of low fluid viscosity and low flow rates the FPP will be close to $\sigma_{h,min}$. The instantaneous shut-in pressure (ISIP) measured after a stop in pumping can provide a more accurate measure of $\sigma_{h,min}$ because it is not influenced by any pressure gradients caused by fluid viscosity. Zoback et al. (2003) and Zoback (2007) provide a detailed explanation of the analysis of (extended) leak-off tests.

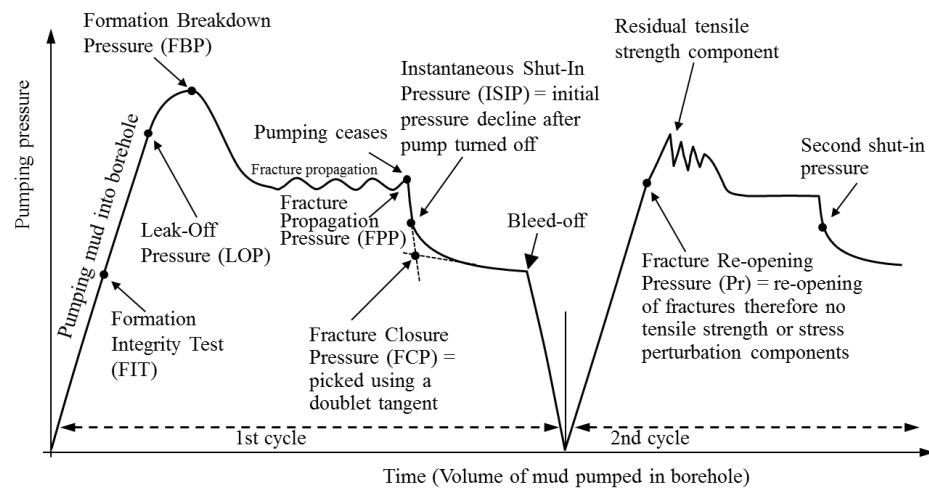


Figure 0.27 Example of an 'ideal' extended leak-off test (redrawn after Lin et al. 2008).

G Additional plots Chapter 4

G.1 D1 figures

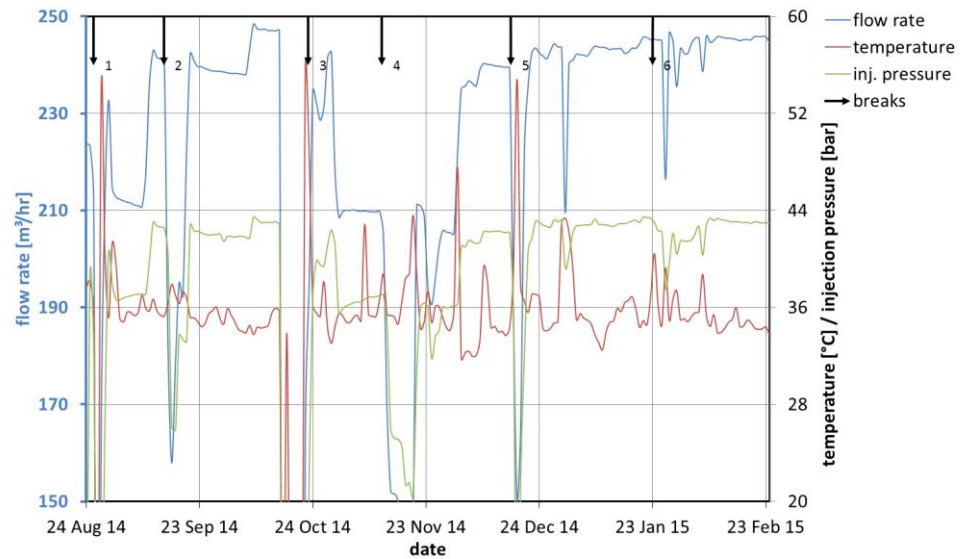


Figure 0.28 Complete production data D1 doublet (daily average) showing flow rate, injection temperature and injection pressure.

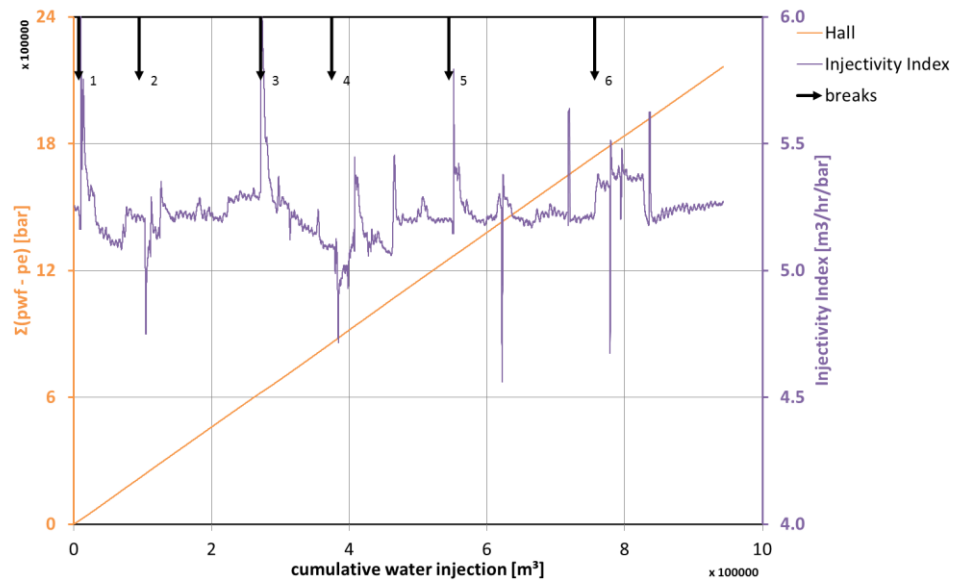


Figure 0.29 Hall plot and injectivity index of the D1 doublet. Arrows indicate changes in injectivity index.

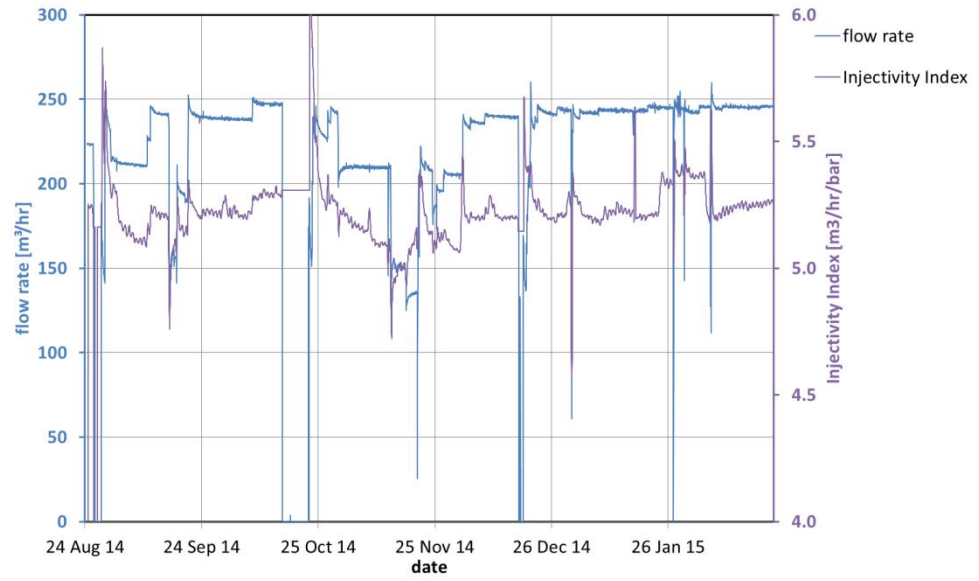


Figure 0.30 Injectivity index and flow rate of the D1 doublet.

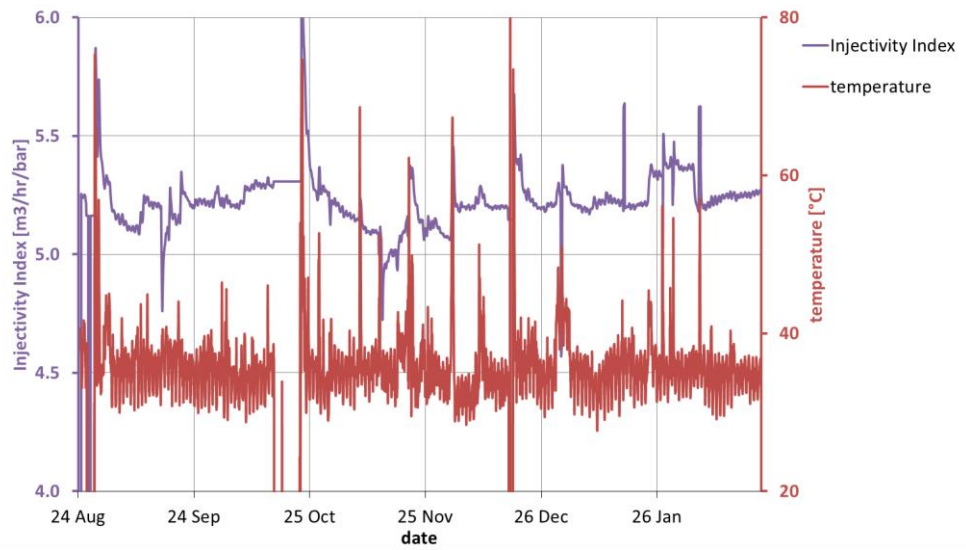


Figure 0.31 Injectivity index and temperature of the D1 doublet.

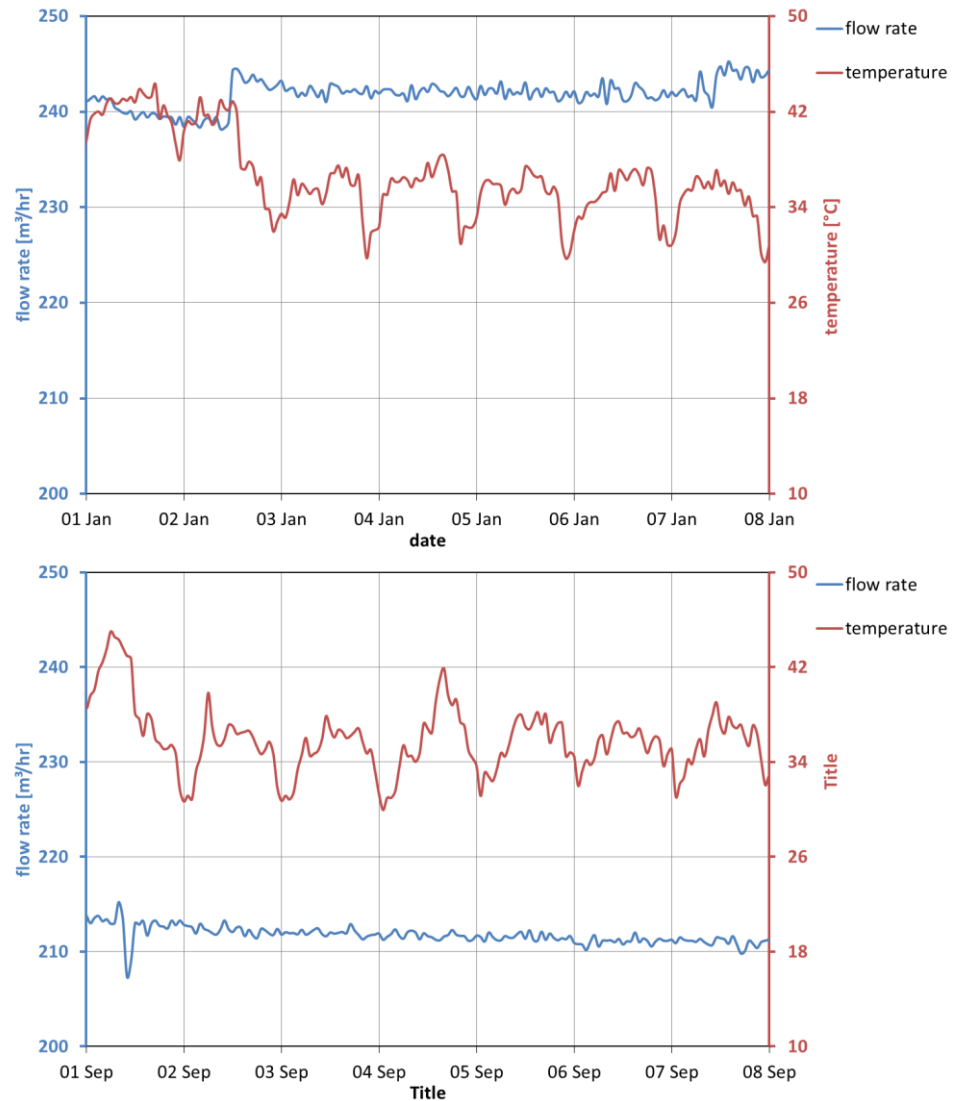


Figure 0.32 Production data D1 doublet for two weeks in January and September showing flow rate and temperature.

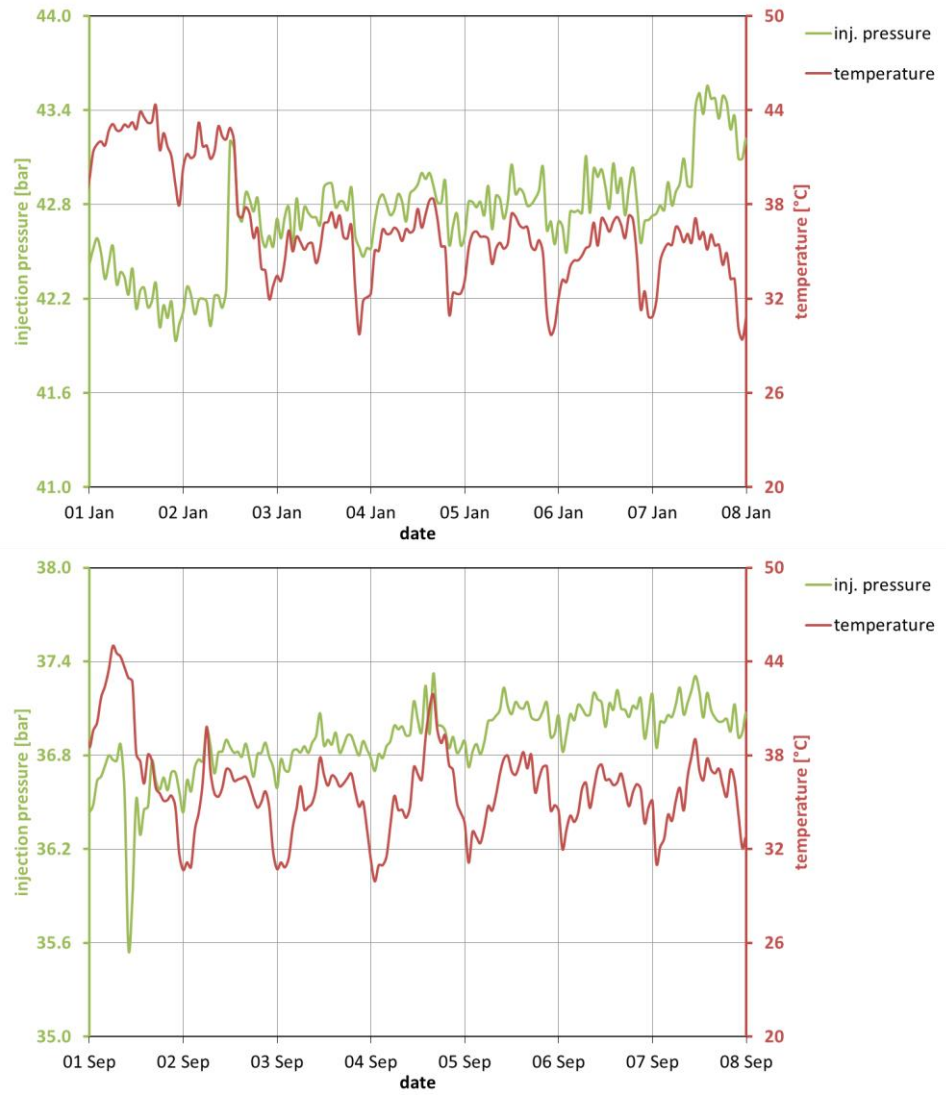


Figure 0.33 Production data D1 doublet for the same two weeks as Figure 0.32 showing injection pressure and temperature.

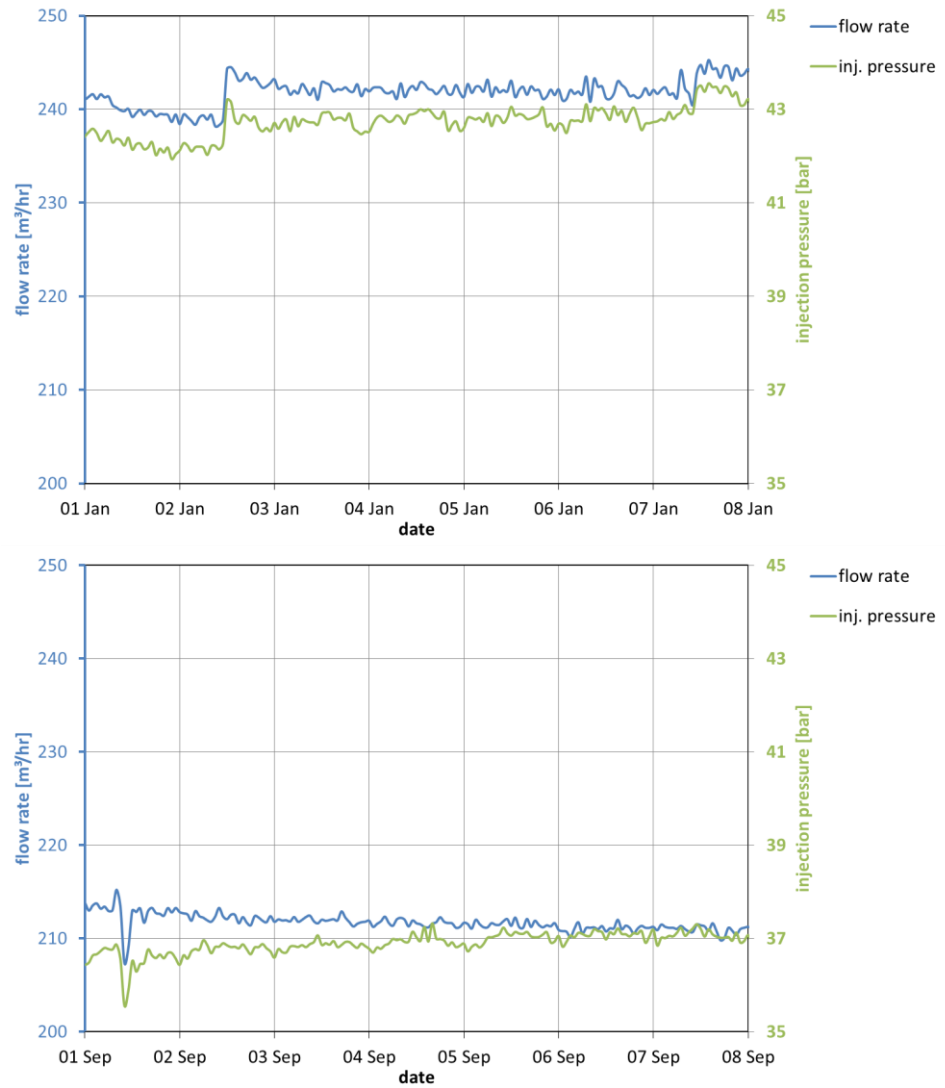


Figure 0.34 Production data D1 doublet for the same two weeks as Figure 0.32, showing flow rate and injection pressure.

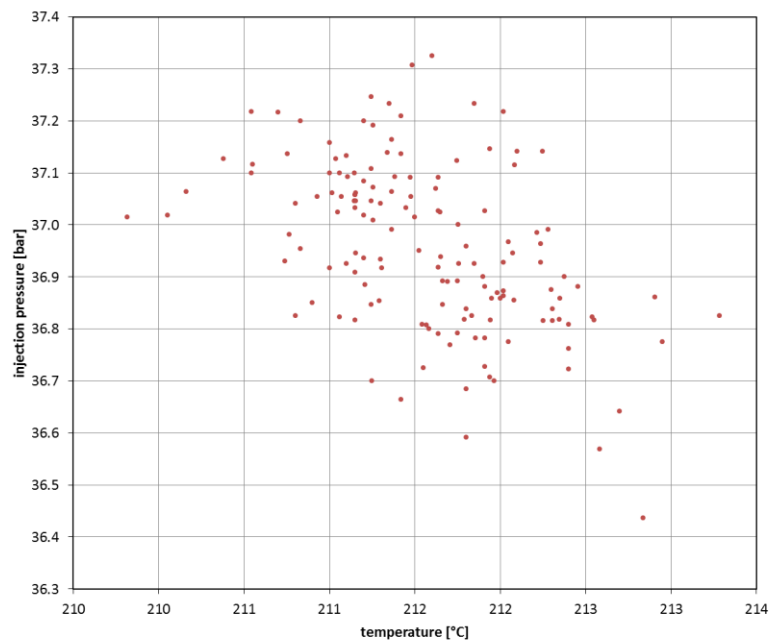
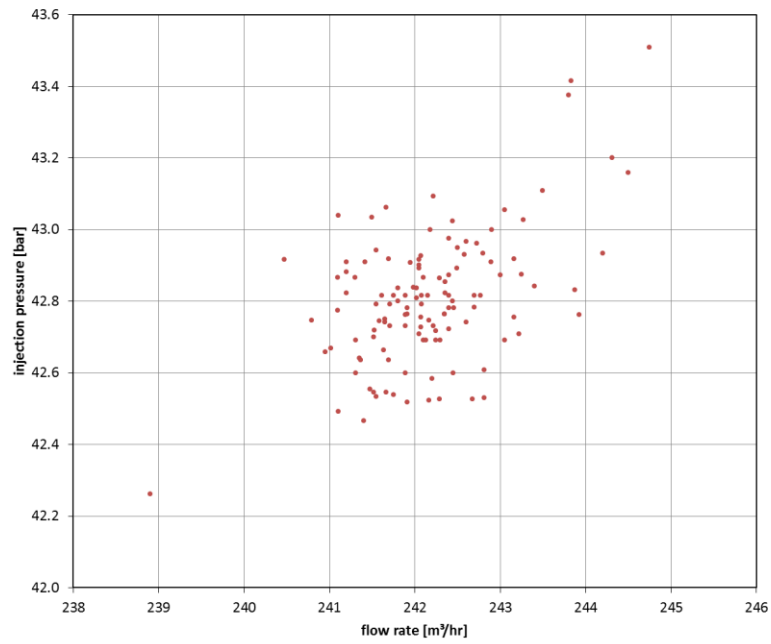


Figure 0.35 Production data D1 doublet for the same two weeks as Figure 0.32, showing injection pressure and temperature. The figure shows the ratio is not the same during the operational period

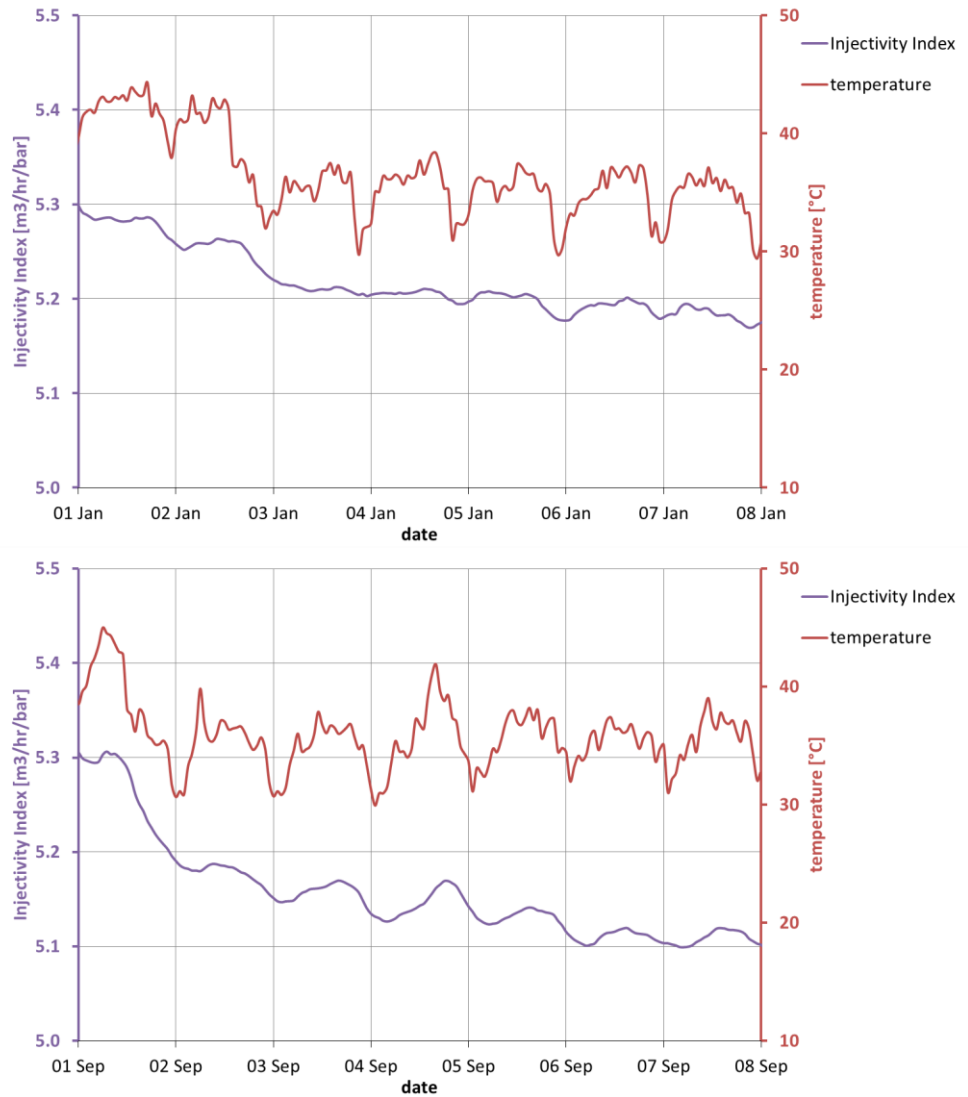


Figure 0.36 Production data D1 doublet for the same two weeks as Figure 0.32, showing injectivity index and temperature

G.2 D3 figures

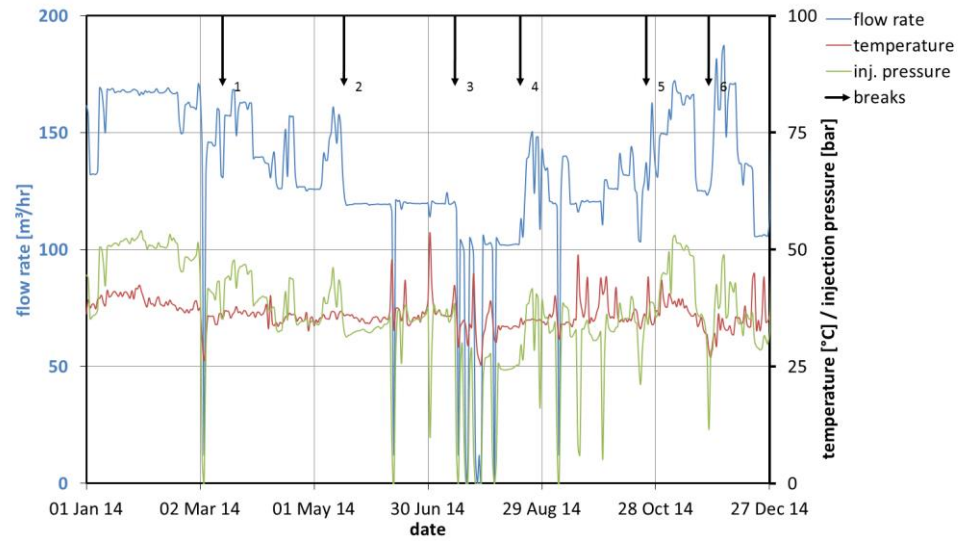


Figure 0.37 Complete production data D3 doublet (daily average) showing flow rate, injection temperature and injection pressure.

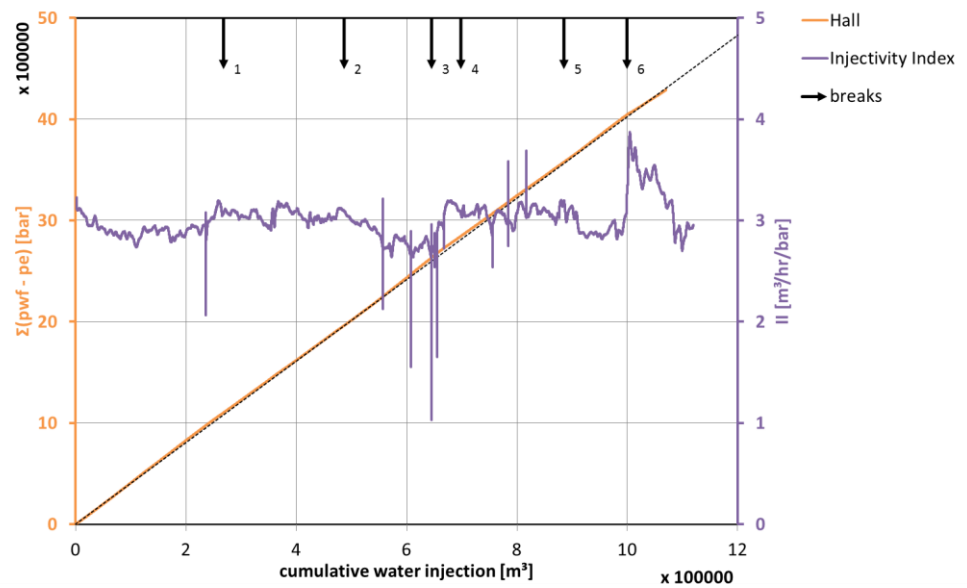


Figure 0.38 Hall plot and injectivity index of the D3 doublet.

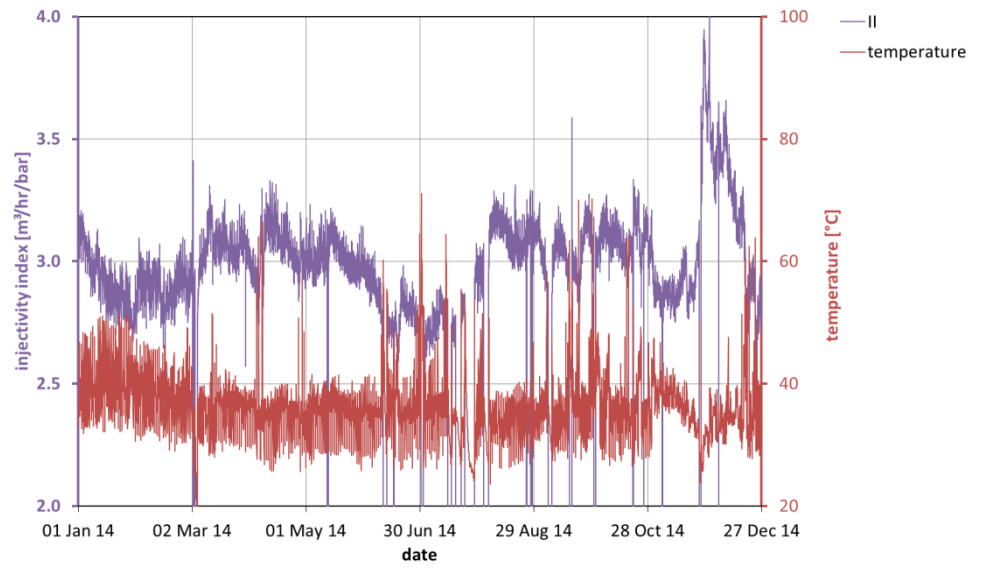


Figure 0.39 Injectivity index and temperature of the D3 doublet.

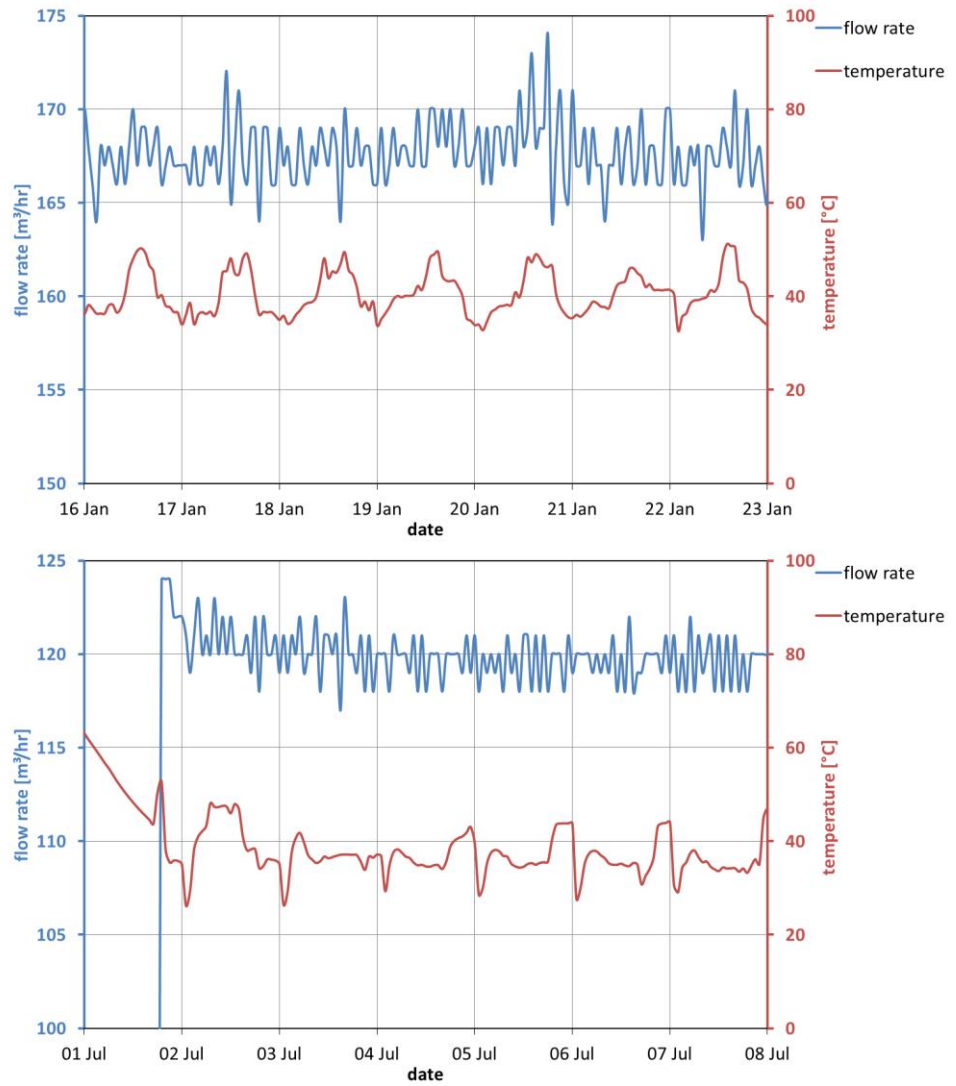


Figure 0.40 Production data D3 doublet for two weeks in January and July (hourly average), showing flow rate and injection temperature.

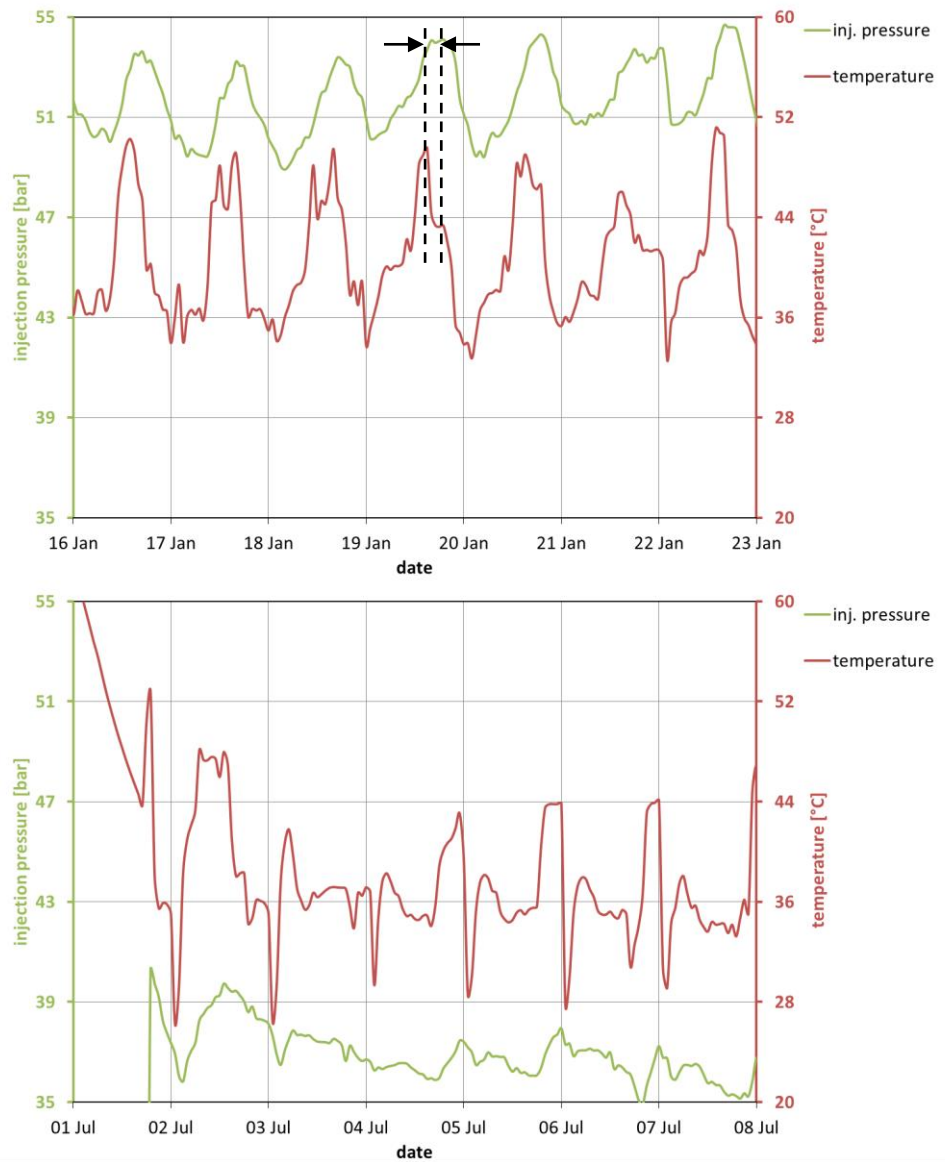


Figure 0.41 Production data D3 doublet for the same two weeks as Figure 0.40, showing injection temperature and pressure. Arrows indicate the time shift between injection temperature reduction and injection pressure reduction.

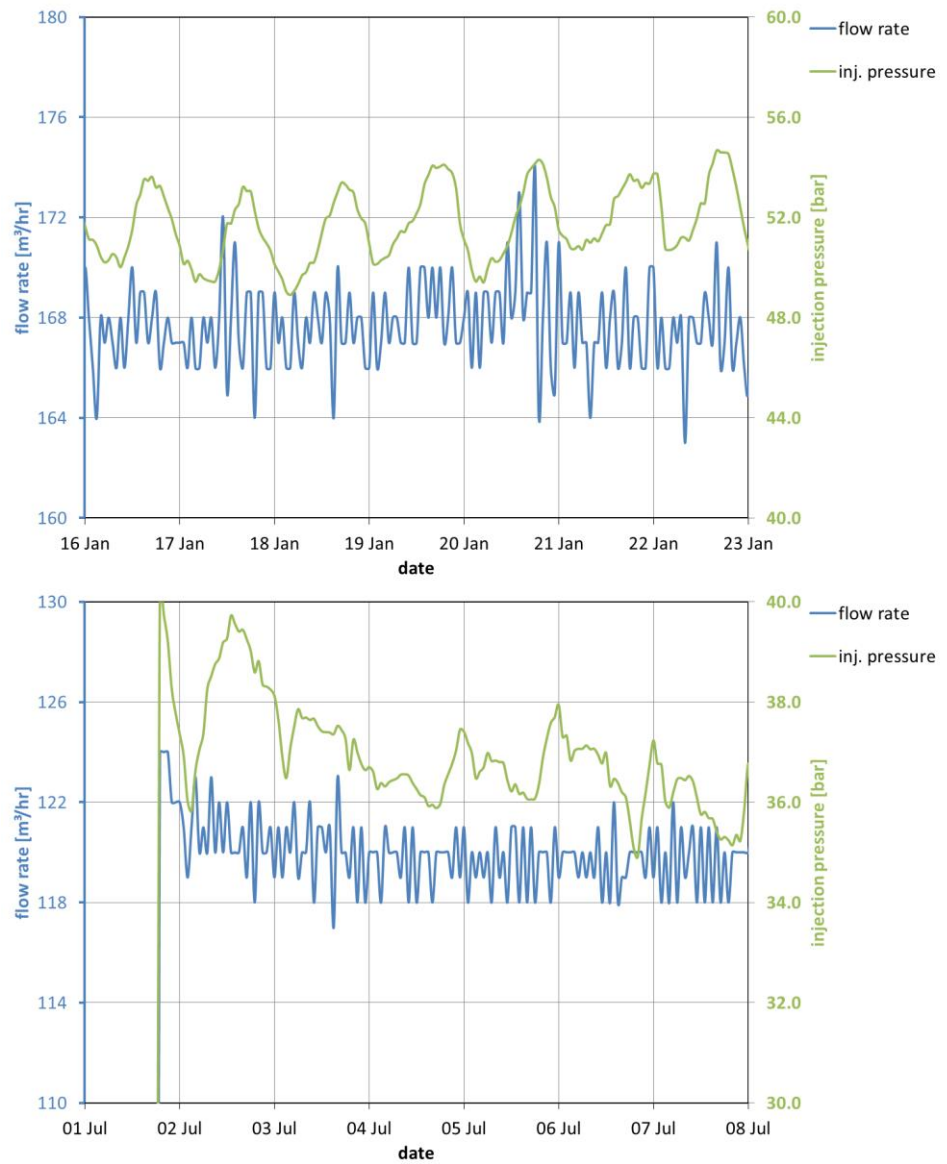


Figure 0.42 Production data D3 doublet for the same two weeks as Figure 0.40, showing flow rate and injection pressure.

G.3 D4 figures

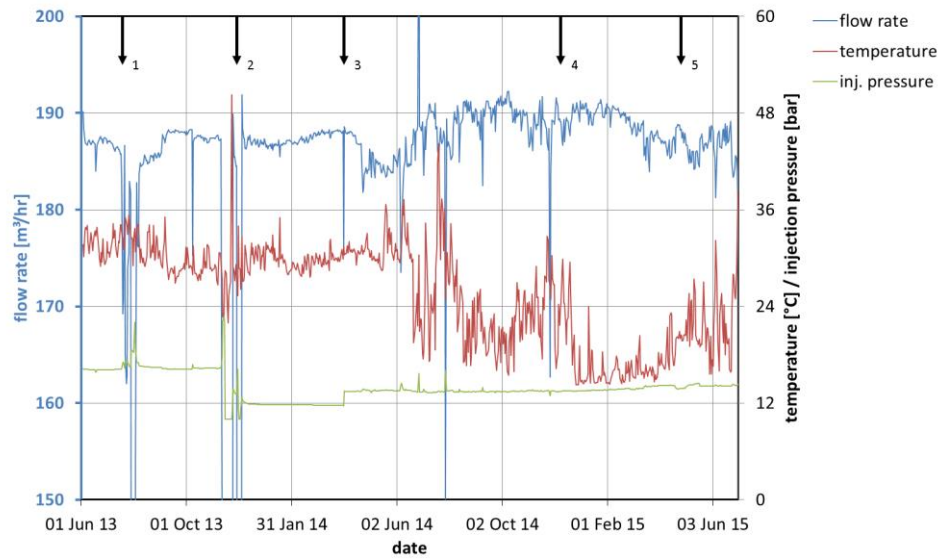


Figure 0.43 Complete production data D4 doublet (daily average), showing flow rate, injection temperature and injection pressure.

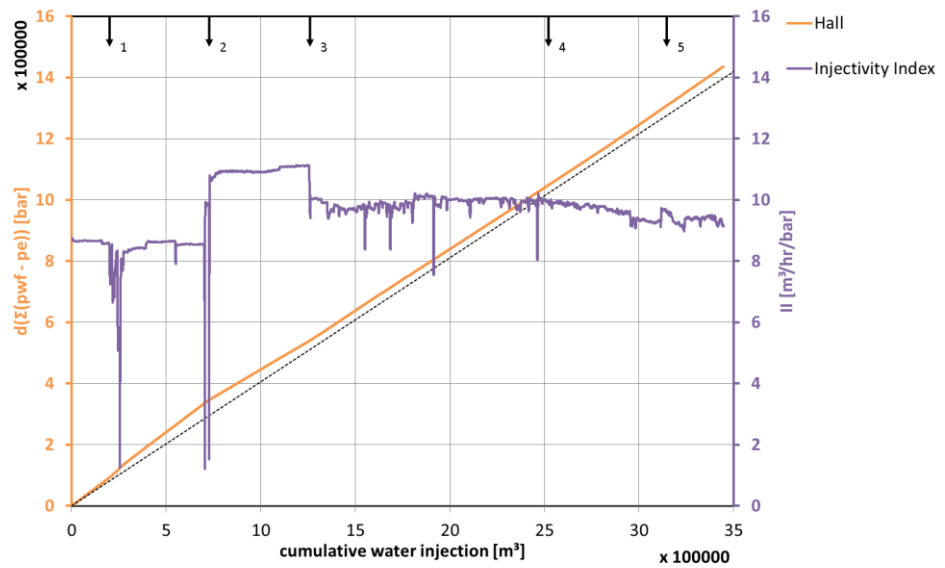


Figure 0.44 Hall plot and injectivity index of the D4 doublet. Arrows indicate changes in injectivity index.

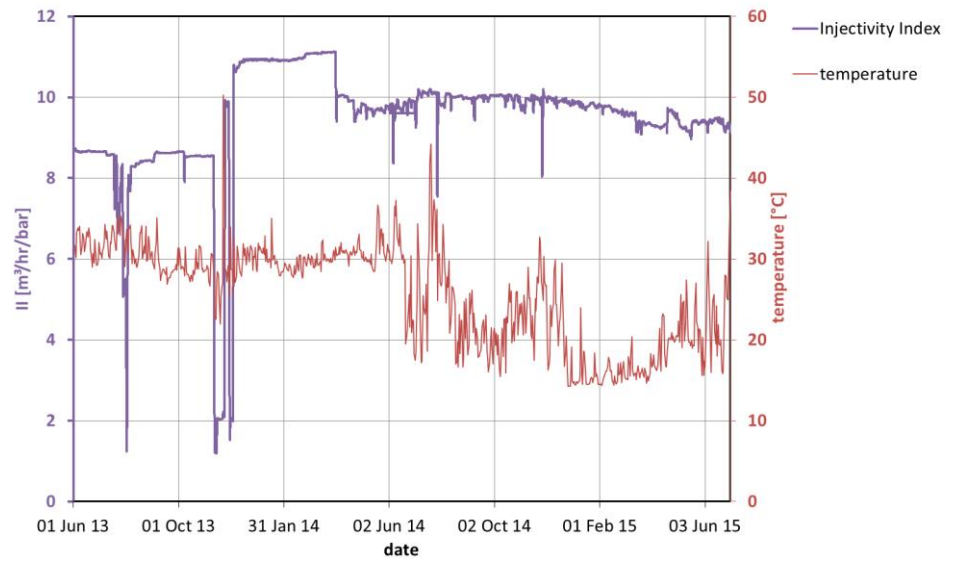


Figure 0.45 Injectivity index and temperature of the D4 doublet.

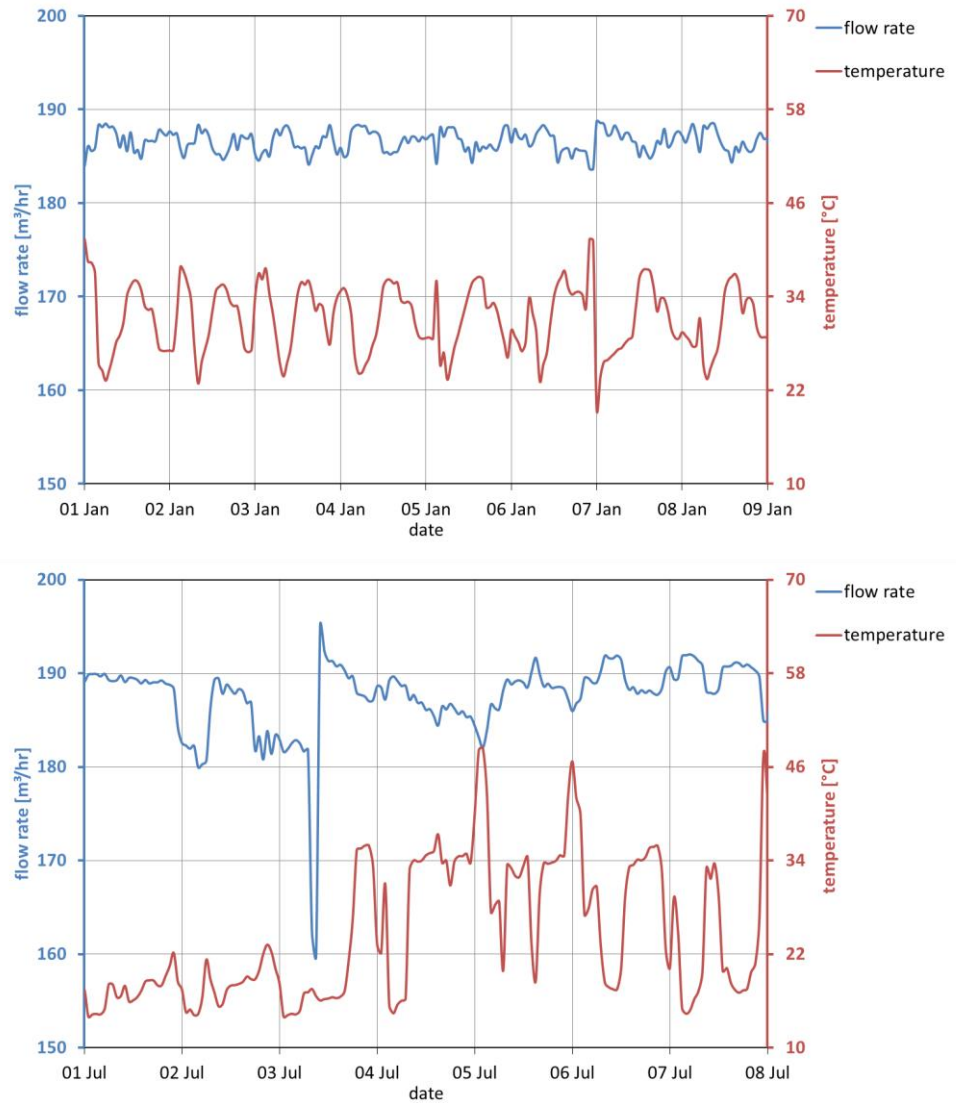


Figure 0.46 Production data D4 doublet for two weeks in January and July (hourly average), showing flow rate and injection temperature.

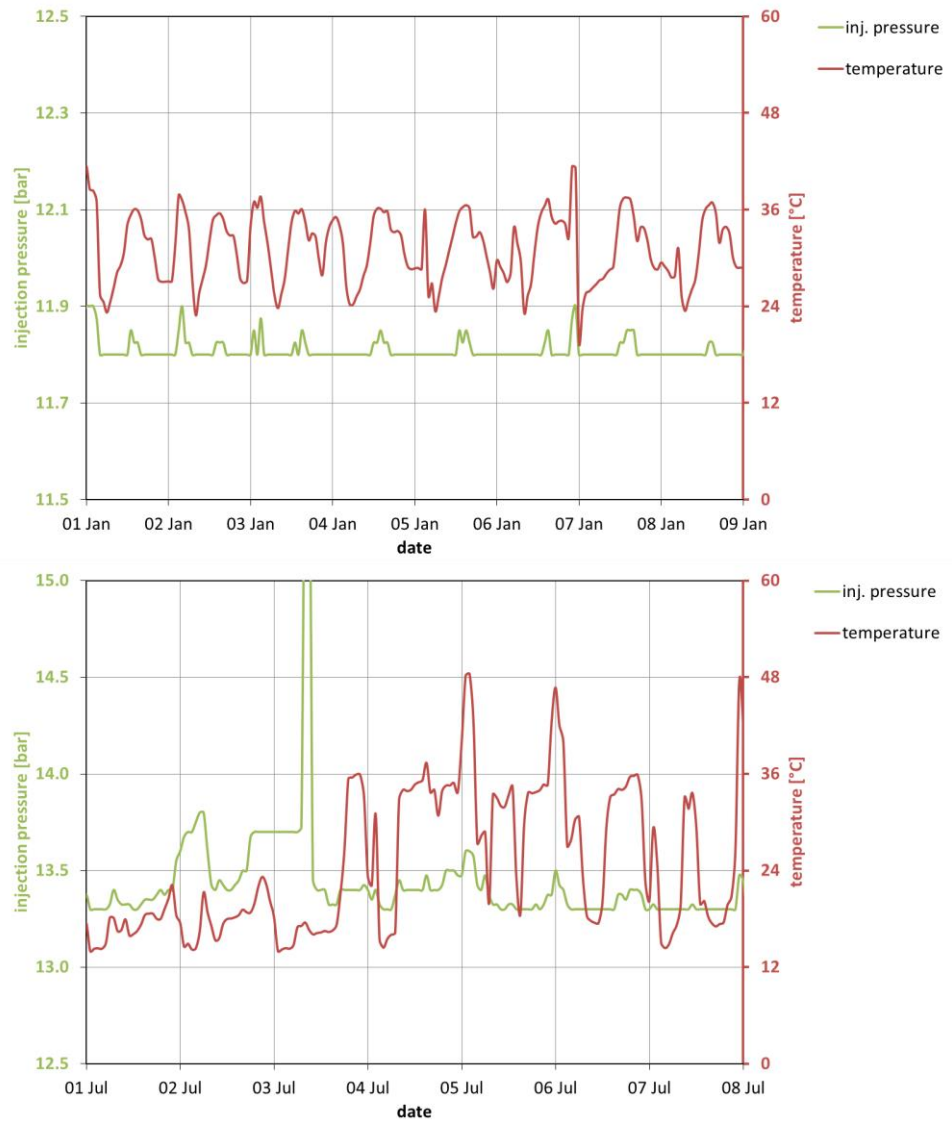


Figure 0.47 Production data D4 doublet for the same two weeks as Figure 0.46, showing injection temperature and injection pressure. The lower injection pressure cut-off at 11.8 bar is suspicious.

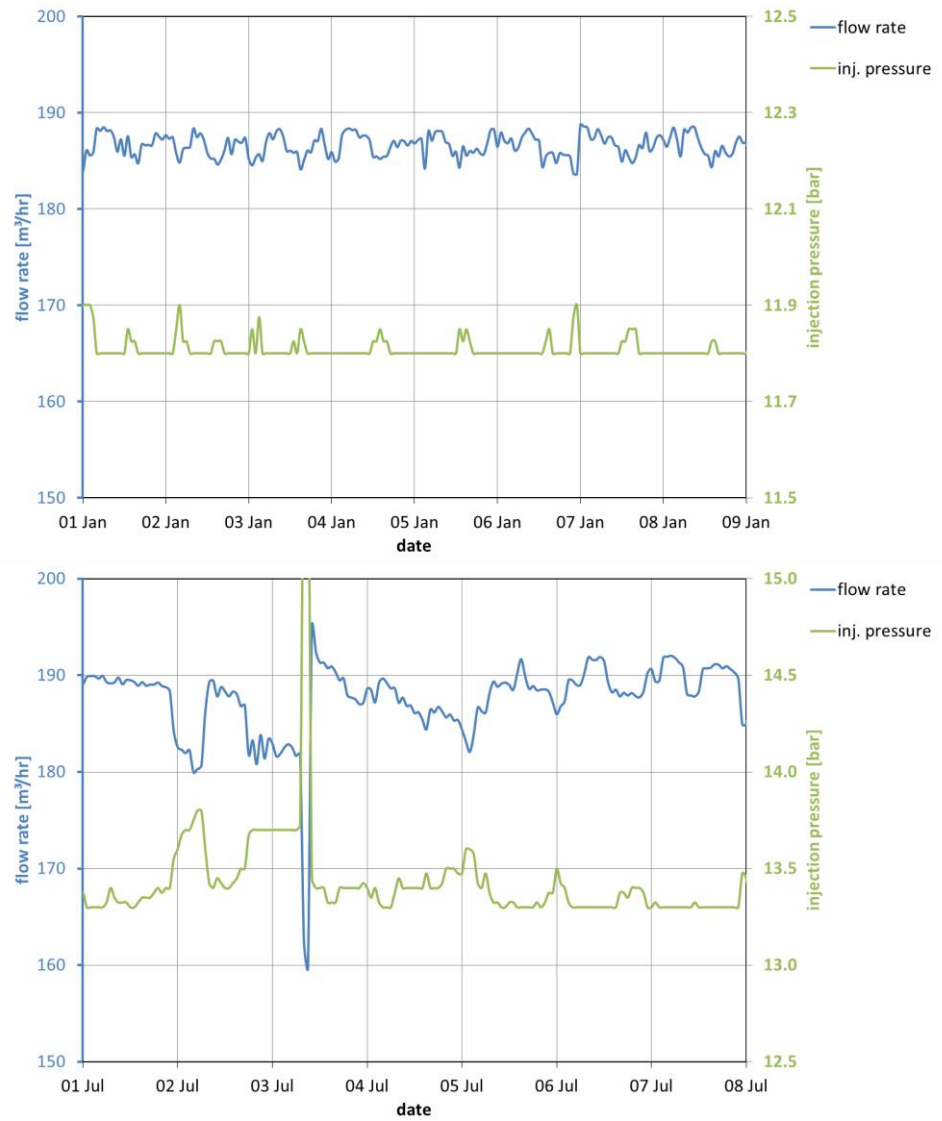


Figure 0.48 Production data D4 doublet for the same two weeks as Figure 0.46, showing flow rate and injection pressure.

H Doublet names (restricted)

Not available in public report.